

# Preferential oxidation of carbon monoxide in microchannels – development of catalysts for the low temperature regime and kinetic study

Dissertation  
zur Erlangung des Grades  
des Doktors der Ingenieurwissenschaften  
der Naturwissenschaftlich-Technischen Fakultät III  
Chemie, Pharmazie Bio- und Werkstoffwissenschaften  
der Universität des Saarlandes

von  
Georgios S. Nikolaidis

Saarbrücken  
2007

Tag des Kolloquiums:

Dekan:

Berichterstatter:

## Acknowledgement/Danksagung

Die vorliegende Arbeit wurde in der Zeit von Januar 2004 bis Dezember 2006 am Institut für Mikrotechnik und an der Universität des Saarlandes, Saarbrücken unter der Betreuung von Herrn Prof. Dr. W. F. Maier und Herrn Dr. G. Kolb angefertigt.

I would like to thank,

- Dr. G. Kolb, for the chance he gave me to work for my Ph.D. at the IMM, the direct supervision of my work all these years, the guidelines and helpful comments always kindly provided and the whole fruitful and friendly cooperation. I am also grateful to him, for providing the opportunity and organising my visit in University of Zaragoza, Spain.
  - Prof. W. F. Maier, for his inspiring and motivating spirit. Further, for his trust and his ability to leave me space to develop own ideas and having a helping mind whenever needed.
  - Prof. V. Hessel, for accepting me in his group and contributing to my work with his helpful and always valuable suggestions.
  - The whole group of Prof. V. Hessel, for the friendly atmosphere during my three years in IMM, the nice cooperation and the help, always provided to me whenever I needed it.
  - Especially the CPT department: Dr. T. Baier, M. Balon-Burger, Dr. V. Cominos, T. Hahn, D. Metzke, C. Krempel, Dr. Y. Men, Dr. H. Pennemann, D. Reinhard, J. Schürer, D. Tiemann, M. Wichert, Dr. A. Ziogas and Dr. R. Zapf, for the wonderful cooperation all these years, the kind knowledge exchange and generally for the warm group working atmosphere in the office and for being the best lab partners. From these people, I am especially thankful to:
    - J. Schürer, who helped me in every aspect of my Ph.D, providing me with know-how and for sharing his valuable experience in the field of micro-engineering.
    - Dr. T. Baier, for his continuous support and assistance with anything concerning the simulation part of the thesis.
    - Dr. H. Pennemann, for his patience to explain me and never being tired to critically discuss “strange” data during my three years in IMM.
    - Dr. V. Cominos, for lots of useful discussion on every question concerning techniques and applications.
-

- Dr. A. Ziogas, for taking the advantage of his knowledge and kindness. He invested a large amount of time to overcome all of my problems associated with analytical chemistry and not only.
  - Dr. R. Zapf and M. Krämer, for kindly providing me with Pt-Rh/ $\gamma$ -Al<sub>2</sub>O<sub>3</sub> and Pt<sub>0.5</sub>Al<sub>1</sub>Mn<sub>7</sub>Co<sub>91.5</sub>O<sub>x</sub> catalysts.
  - Additionally, A. Himmelsbach, who provided me with SEM-photos and EDX-spectra.
  - The mechanic workshop of IMM. All the technical problems during this work would never have been solved without their help.
  - Prof. J. Santamaria, for giving me the opportunity to work in his group at the University of Zaragoza Spain and for his helpful comments and suggestions.
  - The group of Prof. R. Mallada at the University of Zaragoza Spain, for providing me with the XRD-spectra, TEM-photos and their associated analytical data. Especially my office and lab colleagues: Dr. V. Cabeza and Dr. O. De La Iglesia for the measurements, the promising cooperation and their valuable corrections on my manuscripts.
  - Dr. B. Rohland and Dr. E. Fokkens, for giving me the opportunity to perform some of my experiments at the Hydrogen Institute of Applied Technologies in Schwerin Germany and for their helpful comments and suggestions.
  - The “Deutsche Bundesstiftung Umwelt”, for funding the Mikro-Selox project.
  - Dr. Y. Yao of Max-Planck Institute for polymer research Mainz, for his assistance evaluating XRD patterns.
  - My best friends: Dr. T. Atmakidis, Dr. G. Dalakoglou and Dr. I. Vittorias, for correcting my thesis and any manuscript I wrote during the last three years. For their helpful suggestions in science and in life as well, are deeply acknowledged.
  - Furthermore, I am grateful to Dr. K. Antoniadis, Dr. M. Dortsiou, I. Iliopoulos, E. Ilska, Dr. A. Kanaris, Dr. I. Sachpazidis, N. Stieger and A. Weimer, for all the intrinsic discussions we had all these years regarding the broader framework of my thesis, from which I was truly benefited.
  - My family, for their continuous support all these years in any possible way. Without them I wouldn't have achieved anything and there are not enough words, in any language of the world, which can describe my love and my devotion to them.
-

# Zusammenfassung

Ziel der vorliegenden Arbeit war es, die Herstellung von Au/MeO<sub>x</sub> und Zeolite basierten Katalysatoren für die selektive Kohlenmonoxidoxidation für Niedertemperaturbrennstoffzellen zu optimieren und zu bewerten, ob die hohe Aktivität und die Selektivität, die bei idealen Methanol-Reformaten (CO, O<sub>2</sub> und H<sub>2</sub>) beobachtet werden, auch unter realistischen Bedingungen (CO, O<sub>2</sub>, H<sub>2</sub>, bis 20 Vol.% CO<sub>2</sub> und 10 – 20 Vol.% H<sub>2</sub>O) erhalten bleiben. Insgesamt wurde eine Reihe von Katalysatoren getestet. Während sich der Au/Co<sub>3</sub>O<sub>4</sub> Katalysator am aktivsten und empfindlichsten in der Anwesenheit von Kohlendioxid verhielt, haben die Pt-Rh/γ-Al<sub>2</sub>O<sub>3</sub> und Pt<sub>0,5</sub>Al<sub>1</sub>Mn<sub>7</sub>Co<sub>91,5</sub>O<sub>x</sub> Katalysatoren das Kohlenmonoxid in der Anwesenheit des Wasserstoffes und des Kohlendioxides effektiv oxidiert.

Ein besonderer und neuartiger Aspekt in dieser Arbeit sind die Experimente, die für die Untersuchung der Kinetik der selektiven Kohlenmonoxidoxidation in beschichteten Mikroreaktoren durchgeführt wurden. Mittels eines eigens konstruierten Kreislaufreaktors wurde die Kinetik der Reaktion bestimmt. Die Ergebnisse der Verweilzeitverteilung (RTD) für ein CSTR, der durch einen Mikroreaktor mit rückführbarem Strom simuliert wird, weisen einen guten Näherungswert zu den experimentellen Messungen auf. Durch lineare Regressionsanalyse wurde ein kinetisches Modell entwickelt und dessen Validität überprüft. Die Kinetik der selektiven Kohlenmonoxidoxidation und der Wasserstoffoxidation auf Pt-Rh/γ-Al<sub>2</sub>O<sub>3</sub> Katalysator in simuliertem Reformergas in den Mikroreaktoren wurde mit einem Potenz-Ansatz beschrieben.

## Abstract

The aim of this work was to optimize the synthesis of Au/MeO<sub>x</sub> and Zeolite-based catalysts for the preferential oxidation reaction of carbon monoxide for low temperature fuel cells and to evaluate whether the high activity and selectivity observed in idealized methanol-reformate (CO, O<sub>2</sub> and H<sub>2</sub>) are also maintained under more realistic conditions (CO, O<sub>2</sub>, H<sub>2</sub>, up to 20 Vol.% CO<sub>2</sub>, and 10 – 20 Vol.% H<sub>2</sub>O). Among the catalysts tested, the Au/Co<sub>3</sub>O<sub>4</sub> catalyst was the most active and sensitive in the presence of carbon dioxide, while Pt-Rh/γ-Al<sub>2</sub>O<sub>3</sub> and Pt<sub>0,5</sub>Al<sub>1</sub>Mn<sub>7</sub>Co<sub>91,5</sub>O<sub>x</sub> were found to oxidize carbon monoxide effectively in the presence of hydrogen and carbon dioxide.

Another novel aspect of this work are the experiments for the kinetic study of the preferential oxidation reaction of carbon monoxide, which were performed applying catalyst coating in micro reactors. A recycle reactor was constructed to study the kinetics of the reaction. The

---

predictions of the residence time distribution (RTD) for a CSTR simulated by a microreactor with a recycle stream, has been shown to give an adequate approximation of the experimental measurements. Linear regression analysis was used to develop a kinetic model and to validate all the required parameters. The kinetics of the preferential carbon monoxide oxidation and hydrogen oxidation on Pt-Rh/ $\gamma$ -Al<sub>2</sub>O<sub>3</sub> catalyst in simulated reformer gas in the microreactors was well described by a simple power-law expression.

---

# Contents

<b>1 INTRODUCTION.....</b>	<b>1</b>
1.1 MOTIVATION.....	1
1.2 FUEL CELL.....	3
1.2.1 <i>Microreactors</i> .....	5
1.2.2 <i>CO oxidation in H<sub>2</sub>-rich gas streams</i> .....	8
1.3 NOBLE METAL CATALYSTS FOR PREFERENTIAL OXIDATION OF CO .....	10
1.3.1 <i>Gold based catalysts</i> .....	10
1.3.2 <i>Zeolite based catalysts</i> .....	12
1.4 METHODS OF CATALYSTS CHARACTERIZATION .....	17
1.4.1 <i>Brunauer–Emmett–Teller analysis</i> .....	17
1.4.2 <i>Scanning electron microscopy</i> .....	17
1.4.3 <i>Temperature programmed reduction</i> .....	18
1.4.4 <i>X-Ray diffraction</i> .....	18
1.4.5 <i>Transmission electron microscopy</i> .....	19
1.4.6 <i>Gas chromatography</i> .....	20
1.5 REACTOR CHARACTERIZATION.....	21
1.6 KINETIC STUDY .....	23
1.7 FOCUS OF THE RESEARCH .....	24
<b>2 RESULTS AND DISCUSSION .....</b>	<b>25</b>
2.1 SELECTION OF CATALYSTS .....	25
2.2 CATALYSTS CHARACTERIZATION .....	27
2.2.1 <i>Gold and zeolite XRD-spectra</i> .....	27
2.2.2 <i>Zeolite TPR-spectra</i> .....	30
2.2.3 <i>Zeolite SEM-photos</i> .....	32
2.2.4 <i>Gold TEM-photos</i> .....	35
2.3 ACTIVITY MEASUREMENTS.....	38
2.3.1 <i>Gold-catalysts</i> .....	39
2.3.2 <i>Zeolite-catalysts</i> .....	45
2.3.3 <i>Other noble metal catalysts</i> .....	53
2.4 RESIDENCE TIME DISTRIBUTION AND REACTOR MODEL .....	62
2.4.1 <i>Reactor model</i> .....	63

---

---

2.5 KINETIC MEASUREMENTS .....	65
2.5.1 <i>CO oxidation without H<sub>2</sub></i> .....	65
2.5.2 <i>CO oxidation in the presence of H<sub>2</sub></i> .....	69
2.5.3 <i>CO oxidation in the presence of H<sub>2</sub> and CO<sub>2</sub></i> .....	75
2.5.4 <i>CO oxidation in the presence of H<sub>2</sub>, CO<sub>2</sub> and steam</i> .....	78
2.5.5 <i>Comparison with literature values</i> .....	80
2.5.6 <i>H<sub>2</sub> oxidation</i> .....	80
<b>3 EXPERIMENTAL PART .....</b>	<b>83</b>
3.1 SYNTHESIS OF CATALYSTS .....	83
3.1.1 <i>Gold catalysts</i> .....	83
3.1.2 <i>Zeolite catalysts</i> .....	85
3.1.3 <i>Other noble metal catalysts</i> .....	87
3.2 TEMPERATURE PROGRAMMED REDUCTION ANALYSIS .....	89
3.3 EXPERIMENTAL SETUP .....	90
3.3.1 <i>Microreactor as integral reactor</i> .....	90
3.3.2 <i>Determination of the residence time distribution</i> .....	95
3.3.3 <i>Valve actuator</i> .....	96
3.3.4 <i>TCOD IR-Sensor</i> .....	96
3.3.5 <i>Pump</i> .....	96
3.3.6 <i>Gas chromatograph</i> .....	97
3.3.7 <i>Microreactor as recycle reactor</i> .....	97
3.4 CALCULATIONS .....	100
3.4.1 <i>Material balance of a CSTR</i> .....	100
3.4.2 <i>CO conversion and selectivity</i> .....	100
3.4.3 <i>Mechanism of preferential oxidation reaction</i> .....	101
3.4.4 <i>Akaike's Information Criterion (AIC)</i> .....	102
3.4.5 <i>Arrhenius equation</i> .....	102
<b>4 SUMMARY AND PERSPECTIVES .....</b>	<b>104</b>
<b>5 REFERENCES.....</b>	<b>108</b>
<b>6 APPENDIX.....</b>	<b>125</b>
6.1 NOMENCLATURE .....	125

---

## 1.1 Motivation

Air pollution and continuous global warming are serious environmental problems, which can cause the change of climate and damage to the environment. Pollutants, such as carbon monoxide, hydrocarbons, sulphur dioxide and certain nitrogen oxides, are of importance because they influence the formation of smog. In the urban areas, the transportation sector is one of the main contributors to air pollution. For example, in Athens, Los Angeles and Mexico City almost 100% of carbon monoxide emissions come from road vehicles, whereas nitrogen oxides emissions caused by road transport range between 75% and 85% of total emissions [1].

Carbon dioxide is considered to be the main contributor to the greenhouse effect. It is reported that during each of the first eight months of 1998 new record values of global temperature were recorded [2]. Each litre of gasoline combusted in an automobile produces 7.5 kg of carbon dioxide. The transportation sector is responsible for one-third of total carbon dioxide emissions.

Efforts to minimize the environmental damage of rapidly growing automobile industries are focused on end-of-pipe technologies such as catalytic converters and particle traps and recently on producing cleaner gasoline. This strategy has shown a significant decrease of the emissions of the latest produced cars being on the road, but the strategy has its limitations. In order to provide ultra low or zero emission vehicles, the application of fuel cell technology is one of the most prominent solutions. Hydrogen is used as fuel to power the fuel cell. The generation of electricity by a chemical process, combining hydrogen and oxygen to form water, produces no emissions at all. Other advantages of using hydrogen in a fuel cell in

---

---

comparison to the conventional internal combustion engine are higher energy efficiency, lower noise, no formation of soot particles, which can impact the human health. The most promising type of fuel cell for application in the automobile is the low temperature proton exchange membrane (PEM) fuel cell. The prototypes of such passenger cars have been successfully demonstrated by numerous automotive companies [3].

---

## 1.2 Fuel cell

Fuel cells are electrochemical devices in which the energy of fuel and oxidant, continuously supplied to electrodes, is directly converted into electricity, without the intervention of the low efficiency combustion process. There are five different types of fuel cells (alkaline, molten carbonate, phosphoric acid, proton exchange membrane and solid oxide fuel cells). They are differentiated by the type of fuel used, operating conditions (temperatures and pressures) and area of application. A fuel cell combines the fuel with oxygen from the air to electrochemically produce electricity, heat and water. Fuel cell technology has a number of advantages [4]:

- Relatively high efficiency more than 40% (stand alone) to 80% (hybrid) at this moment.
- Substantial heat may be recovered and used for thermal and cooling applications.
- Flexible size.

The choice of any fuel and oxidant for fuel cells depends on their electrochemical activity, cost of fuel and oxidant delivery and removal of reaction by-products. Polymer electrolyte fuel cells (PEFCs) have received significant attention because of their characteristics, essential for transportation applications. They are light in weight, small in size and have high power density at a relatively low operating temperature around 80 °C [4]. PEM fuel cells operating with hydrogen are favored by the major part of automotive industry. PEM fuel cells use a thin, proton-conducting polymer membrane as an electrolyte. Both sides of the membrane are coated with a layer of catalyst material.

In a PEM fuel cell, protons are formed from hydrogen at the catalyst layer, permeate the membrane and react with oxygen at the cathode producing electrical current. A catalyst at the cathode stimulates the formation of water from protons and oxygen (Figure 1).

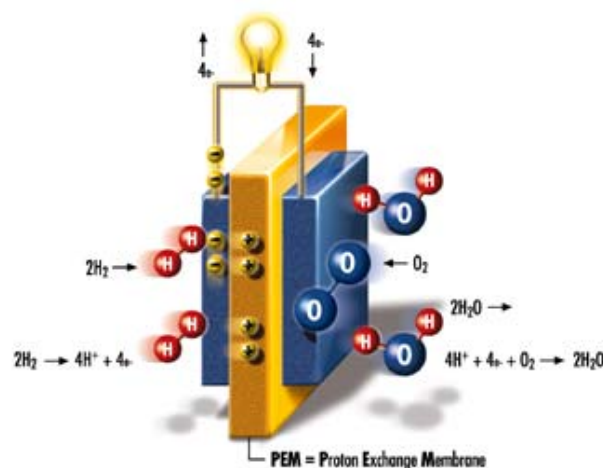


**Figure 1:** Proton exchange membrane.

Individual fuel cells summarized into a unit and connected with each other in series, result in a “stack” of cells (Figure 2).

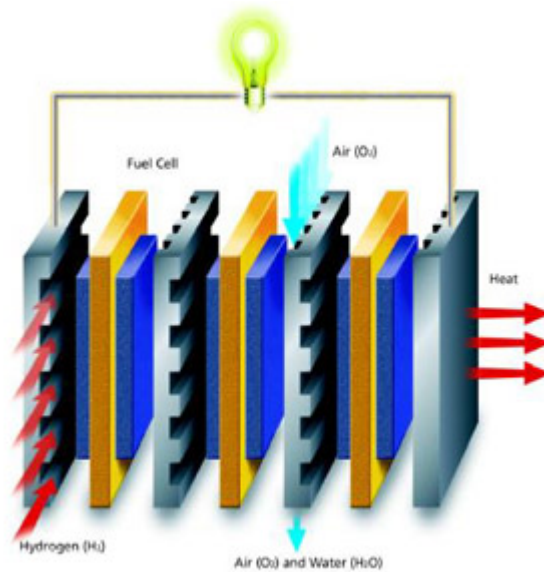


**Figure 2:** *Stack of fuel cell.*

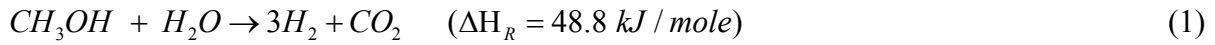
The stack output voltage and power can be varied as desired by adjusting the number of individual cells.

The on-board supply of hydrogen for fuel cell vehicles can generally be divided into three groups:

- Storage of high pressure hydrogen and liquid hydrogen.
- Using of metal-hydride as hydrogen-storage medium.
- Reforming of hydrocarbons and alcohols, such as methanol, ethanol, gasoline, diesel etc.

The lack of hydrogen refueling infrastructure, combined with the complexity of on-board storage and handling of hydrogen, are the drawbacks of applying pure hydrogen on-board. Furthermore, the weight and the volume of the hydrogen tank on-board exceed the size of a gasoline or diesel tank by far, which is an issue owing to the space limitations in automobiles. On top of that, increasing weight increases fuel consumption. The alternative to liquid hydrogen or high pressure hydrogen storage on-board is to carry liquid fuels that have higher energy density. However, they require conversion to a hydrogen-rich gas (reformate) via an on-board fuel cell processor [5].

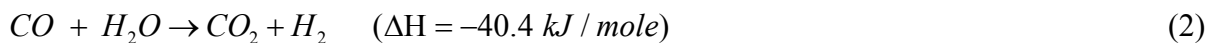
In the first stage, the hydrocarbon fuel is converted (reformed) to a hydrogen-rich gas ( $H_2 + CO + CO_2$ ) with carbon monoxide content of about 1 – 2 Vol.% in case of methanol, and up to 15 Vol.% in case of hydrocarbons. The steam reforming (e.g. of methanol) can be considered as a reverse reaction of methanol synthesis:



Steam reforming of methanol is considered to be the most favorable process of hydrogen production in comparison to the decomposition and partial oxidation of methanol [5]. This is because of the ability to produce gas with high hydrogen concentration (~75 Vol.%) and high selectivity for carbon dioxide. Steam reforming is an endothermic reaction. The energy required for the reaction can be supplied from a catalytic burner device [5].

In order to use hydrocarbon fuels in PEM fuel cell systems, the fuel must first be converted into a hydrogen-rich gas containing little or no carbon monoxide [6]. The most efficient fuel-cell anodes are based on precious metals [7]. However, precious metals are sensitive to deactivation by carbon monoxide adsorption at low temperatures [7]. Above 10 – 100 ppm carbon monoxide poisons the PEM electro-catalyst used in fuel cells severely and irreversibly [1 – 10].

The carbon monoxide clean-up system is regarded to be the most complicated part of the fuel processor. The first stage of the clean-up system is the water gas shift (WGS) reaction, which converts carbon monoxide to carbon dioxide, while increasing the hydrogen content.



In the WGS stage, the carbon monoxide content in the gas is reduced to below 1 Vol.%. The final carbon monoxide clean-up stage, in order to reduce the carbon monoxide content below 100 ppm, involves either preferential oxidation of carbon monoxide to carbon dioxide by addition of air, catalytic methanation or separation of hydrogen by hydrogen permeable membranes [11]. One obvious route is to diffuse hydrogen through a Pd/Ag membrane [12]. However, this requires high-pressure differential and fairly high temperatures. Palladium is also expensive. Carbon monoxide could be methanated, but this consumes 3 molecules of hydrogen per molecule of carbon monoxide and results in the emissions of methane. Additionally carbon dioxide methanation takes place in parallel over unselective catalysts. As a result, most researchers focused on preferential oxidation of carbon monoxide, which has to be achieved in the presence of carbon dioxide with minimum hydrogen oxidation.

### 1.2.1 Microreactors

In the overall design of catalytic processes, such as fuel processing, the choice of the catalyst and its operating conditions is the critical step, which defines system costs against the cost of product recovery and by-product treatment. Candidates for the individual reaction need to be identified by primary screening. For secondary screening of heterogeneous catalysts, two

---

types of reactor concepts exist. i) multi-tubular fixed bed reactor modules and ii) microreactors arrays, in which catalyst coatings are screened frequently [13].

A major issue of secondary gas phase screening reactors is their operation at constant conditions. When the reactor is constructed of materials with a low thermal conductivity, temperature differences of about 5 °C are reported already in the absence of any catalytic reaction. Even higher gradients are expected in the presence of the catalytic reaction, especially when the reactions are significantly exothermic or endothermic. Most of the reactors, apart from ceramic and quartz construction, have a maximum operating temperature around 550 °C, while numerous catalytic applications require higher temperature. Furthermore, these devices are often made from materials with a relatively low thermal conductivity and thus cannot be applied to study the catalyst performance in reactions with strong thermal effects [13].

Microstructured reactors, also called microreactors, are miniaturized reaction systems that are, at least partially, produced using methods of microtechnology or precision engineering [14 and 15]. Typically, microreactors contain fluid channels with a diameter between 10 and 1000  $\mu\text{m}$ , (see Figure 3), which results in a relatively large surface area-to-volume ratio and increased driving forces for heat and mass transport [14 – 19]. One of the first microstructured devices was reported in literature in 1989 [20]. Microreactor engineering has been recognized as a new discipline since the first workshop on Microsystems Technology for Chemical and Biological Microreactors, held in Germany in 1995 [21]. Since then, many research groups have entered the field. Several reviews of the field have already appeared in books and scientific papers [19, 22 – 27].

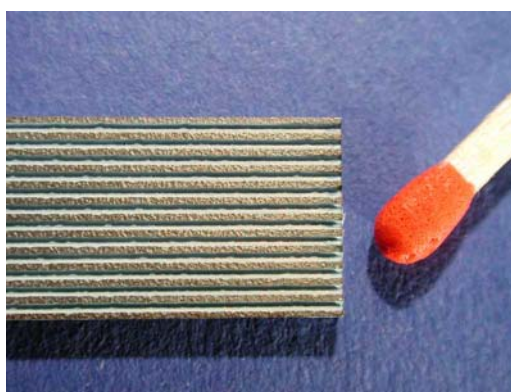


**Figure 3:** Example of a microstructured plate carrying 12 microchannels.

The rate of reactions which are limited by heat or mass transfer in a conventional reactor can be increased by performing them in a microreactor, leading to process intensification. Furthermore, the nonuniformities of temperature, in the case of fast, highly exothermic

---

reactions [23] or concentration when the reactants have to be mixed in the reactor [28], is avoided in a microreactor. This results in improved selectivity and yields. The isothermal conditions also make microreactors well suited for the determination of reaction kinetics [29].

Microchannels also occupy a small volume. When they are used as measurement or analysis devices, decreased space, material, energy consumption, in combination with fast heat and mass transfer and shorter analysis time are some of their characteristic features [30]. These features created large interest in microreactors for high throughput experimentation [31]. The small inventory also makes microreactors safer for handling dangerous chemicals [32]. Hazardous reactions may be performed in the explosive regime leading to increased selectivity and yield and substantially less consumption of diluents.

Another property of microreactors is their modular nature. Scaling-up processes by using a large number of small units or simply by increasing the number and length of channels in a larger device, reveals flow conditions identical to those used in the laboratory and avoids the uncertainties involved in the design of a new process. In case of pharmaceutical products, this might avoid a time-consuming new licensing procedure, which can significantly shorten the time-to-market of a new product [33]. Furthermore, the modular nature of microreactors also facilitates distributed production, where (possibly dangerous) chemicals are produced on-site, avoiding transportation risks and costs.

The short residence time (milliseconds to seconds range) makes microreactors less suitable for slow reactions that require a residence time of minutes or even h [34]. Furthermore, microreactors are more sensitive to corrosion and erosion [21] and require very clean fluids to be used in order to avoid blockage of the microchannels.

Microreactors also differ from conventional reactors in a number of ways, which are of importance for the development of mathematical reactor models [14]. Reactor modelling is an important aspect of chemical engineering, since it is the basis for the design and optimisation of chemical process equipment. Since the flow in microreactors is often laminar, the accuracy of microreactor models can be higher than of conventional reactors, which makes the design of microreactors potentially more reliable. The main differences between microreactors and macro-scale equipment are:

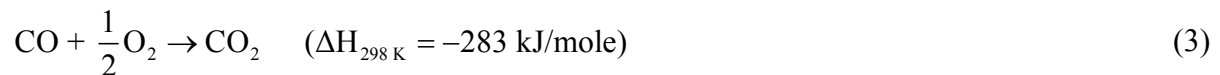
1. The flow in microstructures is in most cases laminar, whereas the flow in macro-scale equipment is usually turbulent.
  2. Heat and mass transfer across boundaries is very fast in microreactors, while it is often a limiting factor in conventional reactors [34].
-

3. The volume fraction of solid wall material is much higher in microreactors than in macroscopic equipment, which makes solid heat conduction an important factor in the first, while it can usually be neglected in conventional reactors [35].
4. The large surface area-to-volume ratio of the microstructures results in an increased importance of surface effects over volumetric effects [36].

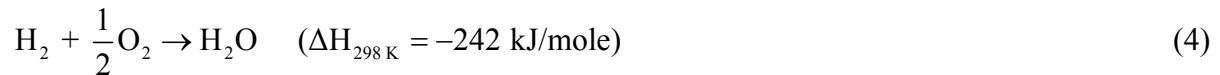
### 1.2.2 CO oxidation in H<sub>2</sub>-rich gas streams

The polymer electrolyte membrane fuel cell, as mentioned above, operating with hydrogen, seems to be the most promising fuel-cell technology for transport applications [37 and 38]. It operates at relatively low temperatures (80 – 120 °C).

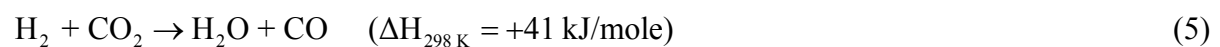
The removal of low concentrations of carbon monoxide from the pre-cleaned reformat of hydrocarbon and ethanol reformers is commonly performed by oxidation with air. Owing to the lower carbon monoxide concentration achieved by the low temperatures of methanol reforming, in this case the reformat goes directly to the preferential carbon monoxide oxidation (PrOx) [24]:



The reaction is accompanied by the undesired side reaction of part of the hydrogen present in the reaction mixture:



Another problem that occurs in preferential oxidation reactors at low load levels is the reproduction of carbon monoxide at the catalyst by the reverse water gas shift reaction:



Generally, the corresponding catalysts tend to have a narrow operation window and heat removal and temperature management of the reaction are crucial [24].

The oxidation of carbon monoxide is an important reaction in emission control, particularly in the cleanup of vehicle emissions [39]. Supported noble metal catalysts are typically used to promote the reaction. The precious metals used are efficient, but full conversion is only achieved at temperatures around 150 °C [40 and 41]. This is true for most conventional catalysts, which are not active at low temperatures and low O/CO ratios because oxygen and carbon monoxide competes for the same sites. Under these conditions, carbon monoxide adsorption dominates the metal surface and prevents oxygen adsorption and surface reaction. On the other hand, oxygen is adsorbed too strongly to be displaced by carbon monoxide over

---

base-metal oxide catalysts at low temperatures. Thus, an efficient low-temperature carbon monoxide oxidation catalyst should accommodate both carbon monoxide chemisorption and the simultaneous dissociative adsorption of oxygen. This suggests the use of composite materials with different components, each having activity for one or the other of these functions [41]. Noble metal reducible oxide combinations, base metal oxides and perovskite-type catalysts have been tested for their carbon monoxide oxidation performance at low temperatures [42 – 44].

If the low-temperature oxidation involves reaction between carbon monoxide adsorbed on one component and oxygen species adsorbed on or originating from a second component, then the interface between the components will be critical. As a result, preparation techniques are crucial for the performance of active catalysts.

For preferential oxidation, three possibilities can be considered. i) It may be possible to find a catalyst that adsorbs carbon monoxide but not hydrogen, and hence favors selective oxidation of carbon monoxide. ii) To operate at a temperature where carbon monoxide is oxidized and hydrogen is not. iii) To find a catalyst where both carbon monoxide and hydrogen are oxidized, but kinetic parameters lead to preferential carbon monoxide oxidation and only minor losses of hydrogen.

In all cases, it is critical to carefully control the O/CO ratio in the preferential oxidation of carbon monoxide as it is an important parameter governing the power generation efficiency of the PEFC system. Moreover, when large amounts of air are added into the reactor, temperature control becomes difficult owing to the heat of reactions. It may be required to use more than one reactor (multi-stage), or integrate a temperature control unit (heat exchanger design). In multi-stage reactors, the addition of air can be reduced by optimizing air feed at each stage. Temperature control at each stage becomes easier, because there is less heat formed at each stage. However, complex hardware is required to control temperatures and oxidant injection along the multi-stage reactors. Hence, the single-stage carbon monoxide removal process is preferable for smaller-scale systems [45].

For most catalysts, carbon monoxide conversion increases with increasing oxygen addition (the stoichiometric ratio being 0.5) within a certain temperature range. This in turn also increases hydrogen losses by unselective oxidation [22].

There are various reports, which specifically report the conversion of carbon monoxide to ppm concentrations levels [22, 46 – 53] and several studies on preferential oxidation of carbon monoxide in compact or microstructured reactors [15, 22, 23, 24, 34, 46, 54 – 56].

---

### 1.3 Noble metal catalysts for preferential oxidation of CO

Possible noble metal catalysts for preferential carbon monoxide oxidation in hydrogen-rich gases are alumina supported platinum, ruthenium, rhodium and palladium catalysts, operating in the range between 120 °C and 160 °C. The catalyst support has the function to enlarge the surface area of the active component and also to provide a catalyst stable under reaction conditions against sintering of the metal particles.

Platinum catalysts have been studied most extensively for preferential oxidation of carbon monoxide. In a hydrogen-rich mixture, containing ~1 Vol.% CO, the carbon monoxide was completely oxidized over alumina-supported platinum catalyst by a four fold stoichiometric excess of oxygen, corresponding to a process selectivity of ~25% [50]. The temperature dependence of the carbon monoxide consumption rate and the carbon monoxide oxidation selectivity in hydrogen-rich gases were investigated for Al<sub>2</sub>O<sub>3</sub> supported platinum catalysts [42, 50, 57 – 59] and zeolite supported platinum [9, 60 and 61].

Other noble metal catalysts, such as Ru/Al<sub>2</sub>O<sub>3</sub> and CuO-CeO<sub>2</sub>, have been also investigated [62 – 64]. The catalytic activities of a wide variety of materials (880 catalysts) have been evaluated by high throughput technologies with the help of emissivity corrected infrared thermography [65 and 66]. After development of several generations of catalysts the mixed oxide Al<sub>1</sub>Mn<sub>7</sub>Co<sub>92</sub> was discovered as catalyst for highly selective carbon monoxide oxidation in hydrogen (100 % selectivity at temperatures between 60 °C and 100 °C and feed gas 1.2 Vol.% CO, 1 Vol.% O<sub>2</sub> in H<sub>2</sub>) [67]. Despite its high activity and selectivity the mixed oxide catalyst deactivated rapidly in the presence of moisture. Doping studies led to a moisture stable variation, the Pt<sub>0.5</sub>Al<sub>1</sub>Mn<sub>7</sub>Co<sub>91.5</sub> mixed oxide, which was not as selective as the platinum-free material, but stable against high loading of carbon dioxide and water in the feed gas.

#### 1.3.1 Gold based catalysts

Coprecipitated catalysts containing small (~10 nm) gold particles and NiO,  $\alpha$ -Fe<sub>2</sub>O<sub>3</sub> and Co<sub>3</sub>O<sub>4</sub> have been tested [68]. These catalysts were highly active for both carbon monoxide and hydrogen oxidation, possibly due to the combined effect of gold and oxides. The oxidation of carbon monoxide on Au/NiO and Au/Co<sub>3</sub>O<sub>4</sub> was found to be complete at 30 °C, even in the presence of 76% relative humidity. In contrast, 50 Vol.% of the hydrogen was oxidized only at 73 °C and 66 °C, respectively.

The general trend observed was that catalytic activity increased with decreasing gold

---

crystallite size in the oxidation of both hydrogen and carbon monoxide. It is interesting that the catalytic activity of coprecipitated Au/ $\gamma$ -Al<sub>2</sub>O<sub>3</sub> was comparable to those of Au/NiO, Au/ $\alpha$ -Fe<sub>2</sub>O<sub>3</sub> and Au/Co<sub>3</sub>O<sub>4</sub>, with similar gold particle sizes, for hydrogen oxidation. However, it was remarkably lower for carbon monoxide oxidation. The activity for hydrogen oxidation depended strongly on the gold particle size exposed, while the choice of support oxide also played a role in carbon monoxide oxidation through either a metal-support interaction or via a bifunctional mechanism. In this mechanism, gold and the support oxide activate different steps of the carbon monoxide oxidation. Hydrogen is assumed not to chemisorb on gold, whereas carbon monoxide chemisorbs weakly on the metal. Thus, the catalytic activity for carbon monoxide oxidation may be a result of the interaction of species adsorbed on the metal and the support. Alternatively, the interaction of gold with the reducible oxide support may change the surface properties of gold particles so that they favor carbon monoxide adsorption. It was reported that at pretreatment temperatures  $\geq 300$  °C, the decomposition of oxidic gold species to metallic gold and formation of crystalline hematite ( $\alpha$ -Fe<sub>2</sub>O<sub>3</sub>) occur to yield hemispherical gold particles of about 4 nm diameter stabilized by epitaxial contact over  $\alpha$ -Fe<sub>2</sub>O<sub>3</sub> [68 – 70].

Various transition metal oxide supports were screened and coprecipitated. Au/MnO<sub>x</sub> was chosen as one of the best catalysts for carbon monoxide removal from hydrogen-rich gases. Because gold catalysts require an oxidative pretreatment, the stability of Au/MnO<sub>x</sub> in a hydrogen-atmosphere was tested. Carbon monoxide oxidation reached 100% conversion at temperatures below 0 °C, whereas hydrogen oxidation occurred only at temperatures above 0 °C [68]. This temperature difference was found to be closely related to the gold content and the Au/Mn atomic ratio in the catalyst. Larger temperature differences obtained at Au/Mn ratios above 1/20. In a feed containing 1 Vol.% CO and 1 Vol.% O<sub>2</sub> in H<sub>2</sub>, an Au/MnO<sub>x</sub> catalyst with Au/Mn = 1/50 selectively oxidized carbon monoxide to give 50% conversion at 16 °C [7]. Conversion above 95% was obtained between 50 °C and 80 °C. Catalyst activity was stable for 2 days and even improved with time-on-stream. At 120 °C, carbon monoxide conversion started to decline, implying that oxygen was competitively consumed by hydrogen oxidation [7].

The preferential oxidation of carbon monoxide in hydrogen-rich gas streams was investigated over a number of Au/ $\gamma$ -Al<sub>2</sub>O<sub>3</sub> catalysts prepared by the deposition-precipitation method [71]. The major finding of this study was, that the oxidation of carbon monoxide at low concentration in a hydrogen-rich gas mixture (H<sub>2</sub>/CO/O<sub>2</sub>/He = 48/1/0.5/50.5) can be achieved with 50% selectivity at 100 °C over Au/ $\gamma$ -Al<sub>2</sub>O<sub>3</sub>. Both activity and selectivity depended on

---

the gold crystallite size, with an optimum particle size below 5 nm, which was in good agreement with results reported for low-temperature carbon monoxide oxidation on gold catalysts in the absence or presence of hydrogen [68, 71 – 74]. The increase in activity with decreasing gold particle size was explained by increasing oxygen activation at the Au-Al<sub>2</sub>O<sub>3</sub> interface as proposed [68] and by the differences in the rates and strengths of adsorption of hydrogen and carbon monoxide on gold particles [7].

The preferential oxidation of carbon monoxide in a fixed bed reactor was investigated over Au/ $\alpha$ -Fe<sub>2</sub>O<sub>3</sub>, using simulated reformat (75 Vol.% H<sub>2</sub>, 1.5% Vol. CO and N<sub>2</sub> in balance) at atmospheric pressure with various O/CO ratios [75]. The  $\alpha$ -Fe<sub>2</sub>O<sub>3</sub> was selected because of the low T<sub>1/2</sub> value (the temperature at which 50% conversion occurs) of Au/ $\alpha$ -Fe<sub>2</sub>O<sub>3</sub> for low temperature carbon monoxide oxidation [69]. A strong initial deactivation of 30% was observed in the first 2 h time-on-stream, which slowed down during the next 8 h and finally reached a steady state. Another group reported similar deactivation behavior for Au/TiO<sub>2</sub> catalysts [69].

When compared with the commonly used Pt/ $\gamma$ -Al<sub>2</sub>O<sub>3</sub> catalyst, which has an optimum temperature window of 180 – 200 °C [50], over the Au/Fe<sub>2</sub>O<sub>3</sub> catalyst comparable activity was achieved at much lower temperature of 80 °C. However, the question remains, how much carbon dioxide existing in reformat can be tolerated by the catalyst. Other open questions are the effect of different gold-precursors on catalyst performance and generally the performance of gold based catalysts inside a microreactor.

### *1.3.2 Zeolite based catalysts*

Zeolites, synonymously called molecular sieves, are crystalline microporous alumina-silicates containing cavities and channels of molecular dimensions, 3 – 10 Å. Few fields of chemistry offer such chemical and structural diversity, although only about 60 different structures or topologies are known, tens of thousands of theoretical structures are possible. Many of the known structures have high thermal and chemical stability, making them useful materials in a wide range of important industrial processes, such as catalysis, separations, purifications and ion exchange [76].

The following six properties make them attractive as heterogeneous catalysts:

- Well-defined crystalline structure.
  - High internal surface area.
  - Uniform pores with one or more discrete sizes.
  - Good thermal stability.
-

- Ability to sorb and concentrate gases.
- Highly acidic sites when ion exchanged with protons.

The primary building unit of the zeolite structure is a tetrahedron of four oxygen atoms surrounding a central silicon atom ( $\text{SiO}_4$ )<sup>-4</sup>. These are connected through their corners of shared oxygen atoms to form a wide range of small secondary building units. These are interconnected to form a wide range of polyhedrons, which in turn connect to form the infinitely extended frameworks of the various specific zeolite crystal structures. Individual structures may comprise only the basic unit or many of them. The record is held by the mineral paulingite which contains five such polyhedrons [77].

Zeolites can be categorized into two groups, namely natural zeolites and synthetic zeolites. The first ones occur in nature in vugs and vesicles of basaltic lava (in such areas as Hawaii, Iceland and Nova Scotia) in specific kinds of rocks subjected to moderate geologic temperature and pressure (the metamorphic zeolite facies) and in altered and reacted volcanic ash deposits. Only the last are of economic importance, in the sense of ready availability in large tonnages at moderate cost in many areas of the world [77].

Synthetic zeolites are high-purity specialty chemicals that serve a wide range of applications. Most synthetic zeolites are thermodynamically meta-stable products formed kinetically under special synthesis conditions. Therefore, they are prepared not only under closely controlled conditions of temperature, pressure and time but with specific reactants and physical reaction environments. These restrictions on their production make their reproducibility an issue [77]. Typically, many zeolite syntheses yield two or more crystalline phases with unreacted gel components. Much development work is, therefore, aimed at the process and compositional control needed to produce a reaction window, where a single-phase fully-crystallized product may be isolated [77].

Framework composition control can be achieved either by manipulation of the original synthesis variables or by one of a series of “secondary synthesis” methods, which in effect are specific chemical reactions involving the framework atoms. Some zeolite framework Si/Al compositions can be varied within a restricted range by changing the compositions of the original reactions gels (some can be made only at a very specific composition). The Si/Al ratio can be manipulated by changing the input stoichiometries.

Figure 4, 5 and 6 show the frameworks of zeolite-Y, ZSM-5 and mordenite.

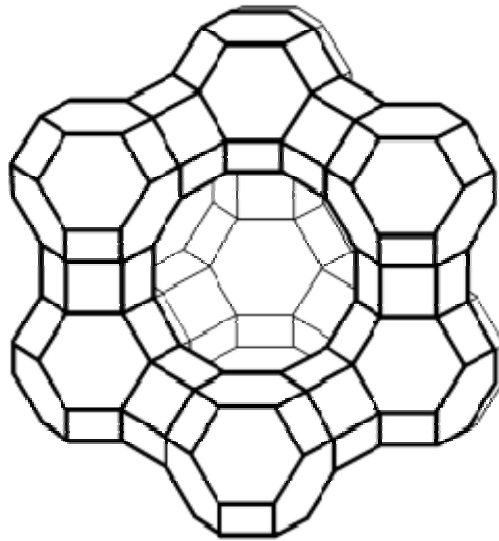


**Figure 4:** Framework structure of zeolite-Y [78].

Zeolite-Y has a 3-dimensional pore structure with pores running perpendicular to each other in the x, y, and z planes and is made of secondary building units. The pore diameter is large at 7.4 Å since the aperture is defined by a 12 member oxygen ring, and leads into a larger cavity of diameter 12 Å. The cavity is surrounded by ten sodalite cages (truncated octahedra) connected on their hexagonal faces. The unit cell is cubic ( $a = 24.7$  Å). Zeolite-Y has a void volume fraction of 0.48, at a Si/Al ratio of 2.43. It thermally decomposes at 793 °C [79].

The most important application of zeolite-Y is as cracking catalyst. It is used in acidic form in petroleum refinery catalytic cracking units to increase the yield of gasoline and diesel fuel from crude oil feedstock by cracking heavy paraffins into gasoline grade naphthas. Zeolite-Y has superseded zeolite X in this use because it is more active and more stable at high temperatures due to the higher Si/Al ratio. It is also used in the hydro-cracking units as a platinum/palladium support to increase the aromatic content of reformulated refinery products.

Zeolite-Y is synthesized in a gelling process. Sources of alumina (sodium aluminate) and silica (sodium silicate) are mixed in alkaline (sodium hydroxide) aqueous solution to give a gel. The gel is then usually heated to 70 – 300 °C to crystallize the zeolite. The zeolite is present in  $\text{Na}^+$  form and must be converted to the acid form. To prevent disintegration of the structure by acid attack, sodium is first ion-exchanged with the  $\text{NH}_4^+$ . Then the acidic form is generated by thermal decomposition of  $\text{NH}_4^+$  to  $\text{H}^+$  and  $\text{NH}_3$ . If a hydrogenation metal such as platinum is required, it may be deposited via impregnation or ion exchange [80].

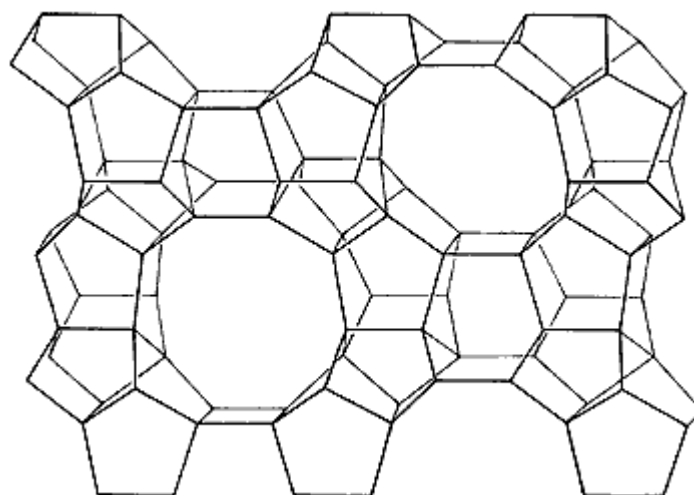


**Figure 5:** Framework structure of ZSM-5 [78].

Another wide-used zeolite catalyst, developed by Mobil Oil, is ZSM-5. This zeolite is an alumina-silicate zeolite with a high Si and low Al content (the ratio Si to Al is denoted with a number attached to the name, e.g.: ZSM-5/100). ZSM-5 is a highly porous material and throughout its structure it has an intersecting two-dimensional pore structure. ZSM-5 has two types of pores, both formed by 10-membered oxygen rings. The first type of pores is straight and elliptical in cross section. The second type of pores intersects the straight pores at right angles, in a zig-zag pattern. The latter pores are circular in cross section [76]. The Al-sites are very acidic. The substitution of  $\text{Al}^{3+}$  in place of the tetrahedral  $\text{Si}^{4+}$  requires the presence of an additional positive charge. When this is  $\text{H}^+$ , the acidity of the zeolite is very high, even though the density of acid sites is rather low owing to the high Si/Al ratio. The reaction and catalysis chemistry of the ZSM-5 is due to this acidity. The ZSM-5 zeolite catalyst is used in the petroleum industry for hydrocarbon interconversion [80].

Mordenite was the third zeolite selected as a catalyst for the preferential oxidation of carbon monoxide. Mordenite is one of the rarer to find members of the zeolite group of minerals. Its pore diameter is near  $7.5 \text{ \AA}$ . It has an orthorhombic crystal structure with straight 12-membered ring channels ( $6.5 \times 7.0 \text{ \AA}$ ) and crossed 8-membered ring channels ( $2.8 \times 5.7 \text{ \AA}$ ). Mordenite has a void volume of  $2827.26 \text{ \AA}^3$  (calculated from unit cell), with a Si/Al ratio in the range of 10 – 200 [78 and 81].

Higher silica-alumina ratio (20 to 60) mordenites are used for the fractionation of the aromatic components of petroleum. Separation of alkylbenzenes, alkyltoluenes and some alkylxylenes from petroleum, are some of these uses [80].

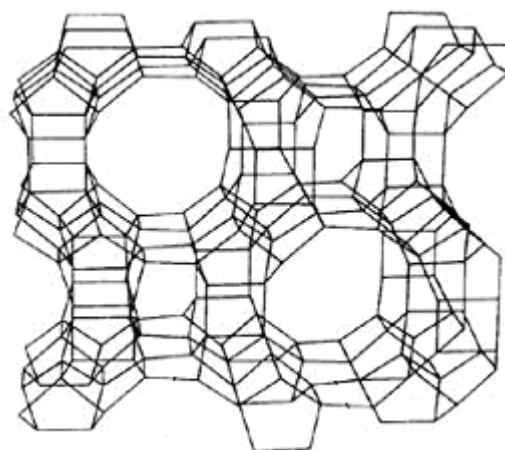


**Figure 6:** *Framework structure of mordenite [78].*

Because these are usually major components of petroleum, their removal facilitates the study of less abundant components. Also the purification of the diaromatic and triaromatic fractions of petroleum by mordenites has led to some novel separations of alkylnaphthalene and alkylphenanthrene isomers and has enabled some of these compounds to be studied for the first time [80].

---

## 1.4 Methods of catalysts characterization

### 1.4.1 Brunauer–Emmett–Teller analysis

The Brunauer–Emmett–Teller (BET) analysis is a well-known rule for the physical adsorption of gas molecules on a solid surface. BET method is used to determine the surface area of the catalysts by nitrogen adsorption/desorption at  $-196\text{ }^{\circ}\text{C}$ . In this method, the adsorption isotherm of a sample of known weight is measured (e.g. the amount of adsorbed gas as a function of pressure at constant temperature). In practice, it offers advantages to plot the relative gas pressure (e.g. the pressure as a function of the saturation pressure,  $P_0$ ) at the temperature of measurement. The Brunauer-Emmett-Teller equation gives surface-area values obtained from these curves.

On the basis of some simplified assumptions BET derives a formula from which the amount of gas ( $V_m$ ) required for covering the surface with a monomolecular layer can be calculated. If the surface area ( $A_m$ ) occupied by one adsorbed gas molecule is known, the total available surface area of the sample can be calculated and thus its specific surface area [82].

All the measurements were made at Institut für Mikrotechnik in Mainz by using a Sorptomatic 1990 (Carlo Erba Instruments).

### 1.4.2 Scanning electron microscopy

The particle morphology of the catalysts is observed by scanning electron microscopy (SEM) using a JEOL JSM -5410 LV scanning microscope operated at 15 kV, at the Institut für Mikrotechnik in Mainz.

Specifically, this analysis involves the evaluation of surface structure and morphology. Origin, distribution, morphology and chemical composition of clays and cements are some of the data which can be obtained. Analysis includes sample preparation, high-quality digital images at various magnifications and positions and image descriptions. A SEM may be equipped with an Energy Dispersive X-ray analysis (EDX) system to enable and to perform compositional analysis on specimen, as well as estimating the relative concentrations for selected components at the surface of the specimen [83].

During SEM inspection, a beam of electrons is focused on a spot volume of the specimen, resulting in the transfer of energy to the spot. These bombarding electrons, also referred to as primary electrons, dislodge electrons from the specimen itself. The dislodged electrons, also known as secondary electrons, are attracted and collected by a positively biased grid or

---

detector, and then translated into a signal.

To produce the SEM-image, the electron beam is swept across the inspected area, producing many such signals. These signals are then amplified, analyzed and translated into images of the topography. Finally, these images are shown on a cathode ray tube.

#### *1.4.3 Temperature programmed reduction*

Temperature programmed reduction (TPR) technique permits to find the most efficient reduction conditions. Furthermore, the supported precursor phases and their interactions with the support can be identified. These experiments are particularly useful in case of multi-metallic systems for the evaluation of the role of the added compounds or doping agents (alloy formations or promotion effects).

In the TPR technique an oxidized catalyst precursor is submitted to a programmed temperature rise, while a reducing gas mixture is flowing over it. The gas mixture consists usually of hydrogen diluted in some inert gas such as argon.

The reduction rates are continuously measured by monitoring the change in composition of the gas mixture downstream the reactor. The decrease in hydrogen concentration in the effluent gas with respect to the initial percentage monitors the reaction progress. An interesting application of this technique is that the TPR analysis may be used to obtain evidence for the interaction between the atoms of two metallic components in the case of bimetallic system or alloy, as already mentioned. The TPR method is also used for qualitative and quantitative analysis of a catalyst. In effect, the spectra produced are characteristic of a specific solid [84].

#### *1.4.4 X-Ray diffraction*

Powder X-ray diffraction (XRD) patterns are used to obtain information about the structure and composition of crystalline materials. The XRD device at the University of Zaragoza was a Rygaku/Max system with a CuK $\alpha$  anode and a fast photon detector.

XRD refers to the principal phase as identified by comparison of its X-ray diffraction pattern with those in literature.

When X-rays are fired at a crystalline sample placed in the X-ray camera, the sample is irradiated with monochromatic X-ray light. Proportions are diffracted by the regular crystal structure and the stray radiation is recorded. These diffracted X-rays produce a pattern of lighter and darker lines on a film (reflexes).

---

This involves the occurrence of interferences of the waves scattered at the successive planes, which are described by Bragg's equation:

$$n \cdot \lambda = 2 \cdot d \cdot \sin(\theta) \quad (6)$$

where  $\lambda$  is the wavelength,  $n = 1, 2, 3, \dots$ ,  $d$  is the lattice plane distance and  $\theta$  is half the diffraction angle. This relation is used for the structure analysis of crystals.

The pattern on the film depends on the composition of the sample and by reference to standard data, this pattern can be used as a kind of "fingerprint" to identify a wide variety of materials.

For comparison with diffraction patterns from the database, it is important to note that routine measurements are often performed with a slit that will expose more than the sample area at low angle. The observed intensities at low angle would therefore be too small compared with these reference patterns and calculated patterns.

In a zeolite laboratory, powder diffraction data are most commonly used to identify a newly synthesized material or to monitor the effects of a post-synthesis treatment. In both cases, the measured pattern is compared with an existing one, whether it is a pattern in the Collection of Simulated XRD Powder Patterns for Zeolites, or an in-house data file. Such comparisons are not trivial for zeolites, especially if the data collection or sample preparation conditions differ from one another [83].

The patterns are then scaled to the same absolute intensity. The diffraction patterns are presented in the as measured condition without any background subtraction or smoothing. Some samples contained elements that produce additional fluorescence such as Fe and Co. No filter or secondary monochromator has been used to remove this radiation.

#### *1.4.5 Transmission electron microscopy*

A light microscope is limited by the wavelength of light. Visible light has wavelengths of 400-700 nm, larger than many objects of interest. Instead, transmission electron microscopy (TEM) uses electrons as a "light source" and their much lower wavelength make it possible to get an improved resolution by a factor of 1000 compared to a light microscope. The wavelength is dependent on their energy and so can be tuned by adjustment of accelerating fields and can be much smaller than that of light. TEM is an imaging technique whereby a beam of electrons is transmitted through a specimen, then an image is formed, magnified and directed to appear either on a fluorescent screen or layer of photographic film.

With TEM-photos objects to the order of a few angstroms ( $10^{-10}$  m) can be seen. For example, study of small details in the cell or different materials down to near atomic levels is

---

---

possible. The possibility for high magnifications has made the TEM a valuable tool in many fields, catalysis-research include. It can provide information on the shape and the surface atomic structure of the metal nanoparticles on supported catalysts, internal structural defects and others.

TEM-images were attained at the University of Zaragoza using a JEOL 2000 FX2 operating at 200 kV [85].

#### *1.4.6 Gas chromatography*

Chromatography is a separation method that exploits the differences in partitioning behavior between a mobile phase and a stationary phase to separate the components of a mixture. Components of a mixture may be interacting with the stationary phase based on charge, relative solubility or adsorption.

Gas chromatography involves a sample (gas or vaporized liquid) injected onto the head of the chromatographic column. The sample is transported through the column by the flow of inert, gaseous mobile phase. Commonly used gases include nitrogen, helium, argon and carbon dioxide. The choice of carrier gas is often dependant upon the type of detector which is used and the components that are going to be identified. The column itself contains a liquid stationary phase which is adsorbed onto the surface of an inert solid.

For optimum column efficiency, the sample should not be too large and should be introduced onto the column as a “plug” of vapor. Slow injection of large samples causes signal broadening and loss of resolution. The most common injection method is where a micro-syringe is used to inject the sample through a rubber septum into a flash vaporizer port at the head of the column. The temperature of the sample port is usually about 50 °C higher than the boiling point of the least volatile component of the sample. Capillary columns, as applied in this work, require much less sample, typically around  $10^{-3}$   $\mu\text{L}$  [86].

---

---

## 1.5 Reactor characterization

As a first step to study the reaction kinetics, the determination of a reactor type, which will be implemented for such experiments, is necessary. Mainly, as a general mode of classification, reactors can be defined as integral or differential [87]. For kinetic measurements, the integral reactor (plug flow reactor) is problematic, as it exhibits a concentration gradient and the solution of its material balance demands integration. On the other hand, the conversion of a differential reactor (continuous stirred tank reactor) represents directly the reaction rate and permits the derivation of simple algebraic reactor model equations.

Nevertheless, the mixing in a continuous stirred tank reactor is often not ideal. The residence time distribution (RTD), also named exit age distribution,  $E(t)$ , indicates the time the fluid elements of a stream remain in the reactor.  $E(t)$  characterizes the non-ideal mixing in a reactor.

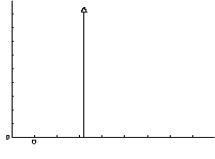
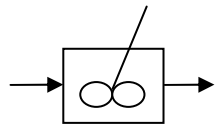
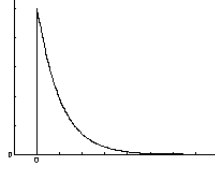
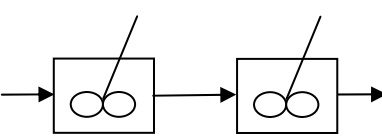
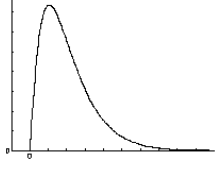
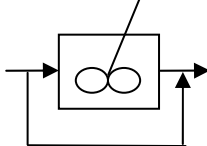
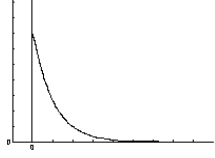
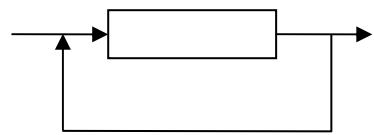
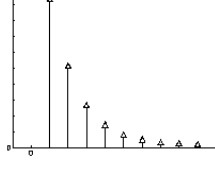
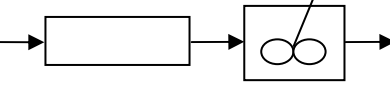
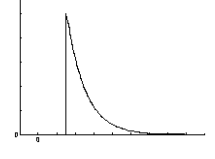
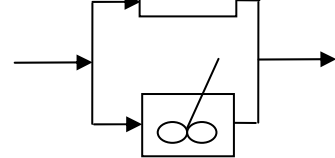
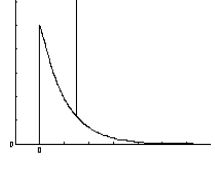
The residence time of individual molecules in the reactor, or more precisely, the distribution of residence times of the fluid can be determined directly by a widely used method of inquiry, the stimulus-response experiment [87 and 88].

Comparison of the measured RTD with that of an ideal reactor allows the identification of non-idealities of the reactor. An appropriate real model of the reactor in combination with kinetics of the reaction is then applied to model the overall reactor performance.

In Table 1, different models and their pulse responses are shown.

---

**Table 1:** Pulse response for various reactor-models [89].

<i>Description</i>	<i>Model</i>	<i>Pulse response</i>
1. Plug flow tank		
2. Ideal mixer		
3. Two ideal mixers connected in series		
4. Ideal mixer with bypass duct		
5. Plug flow tank with circulation		
6. Plug flow tank and ideal mixer connected in series		
7. Plug flow tank and ideal mixer connected in parallel		

---

## 1.6 Kinetic study

The study of reaction kinetics implies measurement of reaction rates under different conditions. In this work, the selected method for the kinetic study is based on the Irving Langmuir approach which is widely accepted for representing catalytic reactions involving the gas-solid phase [90 and 91].

For an appropriate description of the preferential oxidation of carbon monoxide over a precious metal surface (e.g. platinum) the Langmuir-Hinshelwood mechanism is applied [91 and 92]. The power-law form was found to be the most suitable reaction rate expression [50 and 59].

To approach the behaviour of the ideal continuous stirred tank reactor (CSTR) a recycle reactor is constructed. In such a reactor, reactants are continuously re-circulated by means of a pump, a small feed stream is continuously added and a small net-product stream continuously removed. High recycle rates (above 25) lead to perfect mixing similar to that obtained in a CSTR. All the kinetic experiments are then carried out at circulation rates higher than this value [93 and 94].

The reaction rate is measured under various experimental conditions (different feed concentrations of the reactants and temperatures of the reactor) and the effect of these variables is determined.

The study of kinetics requires the determination of reaction rates by estimating parameters using regression analysis and the comparison of the results obtained with those found from the material balance equation of a CSTR.

Estimating a set of parameters simultaneously from experimental data is always affected by numerical, model and experimental errors. Hence, the reliability and precision of the estimates and of the model has to be investigated by means of statistic methods.

---

---

## 1.7 Focus of the research

Polymer electrolyte membrane (PEM) fuel cells, utilizing platinum-catalyzed anodes, are susceptible to carbon monoxide contained in the hydrogen rich reformat product of the fuel processor. The growing interest in low temperature fuel cells has led to the need for research on preferential oxidation reaction catalysts that are capable of minimizing carbon monoxide concentration. Nevertheless, most studies on the preferential carbon monoxide oxidation have been conducted in model atmospheres (“idealized reformat”), consisting only of carbon monoxide, oxygen, hydrogen and an inert component (nitrogen or helium). Realistic methanol steam reformat, however, contains up to 20 Vol.% CO<sub>2</sub> and 10 – 20 Vol.% H<sub>2</sub>O. Aim of this work is to study the influence of these possible species on the preferential oxidation reaction over noble metal catalysts, in order to evaluate whether the high activity and selectivity observed in idealized reformat are also maintained under more realistic conditions.

Another novel aspect of this work is the fact that all the experiments for the kinetic study of the preferential oxidation reaction of carbon monoxide were performed applying catalyst coating in micro reactors. Micro reactors are miniaturized chemical reactions systems, which contain reaction channels with a typical diameter of 10 to 1000 µm. The small channel dimensions lead to a relatively large surface area-to-volume ratio and increased driving forces for heat and mass transport. Therefore, microreactors are especially suited for fast reactions with a large heat effect (exothermic or endothermic), where they allow for nearly isothermal conditions when a micro heat-exchanger is installed.

The influence of various operating parameters, such as pressure, temperature, feed composition and space velocity on the degree of CO-conversion was established by the experiments performed in a single test reactor and in a five fold screening reactor as well.

In **chapter 2** characterization of the catalysts synthesized and their performance are presented. A recycle reactor was constructed to study the kinetics of the reaction. Linear regression analysis was used to develop a kinetic model and to validate all the required parameters.

The **chapter 3** covers the catalyst synthesis protocol information. The chapter contains also catalyst characterization information and a detailed description of the experimental setups used. Additionally, mathematical relations used to determine residence time distribution and kinetics are described in this chapter.

**Chapter 4** reports conclusions and recommendations for future research.

---

## 2.1 Selection of catalysts

The scope of this work was first to develop and test new catalysts as washcoats in microchannels for the low-temperature preferential oxidation of carbon monoxide in a hydrogen-rich reformat stream.

The selection of both noble metal and supports was based on the active catalysts reported in literature for this reaction system. In most works, the effect of carbon dioxide on the activity of the catalyst has not been investigated in detail. However, in realistic reformat mixtures substantial amounts of carbon dioxide is contained, which was taken into account in the present work.

In Table 2 and in Table 3 a summary of the different zeolites and gold-catalysts prepared is presented respectively. As reference for the zeolite-catalysts, three ZSM-5/100 were used with platinum-contents of 0.5, 2.5 and 4.2 wt.%, prepared at the University of Zaragoza.

**Table 2:** *Zeolite-catalysts tested.*

<b>Zeolite</b>	<b>Platinum (wt. %)</b>	<b>Calcination (°C)</b>	<b>Activity</b>
Zeolite-Y	5	400	moderate
Zeolite-Y	5	300	low
ZSM-5/35	5	300	not active
ZSM-5/35	5	400	moderate
Mordenite	4	400	not active
Mordenite-Iron	3.5	400	moderate

**Table 3:** *Gold-catalysts tested.*

Meta oxide	initial pH	Calcination (°C)	Activity
Co <sub>3</sub> O <sub>4</sub>	7	600	not active
Co <sub>3</sub> O <sub>4</sub>	7	500	Very low
Co <sub>3</sub> O <sub>4</sub>	7	300	low
Co <sub>3</sub> O <sub>4</sub>	2	300	not active
Co <sub>3</sub> O <sub>4</sub>	11	300	not active
Fe <sub>2</sub> O <sub>3</sub>	7	300	moderate
TiO <sub>2</sub>	8	300	low
TiO <sub>2</sub>	8	500	not active
CeO <sub>2</sub>	7	300	low
CeO <sub>2</sub>	7	300	not active
CeO <sub>2</sub>	7	500	not active
NiO	7	300	Very low
Al <sub>2</sub> O <sub>3</sub>	7	300	not active
Al <sub>2</sub> O <sub>3</sub>	impregnation	300	low

Not only the choice of the support or the noble metal was important, but also preparation conditions influenced the overall activity of the catalysts. Therefore, several conditions were studied, such as the calcination temperature and pH at which the metal and gold were coprecipitated.

Additionally, two conventional catalysts were also examined for the preferential oxidation of carbon monoxide, namely Pt<sub>0.5</sub>Al<sub>1</sub>Mn<sub>7</sub>Co<sub>91.5</sub>O<sub>x</sub> synthesized by the group of Prof. W. F. Maier [66] and Pt-Rh/ $\gamma$ -Al<sub>2</sub>O<sub>3</sub> developed at the IMM [46].

## 2.2 Catalysts characterization

To characterize the catalysts synthesized in this work, different analysis methods were employed. More specifically, qualitative and quantitative analysis of a catalyst composition was performed by TPR, while XRD gave information about the structure and composition of the catalysts. Information about the surface structure and area was obtained by TEM-photos and BET-analysis respectively. Using SEM-photos the morphology of the washcoat was evaluated.

### 2.2.1 Gold and zeolite XRD-spectra

#### A. Au/Co<sub>3</sub>O<sub>4</sub>-catalyst

XRD-pattern shown in Figure 7 consists of eight reflections. Four typical peaks indicate the existence of Co<sub>3</sub>O<sub>4</sub>, with cubic structure [95], and four peaks testify the presence of gold. XRD-pattern of Au/Co<sub>3</sub>O<sub>4</sub> coprecipitated catalyst shows no strong peaks for gold. However, it has additional short and broad peaks at  $2\theta = 38.2^\circ$ ,  $44.4^\circ$ ,  $64.7^\circ$  and  $77.6^\circ$  [96].

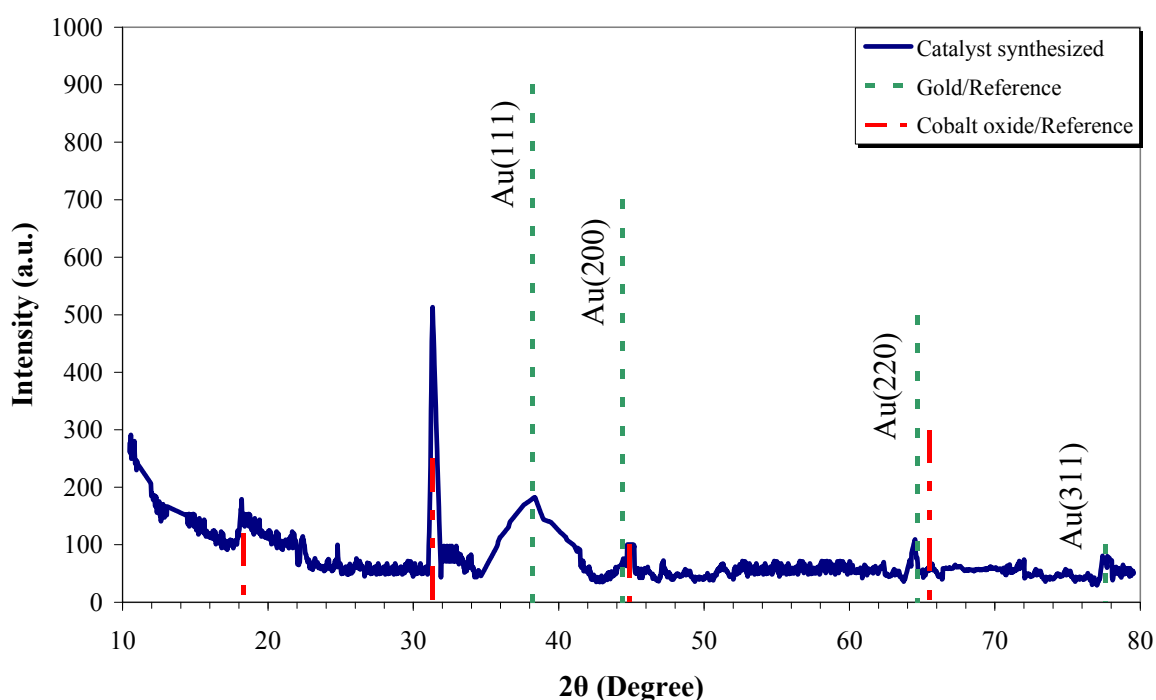


**Figure 7:** XRD-patterns of Au/Co<sub>3</sub>O<sub>4</sub> catalyst.

The peak at  $38.2^\circ$  corresponds theoretically to Au(111). A reactive gold particle must necessarily be small, since that is the only way of assuring a large enough concentration of

those active sites [97 and 98]. The XRD reflections for gold in this pattern are short and relatively wide and thus only very small gold particles are present in this catalyst. To estimate the average size,  $L$ , of the nanoparticles in the studied sample Sherrer's equation was employed.

$$L = \frac{k \cdot \lambda}{B \cdot \cos(\theta)} \quad (7)$$

where  $k = 0.9$ ,  $\lambda$  is the wavelength of the radiation used,  $B$  is the full width at half maximum of the peak in radians and  $\theta$  is the Bragg angle. The average size of the nanoparticles was determined to be 2.4 nm. This estimate is in agreement with TEM investigations showing nanoparticles with sizes in the same range (section 2.2.4).

It is remarkable that the structure of cobalt for the fresh samples corresponds only to  $\text{Co}_3\text{O}_4$ . The same structure was found for a spent sample. No  $\text{CoO}$  phase was detected. Hence, although during carbon monoxide preferential oxidation carbon dioxide is formed over the cobalt-sample, no noticeable reduction of cobalt was noticed. It is suggested, that only the near surface oxygen atoms, known as highly mobile species, have an active role in the carbon monoxide oxidation and the temperature and reaction conditions used were not sufficiently high to convert  $\text{Co}_3\text{O}_4$  [96].

Therefore, carbon monoxide is most likely oxidized over  $\text{Au}/\text{Co}_3\text{O}_4$  by highly mobile oxygen species. However, cobalt oxide alone is not able to oxidize carbon monoxide to a significant extent. Hence, gold and cobalt oxide are both needed for high activity. Carbon monoxide was probably activated on gold [96].

## B. Platinum/Zeolite-catalyst

XRD-patterns obtained for zeolites present peculiar characteristics and thus, few practical considerations are briefly presented. The low angle lines in Figure 8 and Figure 9 are the ones most strongly affected by non-framework species. In general, these lines are more intense in the calcined material than in the as-synthesized-form. Similar materials containing different cations have quite different relative intensities at low angles. However, the intensities of the higher angle reflections are generally dominated by the positions of the framework atoms, so these can be compared quite well.

Different synthesis conditions or different post-synthesis treatments can cause subtle distortions in a zeolite framework structure that can complicate identification. The symmetry may be reduced (and thereby produce a high number of additional peaks in the pattern), although the basic framework topology (connectivity) remains unchanged. In such a case,

indexing the pattern to obtain the dimensions of the unit cell can facilitate the identification [83].

XRD can be used to identify the bulk phases of catalyst samples. The big differences in the preparation procedure during ion-exchange might have affected the structure of the zeolite as well as the nature and the distribution of the platinum deposited on the catalysts. The ZSM-5/35 zeolite was ion-exchanged with an aqueous  $[\text{Pt}(\text{NH}_3)_4](\text{NO}_3)_2$  solution by two different routes (methods). By the first method (Method 1) the microreactor was impregnated with the platinum-solution for 24 h at room temperature. By the second method (Method 2) the duration of the impregnation was reduced to 4 h but at an elevated temperature of 80 °C.

The XRD-patterns of the platinum ZSM-5/35 and platinum-mordenite catalysts are shown in Figure 8 and Figure 9 respectively. The full width at half maximum (FWHM) of the peaks on both figures indicates that the crystallinity was high [99].

Neither a degradation of the zeolite framework nor the platinum peak at 39.8° explains the low activity of the samples, which will be discussed later.

On the other hand, the structure of the zeolites examined seemed to be unaffected by the different cation exchange procedures. The TPR-spectra discussed below confirmed the correctness of the method used.

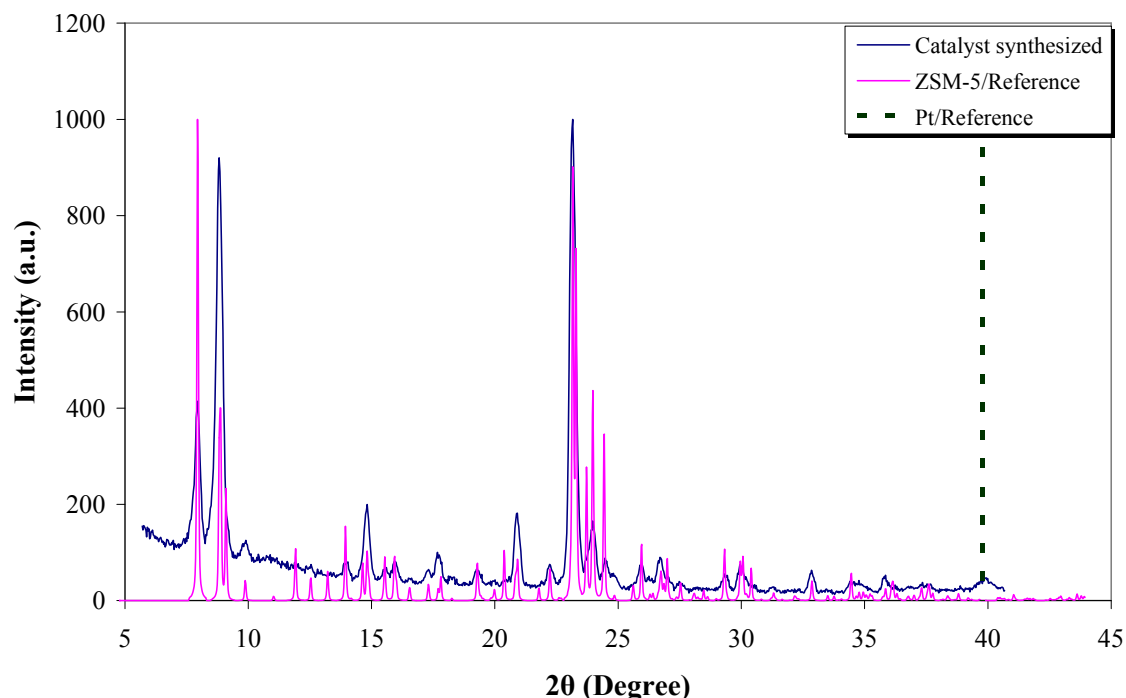


**Figure 8:** XRD-patterns of platinum supported ZSM-5, ion-exchanged by Method 1.

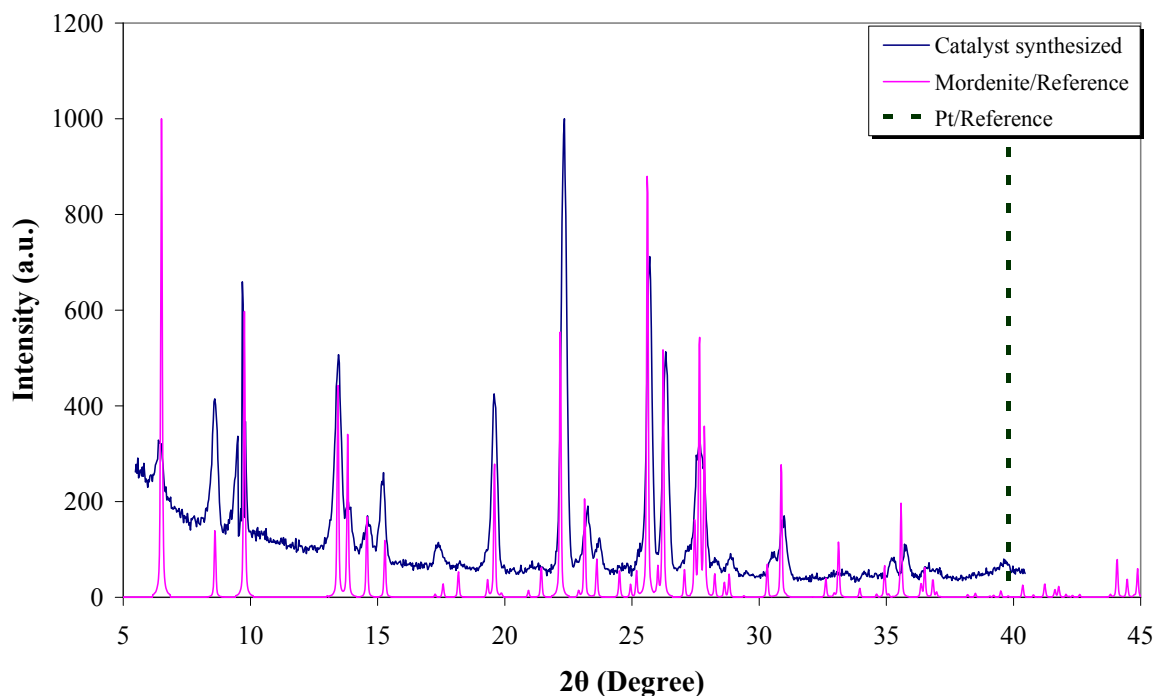


**Figure 9:** XRD-patterns of platinum supported mordenite, ion-exchanged by Method 2.

The above results indicate that zeolites had been successfully synthesized in the microchannel reactor and that ion-exchange was also successful, since the reference pattern matches well with the patterns obtained for the zeolite synthesized.

### 2.2.2 Zeolite TPR-spectra

The TPR-spectra for zeolite catalyst obtained are shown in Figure 10 and Figure 11. The essential difference between these spectra is due to the different distribution of platinum inside the cavities of the zeolite and over the surface as well. Thus, the proper pretreatment method was chosen judging from the curves.

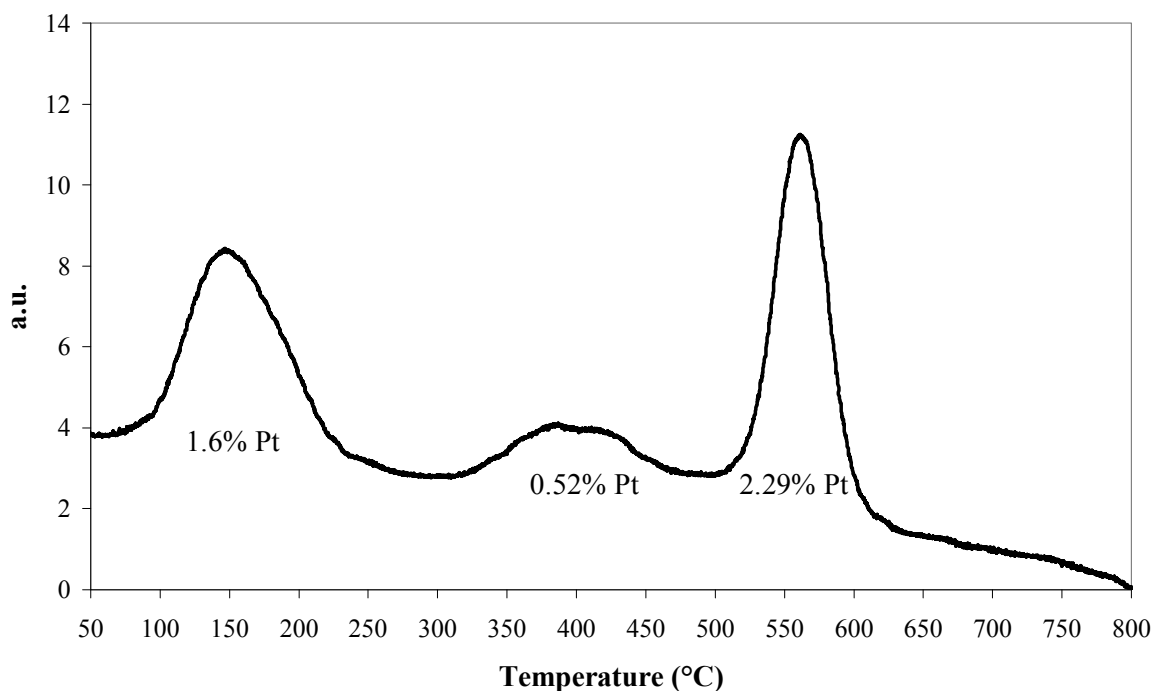


**Figure 10:** TPR-plot of platinum supported ZSM-5/35, ion-exchanged by Method 1.

The first peak in Figure 10 shows the amount of platinum on the surface of the catalyst. For the catalyst prepared by Method 1 we obtained 1.6 wt.% Pt. The bigger this amount is, the worse the catalyst performs, since the activity is gained by platinum present in the zeolite pores. This is represented by the second and third peak, here 2.81 wt.%.

In contrary to that, in Figure 11 it is depicted that large amount of platinum, about 5.75 wt.%, covers the surface and only 1.08 wt.% is ion-exchanged inside the cavities of the zeolite.

It is expected the amount of platinum present on the surface inhibits the gas to enter the zeolite pores, where the active sites are located. From Figure 10 and Figure 11, it is clear that Method 1 (24 h at room temperature), for ion-exchange, gives better results, according to the TPR-measurements.

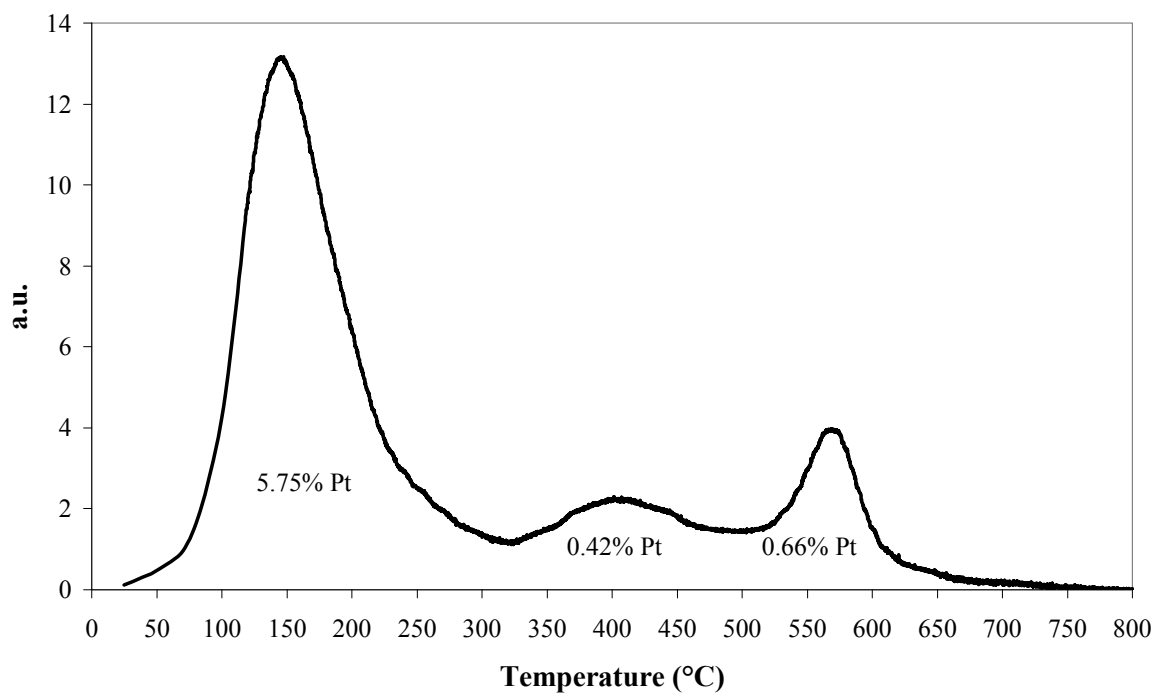
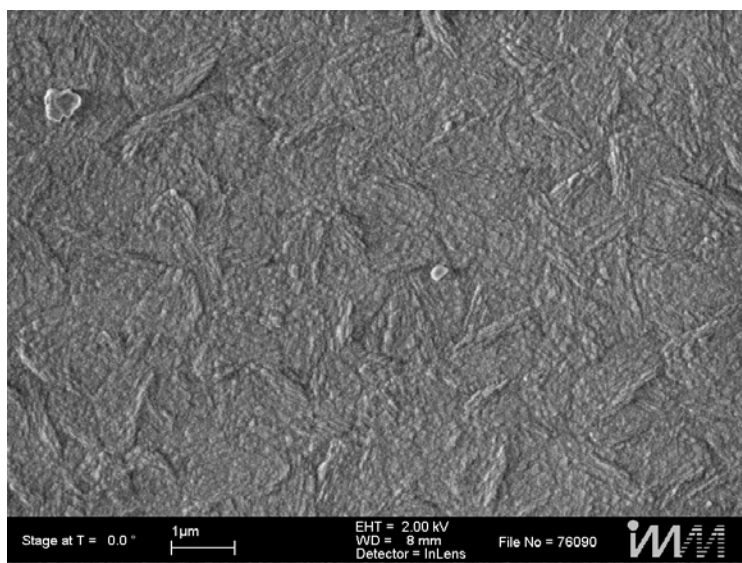


**Figure 11:** TPR-plot of platinum supported ZSM-5/35, ion-exchanged by Method 2.

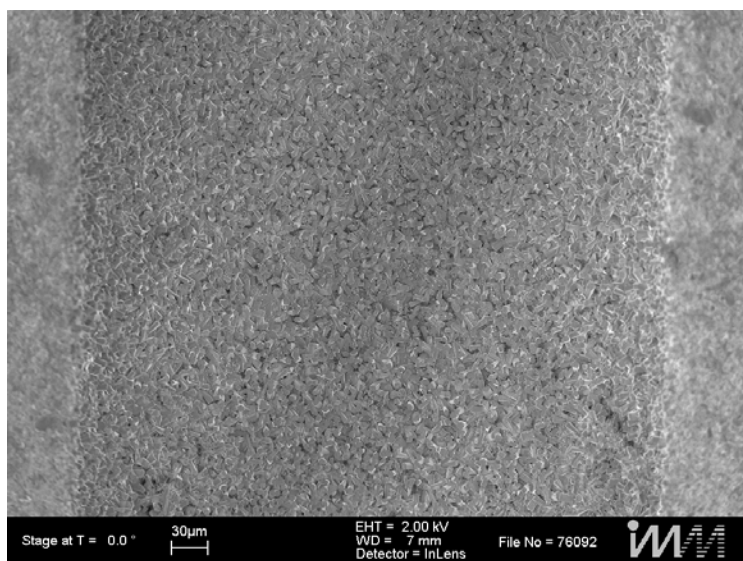
### 2.2.3 Zeolite SEM-photos

In order to determine the orientation of zeolite crystals and the homogeneity of the coating over the microreactors SEM-photos were prepared.

In Figure 12 and Figure 13, characteristic coatings over ZSM-5/35 and mordenite are depicted.

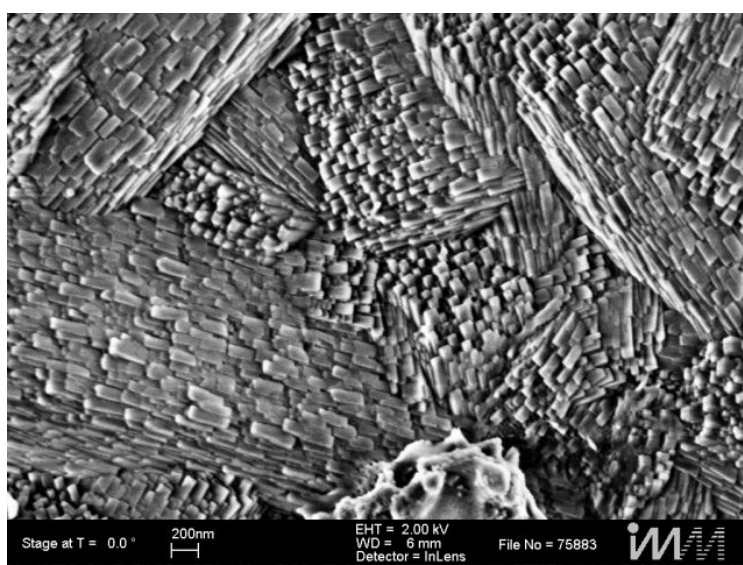


**Figure 12:** SEM-photo of a reactor coated with ZSM-5/35.



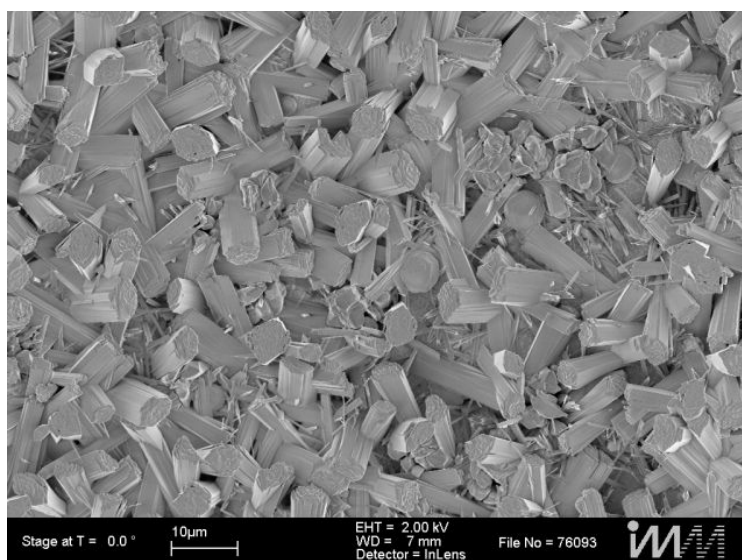
**Figure 13:** SEM-photo of a reactor coated with mordenite.

Figure 14 depicts a more detailed view (zoom in) of a microreactor coated with ZSM-5/35.



**Figure 14:** Detailed view of a reactor coated with ZSM-5/35 at 2 kV.

Figure 15 and Figure 16 shows magnifications of mordenite SEM-photos at 2 and 5 kV respectively.



**Figure 15:** Detailed view of a reactor coated with mordenite at 2 kV.

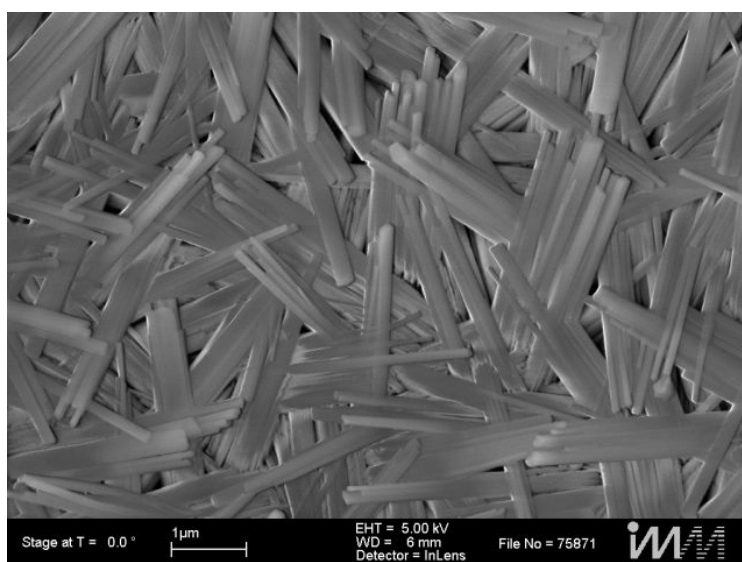


**Figure 16:** Detailed view of a reactor coated with mordenite at 5 kV.

As can be noticed, mainly from Figure 14 – Figure 16, our samples were successfully prepared and synthesized in terms of needles orientation and homogeneity over the microreactors. A well grown zeolite having the right orientation provides a better access of the gas mixture to the active sites. In this respect, high performance of the catalyst was expected.

### 2.2.4 Gold TEM-photos

The TEM-pictures of 1 wt.% Au/CeO<sub>2</sub> and 5 wt.% Au/Co<sub>3</sub>O<sub>4</sub> coprecipitated catalysts shown in Figure 17 and Figure 18, reveal the presence of the gold particles as dark spots in the catalyst. For both ceria and cobalt coprecipitated catalysts, the gold particles are seen as high contrast spots both on and inside the support, where the average particle size of gold is less than 2 nm [97].

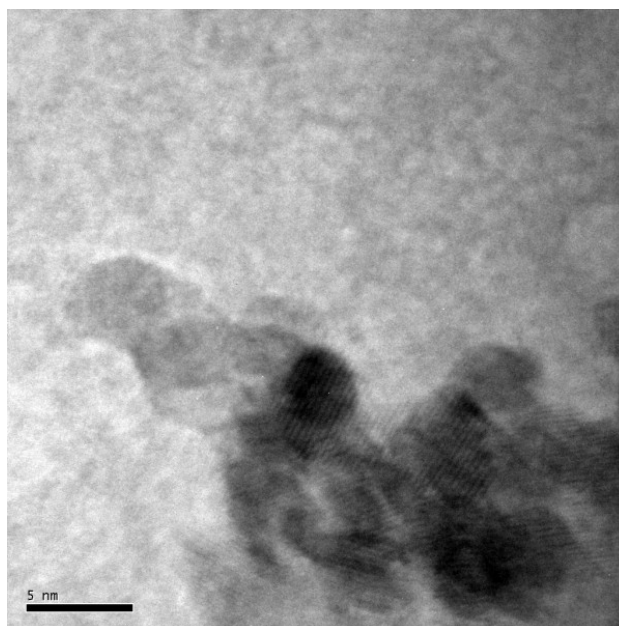


**Figure 17:** TEM-image of 3wt.% Au/CeO<sub>2</sub>.

The coprecipitated catalysts were calcined at 300 °C, which was thought to be the optimum calcination temperature to obtain very small particles. From the pictures it can also be observed, that the small gold particles did not show sufficiently homogeneous dispersion neither on ceria nor on cobalt oxide.

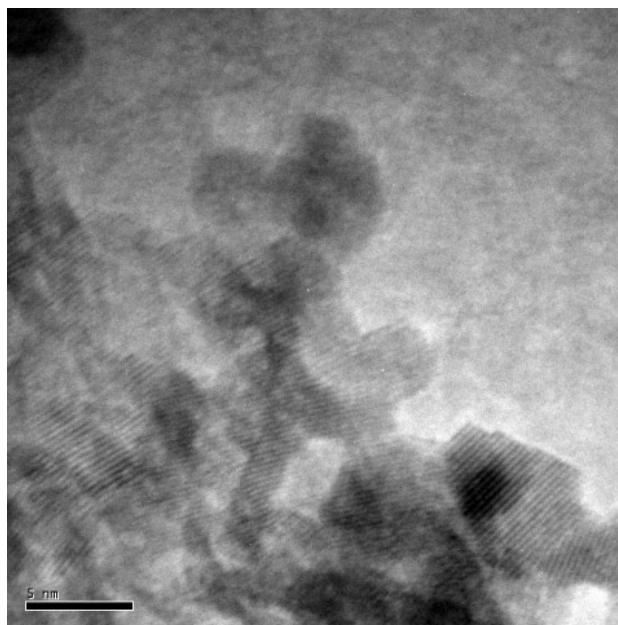


**Figure 18:** TEM-image of 5 wt.% Au/Co<sub>3</sub>O<sub>4</sub>.

In general, gold is deposited with its 111 plane in contact with the metal oxide [100]. However, it is not possible to know its exact structure, because the samples were in powder form and the gold particles were in both samples too thick (approximately 2 nm). Thus, gold appeared as tiny shadowed spots [101]. In Table 4 median particle diameters of various metal oxides calcined at 300 °C are presented. Hydrogen chemisorption was used by the University of Zaragoza Spain, to determine the mean particle size.

**Table 4:** Median gold-particle diameter for 3 wt.% Au catalysts over various metal oxides.

<b>Metal oxide</b>	<b>Median particle diameter (nm)</b>
<b>Co<sub>3</sub>O<sub>4</sub></b>	<2
<b>Fe<sub>2</sub>O<sub>3</sub></b>	4
<b>TiO<sub>2</sub></b>	<2
<b>CeO<sub>2</sub></b>	<2
<b>NiO</b>	3
<b>Al<sub>2</sub>O<sub>3</sub></b>	4

Gold particle sizes on the various samples are similar, when calcined at the same temperature. The presence of gold particles on cobalt and ceria oxide support was verified by EDX-spectra (Figure 19 and Figure 20), focusing on the regions containing high contrast spots under TEM.

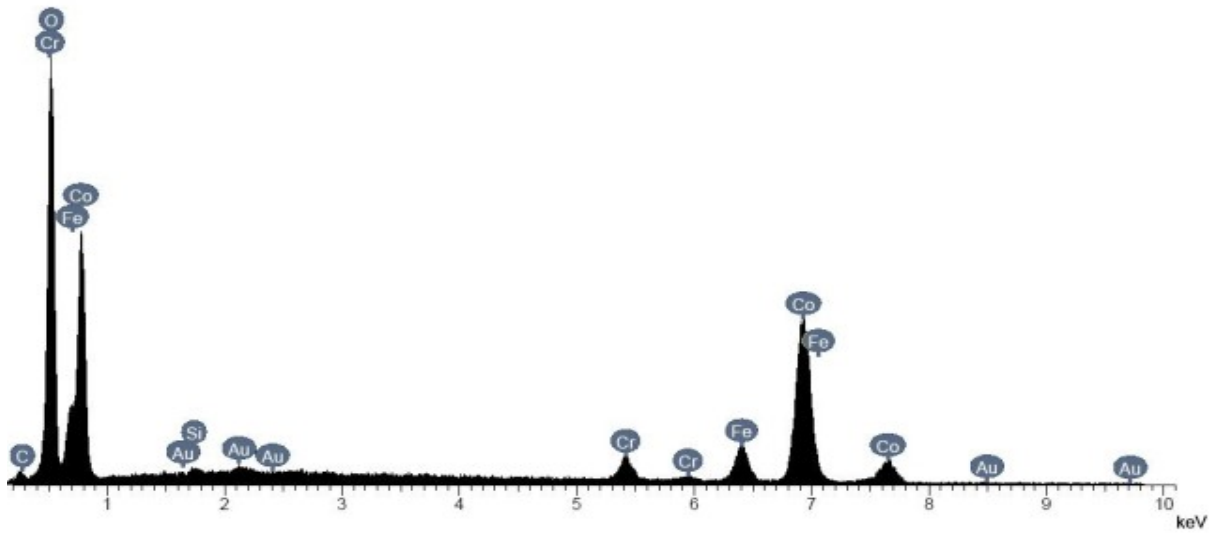


**Figure 19:** EDX-analysis of 5 wt.% Au/Co<sub>3</sub>O<sub>4</sub>.

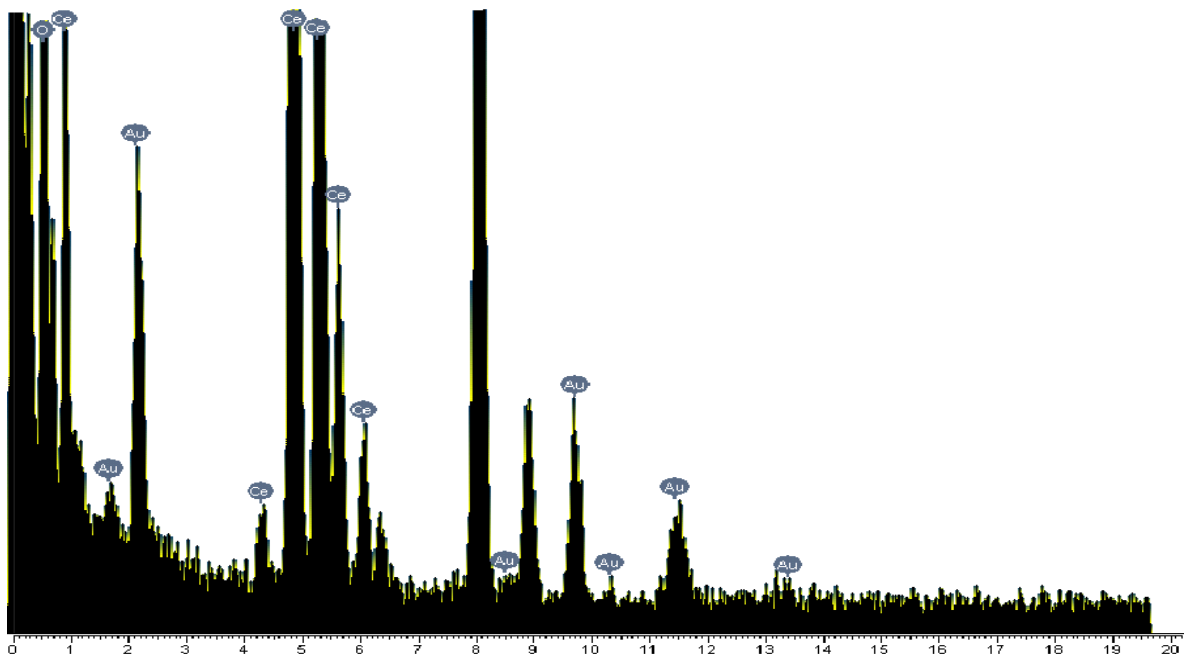


**Figure 20:** EDX-analysis of 3 wt.% Au/CeO<sub>2</sub>.

### 2.3 Activity measurements

With the results reported in the previous section, the optimum synthesis conditions for gold and zeolite catalysts were selected. In this chapter, catalysts prepared as washcoats are presented as they were tested in microreactors for the preferential oxidation of carbon monoxide in hydrogen-rich stream in the presence of carbon dioxide.

Aim of these preliminary tests was to select the most promising catalyst. For this selection two criteria were used, namely the activity and selectivity of each catalyst at temperatures below 200 °C and at maximum weight hourly space velocity (WHSV) of 180 Ndm<sup>3</sup>/h·g<sub>cat</sub>. In Table 5, the physical properties of the metal oxides over gold catalysts, tested in the five fold reactor, are listed. Samples were calcined at 300 °C. Both median pore diameter and the surface area were determined by nitrogen adsorption.

**Table 5:** Surface area and pore diameter for 3 wt.% Au catalysts over various metal oxides.

<b>Metal oxide</b>	<b>Surface area (m<sup>2</sup>/g)</b>	<b>Median pore diameter (nm)</b>
<b>Co<sub>3</sub>O<sub>4</sub></b>	59.50	15
<b>Fe<sub>2</sub>O<sub>3</sub></b>	25.95	20
<b>TiO<sub>2</sub></b>	41.95	3
<b>CeO<sub>2</sub></b>	78.10	46
<b>NiO</b>	19.05	34
<b>Al<sub>2</sub>O<sub>3</sub></b>	179.10	4

The different Au/MeO<sub>x</sub> investigated catalysts exhibit significant activity differences in the carbon monoxide oxidation reaction in reformat gas-stream. There was a strong variation of the physical properties, which are depended on the metal oxide nature. The surface area of Al<sub>2</sub>O<sub>3</sub> was ten times higher compared with NiO. The pore radius of Fe<sub>2</sub>O<sub>3</sub> was more than five times larger compared with Al<sub>2</sub>O<sub>3</sub>. Since the gold particle sizes on the various samples are rather similar, when calcined at the same temperature, particle size effects cannot be held responsible for these differences. Consequently, the differences are related to the different support materials with easily reducible metal oxides. It was thus expected that the metal support will strongly influence the reaction rate.

The same implied also for zeolite catalysts. The differences of the framework structure between ZSM-5/35, ZSM-5/100, zeolite-Y and mordenite are related to different physical and chemical properties.

### 2.3.1 Gold-catalysts

The influence of several parameters was examined. All measurements with gold-catalysts were carried out using a synthetic methanol reformat stream, which contained 1.27 Vol.% CO, 72 Vol.% H<sub>2</sub>, 20 Vol.% CO<sub>2</sub>, and O<sub>2</sub> (depending on O/CO ratio), in the five fold reactor (section 3.3.1).

The first parameter examined was the calcination temperature and its effect on the activity of the catalyst. When the calcination temperature is below 200 °C, gold can exist as an oxidic species, Au<sub>2</sub>O<sub>3</sub>, similar to gold hydroxide (Au(OH)<sub>3</sub>). Above 300 °C the oxidic gold species are decomposed into metallic species and gold-sintering occurs. At 500 °C almost all oxidic gold species are reduced to metallic species [69, 102 and 103]. This was proven also by the presence of peaks of metallic gold species in the XRD patterns.

The same conclusion for the relation between calcination temperature and change of oxidic gold to metallic gold which causes catalyst inactivity through sintering stands for the relation between calcination temperature and physical properties of the catalyst. In Table 6 the influence of calcination temperature on particle diameter and surface area is presented.

**Table 6:** *Surface area and gold particle diameter dependence on calcination temperature for 3 wt.% Au over Fe<sub>2</sub>O<sub>3</sub> catalyst (University of Zaragoza Spain).*

Calcination temperature (°C)	Surface area (m <sup>2</sup> /gr)	Gold Particle diameter (nm)
400	25.95	6.50
450	20.68	8.31
500	14.62	9.04
600	10.89	9.31

The suggestion [71 and 73] that increasing calcination temperature corresponds to an increment in gold particle size is confirmed by the above measurements. By varying the calcination temperature of the washcoat, its properties are affected significantly.

In particular, by increasing the calcination temperature not only particle diameters increased, which is reported to be a disadvantage [104], but also the surface area and hence the oxidation capabilities of the catalyst decreased. In Figure 21 the carbon monoxide conversion as a function of temperature for two different calcination temperatures is shown. When the calcination temperature was above 300 °C, deactivation of the gold-catalyst occurred. Therefore, a calcination temperature of 300 °C was selected.

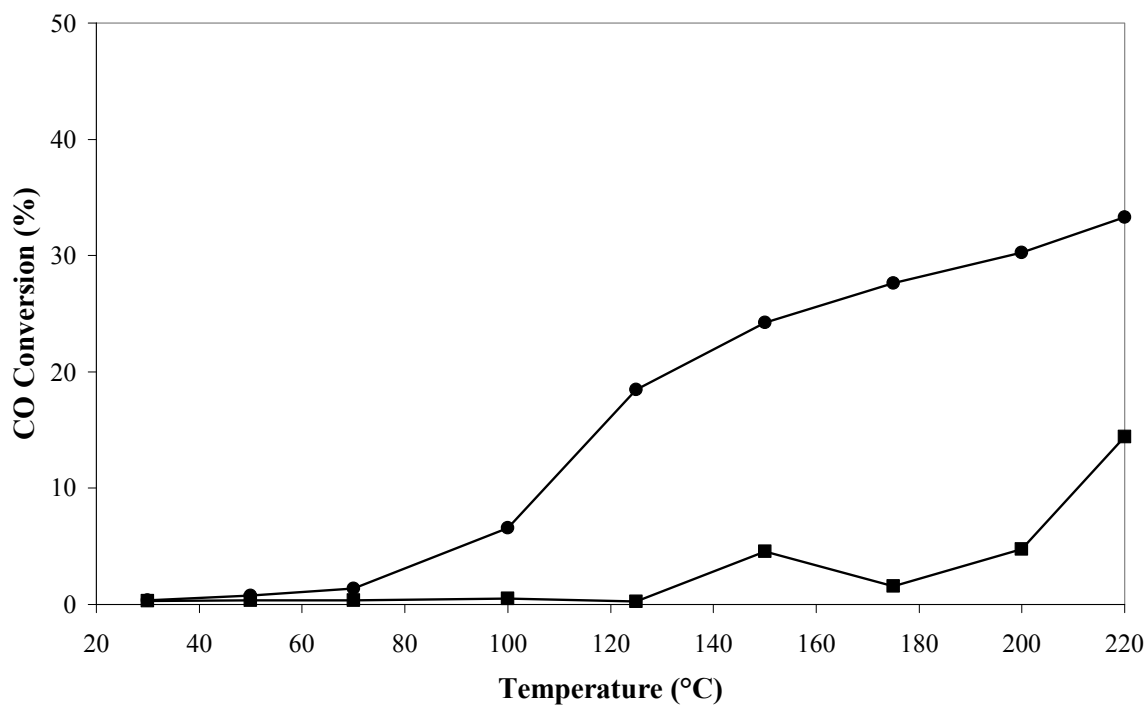


**Figure 21:** CO conversion achieved vs. reaction's temperature over catalyst containing 3 wt.% Au/Co<sub>3</sub>O<sub>4</sub>, feed O/CO = 4, WSHV = 180 Ndm<sup>3</sup>/h·g<sub>cat</sub> at (■) 500 °C and (●) 300 °C calcination temperature (five fold reactor).

In Figure 22, the carbon monoxide conversion over various gold-metal oxides is shown.

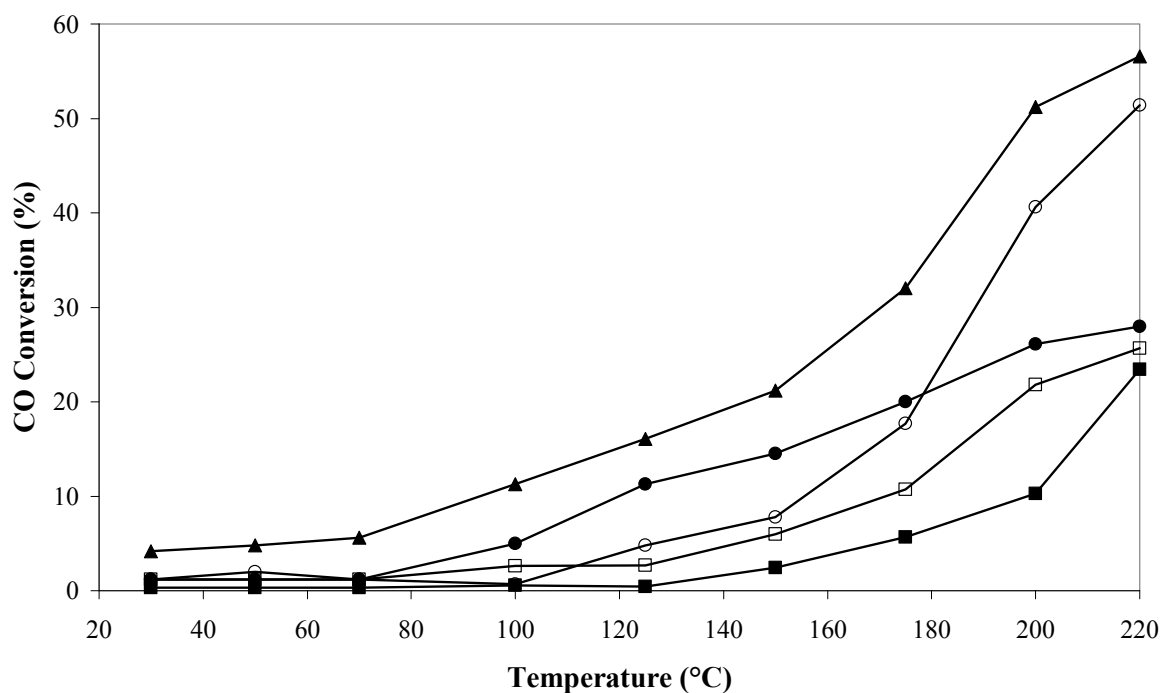


**Figure 22:** CO conversion achieved vs. reaction's temperature over various catalysts containing 3 wt.% Au, feed O/CO = 8, WSHV = 90 Ndm<sup>3</sup>/h·g<sub>cat</sub> over (■) NiO<sub>2</sub>, (□) CeO<sub>2</sub>, (●) TiO<sub>2</sub>, (▲) Co<sub>3</sub>O<sub>4</sub> and (○) Fe<sub>2</sub>O<sub>3</sub> (five fold reactor).

As shown in Figure 21 and 22, both Au/Co<sub>3</sub>O<sub>4</sub> and Au/Fe<sub>2</sub>O<sub>3</sub> catalysts present remarkable activity at high temperatures for the carbon monoxide oxidation in the presence of carbon dioxide. In contrary, at temperature below 180 °C only Au/Co<sub>3</sub>O<sub>4</sub> shows moderate activity. The other metal oxides shown in Figure 22, namely TiO<sub>2</sub>, NiO<sub>2</sub> and CeO<sub>2</sub>, present very low activity under the specific conditions investigated.

As mentioned, the preparation method plays also a significant role to the activity of the catalyst. In Figure 23, two Au/ $\gamma$ -Al<sub>2</sub>O<sub>3</sub> catalysts are compared. The first-one was prepared by impregnation method, while the second-one by coprecipitation method. The inlet O/CO ratio was 4 and the WHSV = 180 Ndm<sup>3</sup>·h<sup>-1</sup>·g<sub>cat</sub><sup>-1</sup>.

The difference between the two Au/ $\gamma$ -Al<sub>2</sub>O<sub>3</sub> catalysts is remarkable. More specifically, conversion of the impregnated gold is significantly higher than the conversion exhibited by the coprecipitated Au/ $\gamma$ -Al<sub>2</sub>O<sub>3</sub> catalyst. The impregnated gold-catalyst exhibited conversion and performance similar to those achieved over Au/Co<sub>3</sub>O<sub>4</sub> for the whole temperature range.

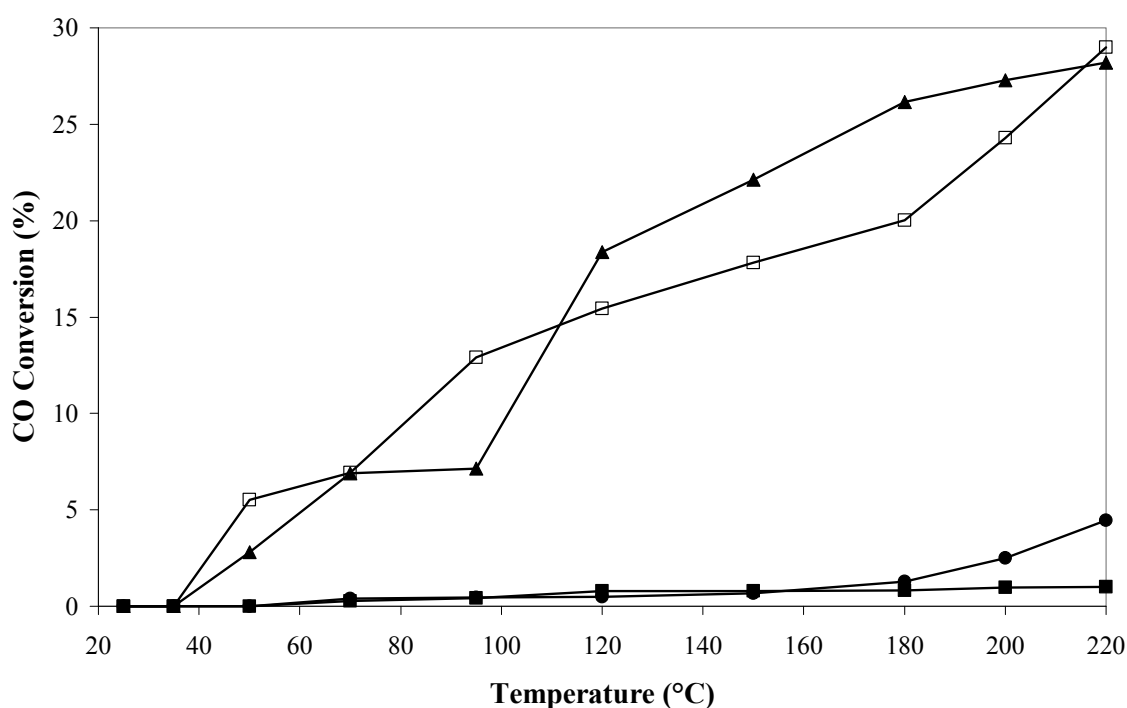


**Figure 23:** CO conversion achieved vs. reaction's temperature over various catalysts containing 3 wt.% Au, feed O/CO ratio = 4, WSHV = 180 Ndm<sup>3</sup>/h·g<sub>cat</sub> over (■) co-precipitated  $\gamma$ -Al<sub>2</sub>O<sub>3</sub>, (▲) impregnated  $\gamma$ -Al<sub>2</sub>O<sub>3</sub>, (□) Co<sub>3</sub>O<sub>4</sub> and (●) CeO<sub>2</sub> (five fold reactor).

Furthermore, the enormous influence of carbon dioxide on the activity of the gold-catalysts synthesized by coprecipitation was confirmed. The resistance of the Au/Co<sub>3</sub>O<sub>4</sub> catalyst on carbon dioxide was tested in a quartz tube with an inner diameter of 4 mm. It was filled with

catalyst diluted by  $\text{Al}_2\text{O}_3$ . Reaction rate and selectivity were determined as a function of temperature.

For this purpose 130 mg of catalyst were used, diluted by 50 wt.%  $\text{Al}_2\text{O}_3$  and an inlet concentration of 5,000 ppm CO. This mixture ensured thermal homogeneity and reasonable pressure drop inside the fixed bed reactor. The concentrations of the gases components were measured for both inlet and the outlet of the reactor, using an NGA 2000 detector from Fisher Rosemount, with IR detectors for carbon monoxide and carbon dioxide, a paramagnetic sensor for oxygen and a thermal conductivity sensor for hydrogen. All measurements were carried out at O/CO ratio of 8, using a total flow of 390 Nml/min synthetic methanol reformat, consisted of 0.5 Vol.% CO, 70 Vol.%  $\text{H}_2$ , 0 – 20 Vol.%  $\text{CO}_2$ , 2 Vol.%  $\text{O}_2$  and  $\text{N}_2$  in balance. In Figure 24 the carbon monoxide conversion and selectivity is shown as a function of time.

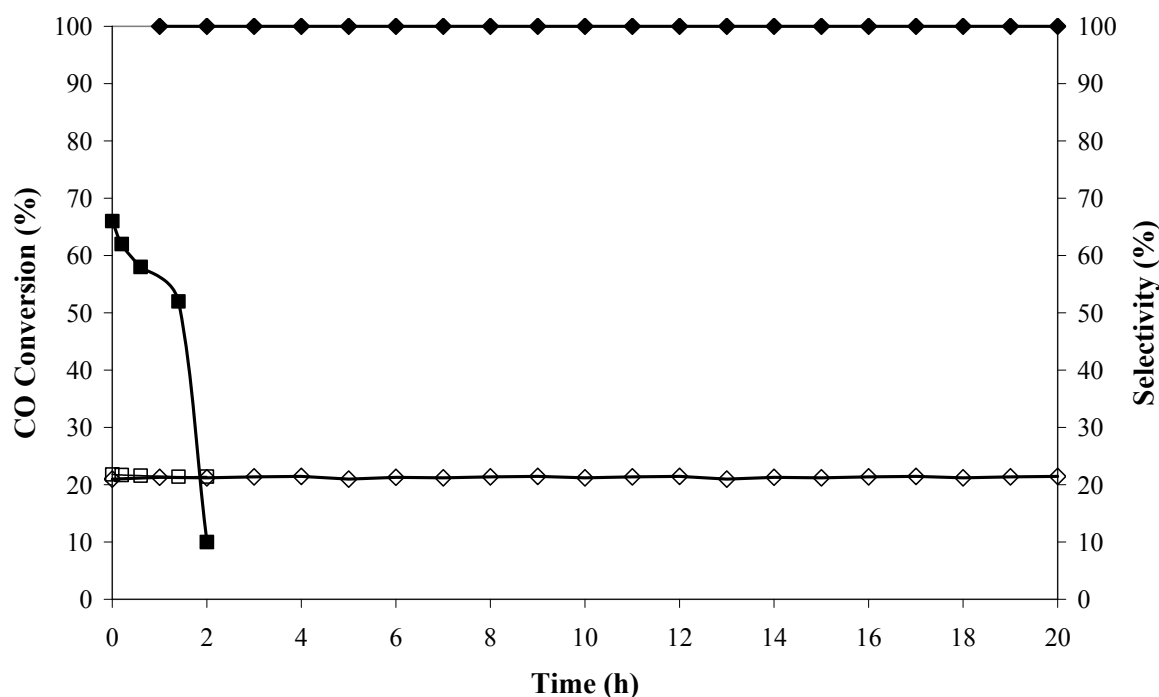


**Figure 24:** CO conversion and selectivity achieved vs. time on stream over catalyst containing 3 wt.% Au/ $\text{Co}_3\text{O}_4$ , feed O/CO = 8, at 50 °C,  $WSHV = 180 \text{ Ndm}^3/\text{h}\cdot\text{g}_{cat}$  with (■) 20 Vol.%  $\text{CO}_2$ , or without (◆)  $\text{CO}_2$  in the reaction mixture. Solid and open symbols denote, respectively, conversion and selectivity.

In the presence of carbon dioxide, conversion drops rapidly within 2 h, while in the absence of carbon dioxide remained 100% for more than 20 h. Looking at the selectivity as a function of gas composition, we can assume that the presence of carbon dioxide hindered the oxidation of carbon monoxide, without affecting the oxidation of hydrogen.

A possible explanation for this behaviour was given by Schubert et al. [74]. They found similar effects of carbon dioxide presence in the synthetic reformat on the activity of preferential carbon monoxide oxidation for the Au/Fe<sub>2</sub>O<sub>3</sub> system. The authors assumed co-adsorption of carbon dioxide at the gold-metal oxide interface to be responsible for the decreased activity.

The pH influenced significantly the activity, as shown in Figure 25. The pH of the buffer solution at which gold and metal solutions coprecipitated depends on the metal. To examine the pH, it was necessary to vary the pH, from low or high values to the final pH value where the solvate precipitates.

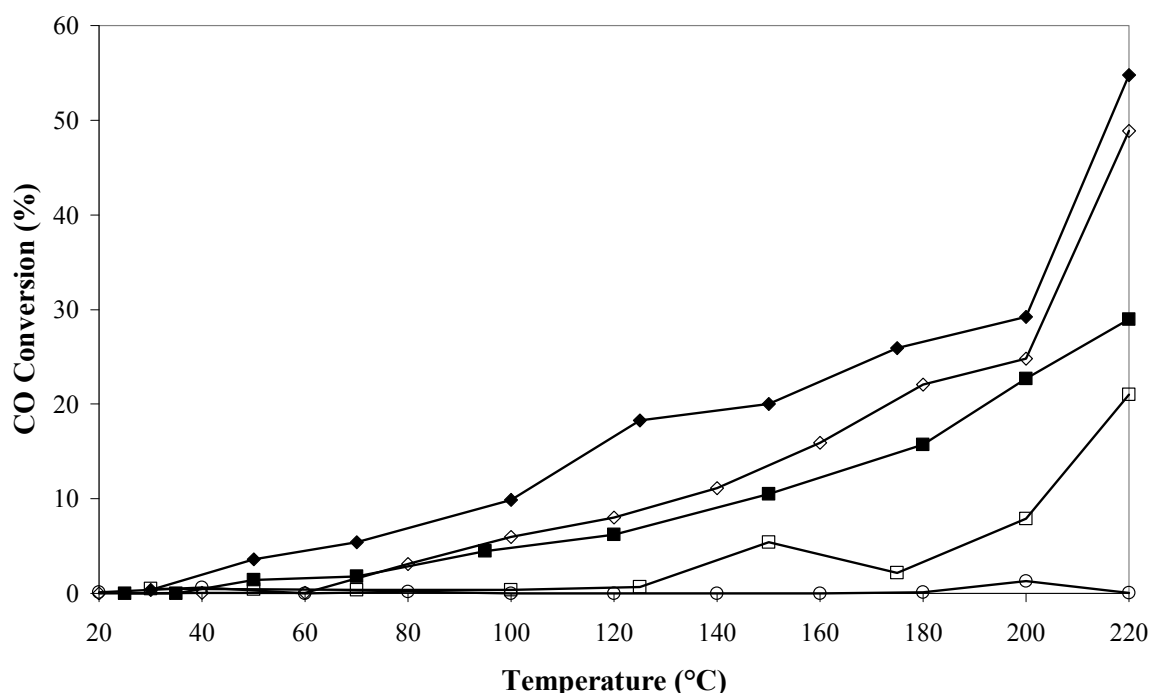


**Figure 25:** CO conversion achieved vs. reaction's temperature over catalyst containing 5 wt.% Au/Co<sub>3</sub>O<sub>4</sub>, feed O/CO = 8, WSHV = 180 Ndm<sup>3</sup>/h·g<sub>cat</sub> at a pH ranging (○) from 2 to 7, (◊) 7 and (◑) from 11 to 7. Solid and open symbols denote, respectively, 300 °C and 400 °C calcination temperature (five fold reactor).

It has been found that preparation at a constant pH was preferable, ranging from 7 to 8 depending on the oxide support. For cobalt oxide this value was set to 7, as it was suggested [105 – 107] and thus higher activity was achieved. Any other pH-conditioning derived to inactive catalyst.

Other parameters thought to influence the activity of gold-catalysts were also investigated [108 and 109]. The need to activate the sample in an oxygen or hydrogen atmosphere (60 – 200 ml/min) at moderate temperature (100 – 300 °C) was not verified by the experiments

carried out. It was also suggested [106] that the gold-precursor could affect the activity. Apart from gold tetrachloroauric acid ( $\text{HAuCl}_4$ ) used in all the previous experiments, gold-acetate ( $\text{Au}(\text{O}_2\text{CCH}_3)_3$ ) was tested as alternative precursor. Figure 26 discourages the usage of  $\text{Au}(\text{O}_2\text{CCH}_3)_3$  as gold-precursor for synthesizing such a catalyst, as it is little soluble in water and can not be used in coprecipitation or in any other similar method.

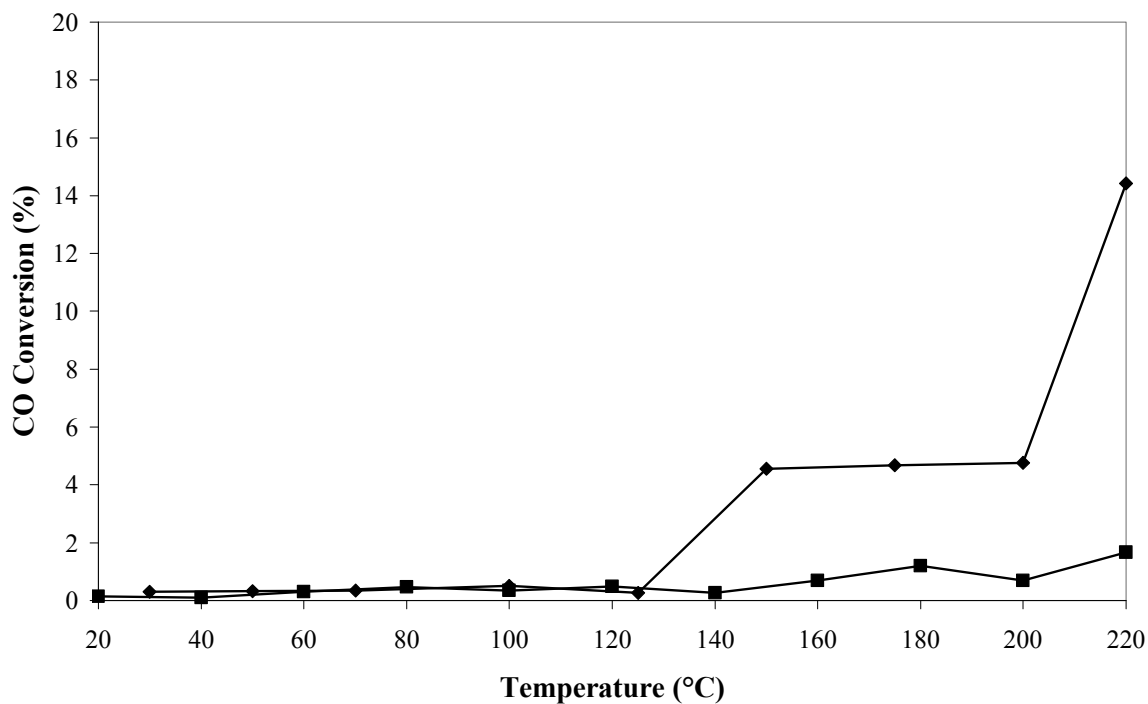


**Figure 26:** *CO conversion achieved vs. reaction's temperature over catalyst containing 3 wt. % Au/CeO<sub>2</sub>, feed O/CO = 4, WSHV = 180 Ndm<sup>3</sup>/h·g<sub>cat</sub> with (◆) HAuCl<sub>4</sub> and (■) Au(O<sub>2</sub>CCH<sub>3</sub>)<sub>3</sub> as gold-precursor (five fold reactor).*

### 2.3.2 Zeolite-catalysts

For all the experiments carried out with zeolites in the single reactor (section 3.3.1), the reaction mixture consisted of 1.27 Vol.% CO, 26.3 Vol.% CO<sub>2</sub> and 72.43 Vol.% H<sub>2</sub>. Oxygen was also present in various concentrations (O/CO ratio).

The ZSM-5/100 catalysts, prepared at the University of Zaragoza, contained 4.2 wt.%, 1.5 wt.% and 0.5 wt.% Pt, respectively.

In Figure 27, the conversion of carbon monoxide and the selectivity as a function of the temperature are shown for ZSM-5/100 catalyst with 4.2 wt.% Pt.

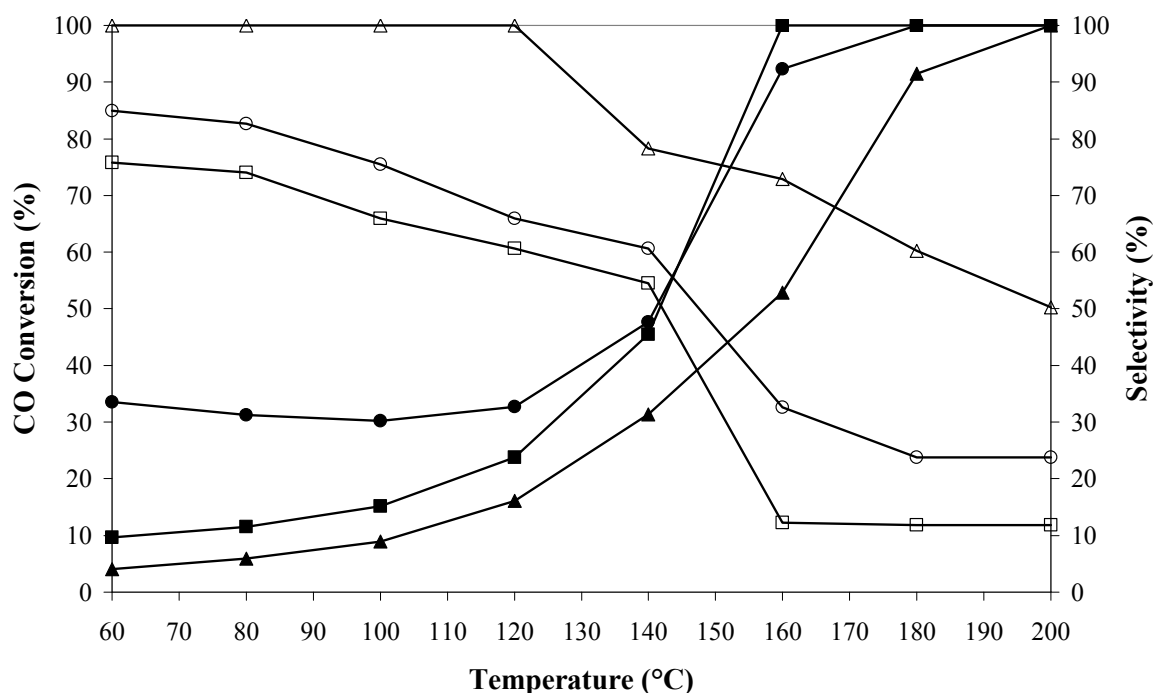


**Figure 27:** CO conversion and selectivity achieved vs. reaction's temperature over catalyst containing 4.2 wt.% Pt ZSM-5/100,  $WSHV = 180 \text{ Nm}^3/\text{h}\cdot\text{g}_{\text{cat}}$  at feed (■) O/CO = 8, (●) O/CO = 4 and (▲) O/CO = 2. Solid and open symbols denote, respectively, the CO conversion and selectivity.

As expected, the O/CO ratio increases the overall conversion. Conversion of 100% (carbon monoxide below 5 ppm was the detection limit of the GC) was achieved for temperatures higher than 160 °C, 180 °C and 200 °C at O/CO ratio of 8, 4 and 2 respectively.

Primary aim for a carbon monoxide catalyst for fuel cell application is to convert carbon monoxide to at least 50 ppm (if not to 10 ppm) and maintain stable activity. It is also, though, important to investigate the extent of hydrogen loss due to the catalyst selectivity properties at varying O/CO ratio. Hydrogen oxidation is strongly inhibited by the presence of carbon monoxide due to the stronger carbon monoxide chemisorption on the noble metal surfaces as

compared with hydrogen and oxygen chemisorption. Consequently, carbon monoxide covers these active sites allowing hydrogen and oxygen species to weakly chemisorb when temperatures are high enough to desorb some of the carbon monoxide. Thus, once this stage is reached, there is simultaneous hydrogen and carbon monoxide oxidation taking place at different rates. As it was expected the catalyst is more selective when less oxygen ( $O/CO = 2$ ) is present at the reaction mixture. Increasing the amount of oxygen inevitably led to an increase in hydrogen loss.

It is important to mention that at low temperatures the catalyst is most active at  $O/CO = 4$ .

In Figure 28, the results obtained with 1.5 wt.% Pt ZSM-5/100 catalyst are presented.

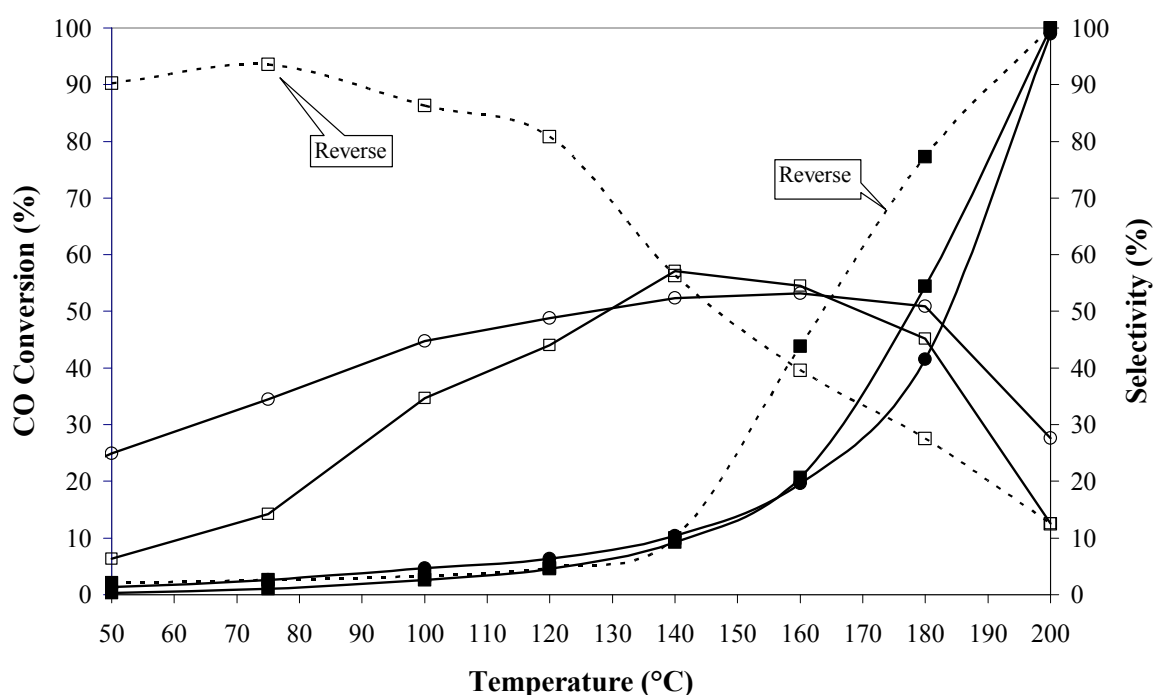


**Figure 28:** CO conversion and selectivity achieved vs. reaction's temperature over catalyst containing 1.5 wt.% Pt ZSM-5/100,  $WSHV = 180 \text{ Ndm}^3/\text{h}\cdot\text{g}_{\text{cat}}$  at feed ( $\blacksquare$ )  $O/CO = 8$  and ( $\bullet$ )  $O/CO = 4$ . Solid and open symbols denote, respectively, the CO conversion and selectivity.

Compared to the previous measurement, this catalyst is less active. Acid sites on the zeolite are formed by ion exchange. The more platinum is exchanged the more acidic the zeolite is and thus, more active. Consequently, it was expected lower activity for a catalyst with lower platinum content.

As mentioned before, at low temperatures the catalyst is more active when  $O/CO = 4$  and not when  $O/CO = 8$  (which means more oxygen in the reaction mixture). In both cases, experiment were made firstly at  $O/CO = 8$  and then at  $O/CO = 4$ . This seems to cause an

increase of the catalyst activity. Besides, as it is depicted in Figure 28, the catalyst shows higher activity and selectivity by a second pass (reverse route), indicating the need of a pretreatment in flow before each test.

Figure 29 illustrates the carbon monoxide conversion and selectivity over 0.5 wt.% Pt ZSM-5/100 catalyst.

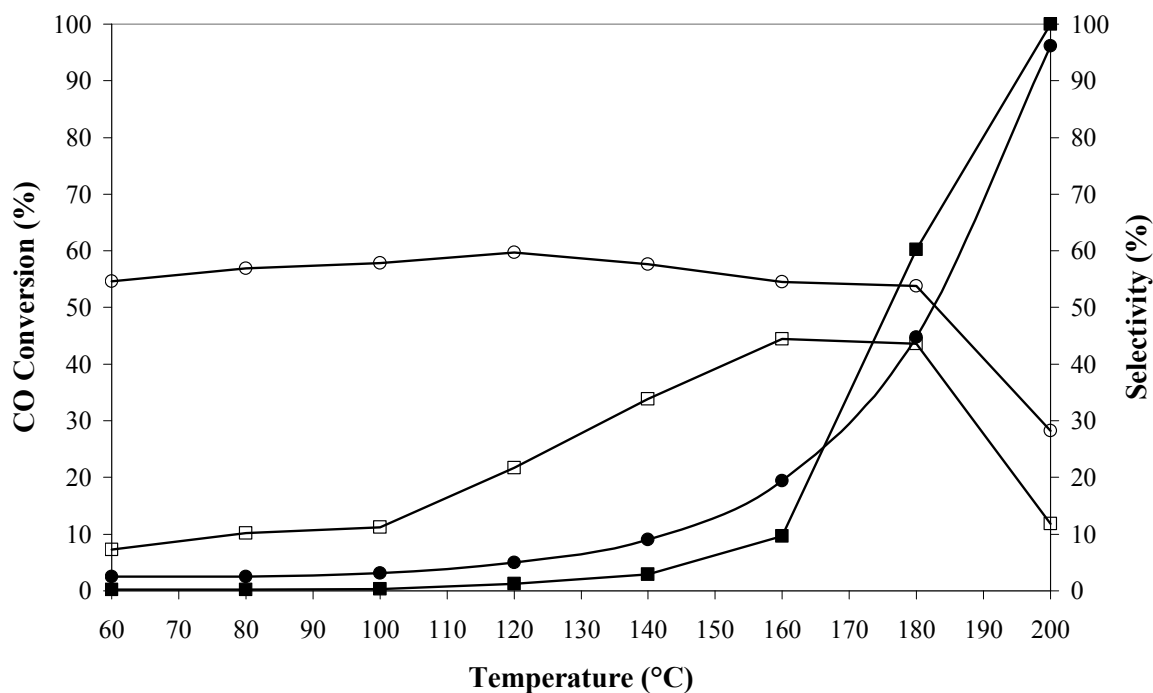


**Figure 29:** CO conversion and selectivity achieved vs. reaction's temperature over catalyst containing 0.5 wt.% Pt ZSM-5/100,  $WSHV = 180 \text{ Ndm}^3/\text{h}\cdot\text{g}_{\text{cat}}$  at feed (■)  $O/CO = 8$  and (●)  $O/CO = 4$ . Solid and open symbols denote, respectively, the CO conversion and selectivity.

The catalyst remained little active at temperatures below 160 °C. Nevertheless, 100% conversion was achieved at a temperature of 200 °C. The O/CO ratio did not have any effect on the conversion over 0.5 wt.% Pt ZSM-5/100. In contrast, 0.5 wt.% Pt ZSM-5/100 presented higher selectivity when less oxygen was in the feed, especially at lower temperatures. This was because there were not enough acidic sites to catalyze carbon monoxide reaction (low platinum content). The remainder of oxygen caused hydrogen combustion leading to lower selectivity [9]. However, at higher temperatures, oxygen species can easier react preferentially with carbon monoxide, concentrated in the zeolite pores [9]. This can explain the increase of the selectivity at temperatures between 100 °C and 160 °C. At low conversion and as the temperature increased above 140 °C some active sites get available for oxygen adsorption and the conversion of carbon monoxide gets accelerated.

Since the application of the present preferential oxidation catalyst is for a fuel cell system, it was important to determine the effect of space velocity on its performance. Figure 30 shows the effect that weight hourly space velocity (WHSV) has on the activity of a ZSM-5/100 catalyst, containing 4.2 wt.% Pt. The tests were carried out over the same microreactor and in both cases the flow was laminar.

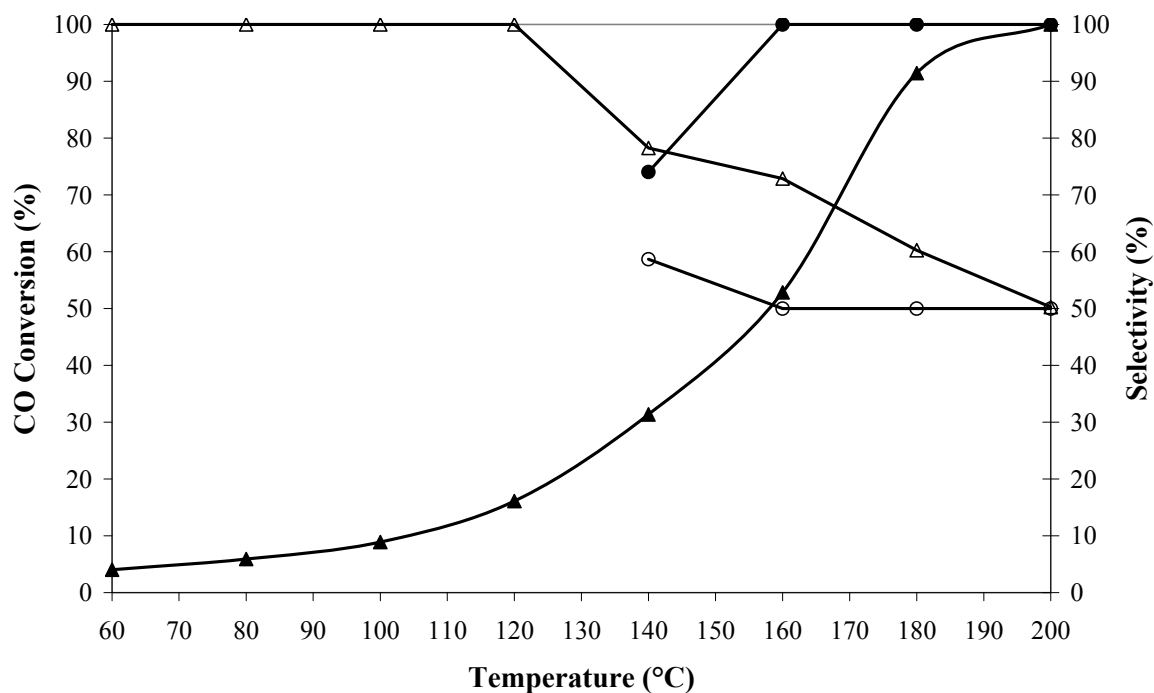


**Figure 30:** CO conversion and selectivity achieved vs. reaction's temperature over catalyst containing 4.2 wt.% Pt ZSM-5/100, feed O/CO = 2, ( $\blacktriangle$ ) WHSV = 180 Ndm<sup>3</sup>/h·g<sub>cat</sub> and ( $\bullet$ ) WHSV = 120 Ndm<sup>3</sup>/h·g<sub>cat</sub>. Solid and open symbols denote, respectively, the CO conversion and selectivity.

As shown in Figure 30, with higher space velocity the reactant gases had less time over the catalyst to achieve adsorption thus leading to a lower carbon monoxide conversion at a specific temperature. To achieve 100% carbon monoxide conversion, at 180 Ndm<sup>3</sup>/h·g<sub>cat</sub> space velocity, a temperature of ca. 200 °C was required. This was 40 °K higher than the temperature required to achieve full conversion with a space velocity of 120 Ndm<sup>3</sup>/h·g<sub>cat</sub>. At a space velocity of 180 Ndm<sup>3</sup>/h·g<sub>cat</sub> and 75% conversion, a carbon monoxide selectivity of ca. 65% was achieved which was nearly 10% higher than the selectivity achieved at a space velocity of 120 Ndm<sup>3</sup>/h·g<sub>cat</sub> and conversion of 75%. This implies that at high space velocities the rate of hydrogen conversion decreased with respect to the rate of carbon monoxide conversion as hydrogen adsorption rate was lower than that of carbon monoxide.

At higher temperatures, where nearly all of the oxygen has been depleted, selectivity

decreased in both cases to the level of ca. 50% which is to be expected at O/CO ratio of 4.

Figure 31 presents long term testing of the 4.2 wt.% Pt ZSM-5/100 catalyst.

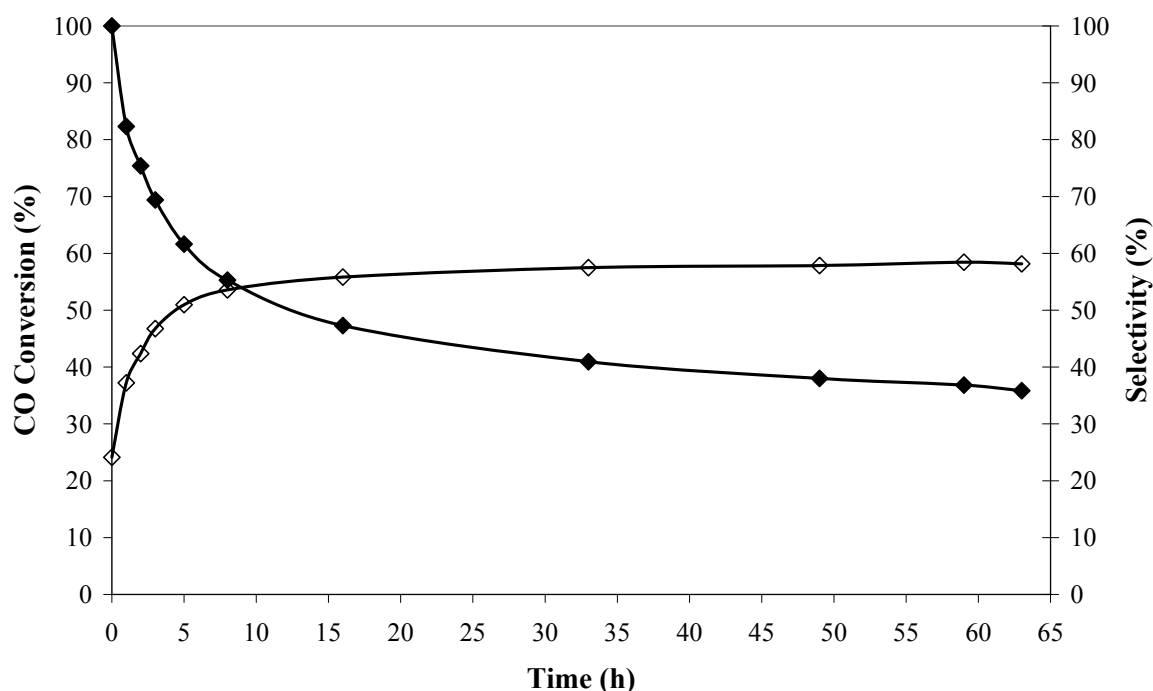


**Figure 31:** 4.2 wt.% Pt ZSM-5/100 catalyst operation with time at 190 °C, feed O/CO = 4 and WSHV = 180 Ndm<sup>3</sup>/h·g<sub>cat</sub>. Solid and open symbols denote, respectively, the CO conversion and selectivity.

Zeolite ion-exchanged catalyst exhibited remarkable activity and selectivity, although rapidly deactivation occurred even at relatively high temperatures. After 35 h, the conversion had decreased to 40% and remained there for 30 h.

The performance exhibited by platinum-exchanged ZSM-5/100 catalysts was promising. It is reported elsewhere, that other zeolites (e.g. mordenite, ZSM-5/35 and zeolite-Y) exhibit superior performance compared to ZSM-5/100 [9]. The Si/Al ratio plays an important role in the catalytic activity (difference between ZSM-5/35 and 100). When this ratio is decreased, the acid sites density is increased, leading theoretically to higher conversions [110 and 111].

The zeolite-Y was selected in the present study, since the diameters of the entrance and supercage of Y-type zeolite are 0.74 and 1.3 nm, respectively, and carbon monoxide and oxygen molecules can enter the micropores with an enough clearances.

In Figure 32, comparison of the above catalysts is depicted. The catalysts did not demonstrate the superior behavior of ZSM-5/100. Several parameters were investigated to ensure that synthesis and pretreatment conditions were ideal and suitable for the proposed zeolite. Experiments were carried out at inlet O/CO ratio of 4 and WSHV of 180 Ndm<sup>3</sup>/h·g<sub>cat</sub>.

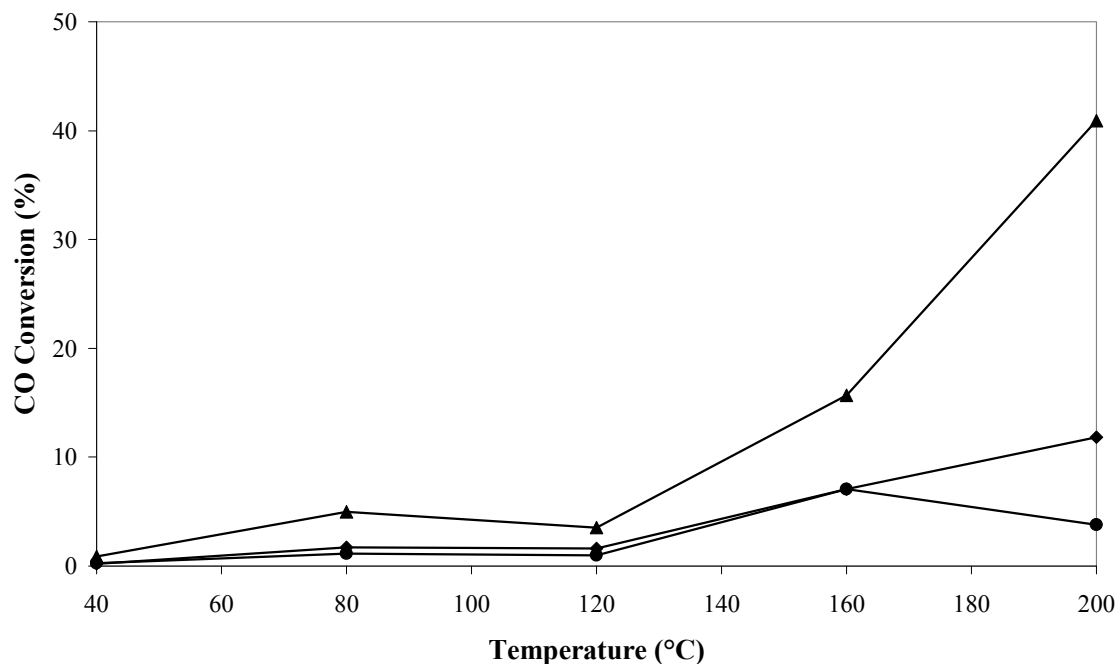


**Figure 32:** CO conversion achieved vs. reaction's temperature at  $WHSV = 180 \text{ Ndm}^3/\text{h}\cdot\text{g}_{cat}$ , feed  $O/CO = 2$  over (▲) Zeolite-Y, (◆) ZSM-5/35 and (●) Mordenite catalyst.

Zeolite Y exhibited higher activities than mordenite and ZSM-5/35. Similar results were also obtained under different experimental conditions (Figure 33).

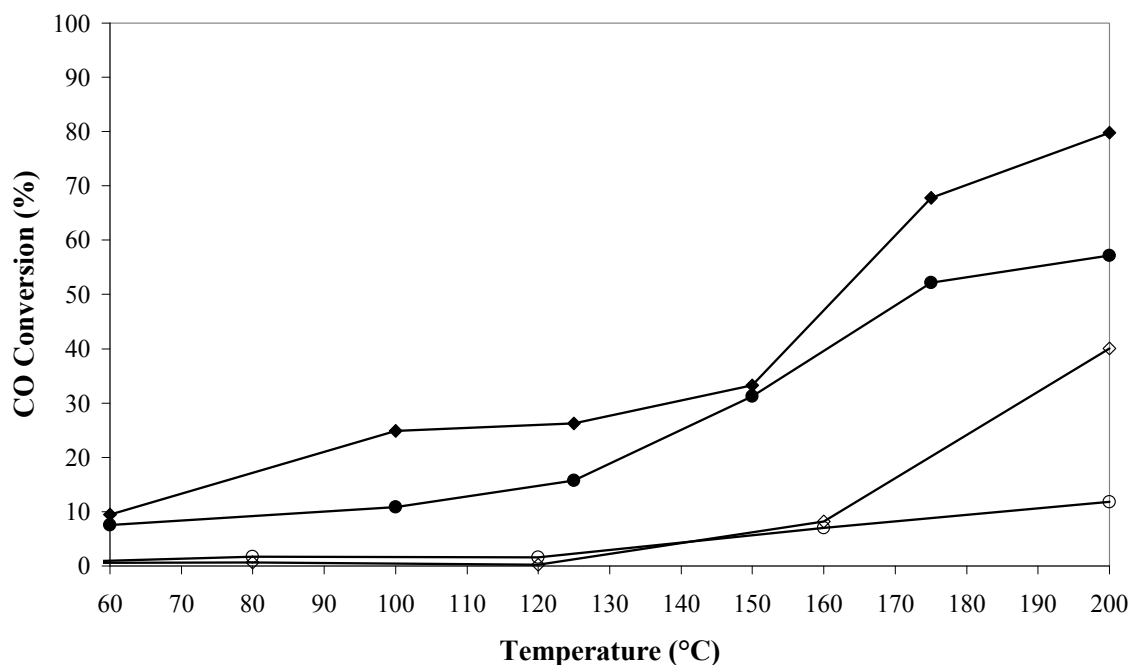


**Figure 33:** CO conversion achieved vs. reaction's temperature at  $WHSV = 180 \text{ Ndm}^3/\text{h}\cdot\text{g}_{cat}$ , feed  $O/CO = 4$  over (◆) Zeolite-Y and (●) ZSM-5/35 catalyst. Solid symbols denote calcination at  $400 \text{ }^\circ\text{C}$  and reduction at  $60 \text{ }^\circ\text{C}$  under  $60 \text{ ml/min H}_2$  flow. Open symbols denote calcination at  $300 \text{ }^\circ\text{C}$  without reduction.

As mentioned before, the catalytic activity of zeolite catalysts for the preferential oxidation of carbon monoxide depends on aluminium loading. The higher loading of aluminium on the surface of Y-type zeolite can prevent the sintering of metal species providing a more hydrophilic environment for them; therefore, higher catalytic activity for carbon monoxide oxidation can be achieved.

As it is depicted in Figure 32 and Figure 33, the catalytic activity and the stability of Y-type zeolite were higher than those of mordenite or ZSM-5/35. Mordenite can possibly facilitate the sintering of platinum. In contrast, the pores in Y-type zeolite can prevent the sintering of platinum during carbon monoxide oxidation [112].

The influence of the calcination temperature and the pretreatment method on the activity was also remarkable. It is reported, that each zeolite requires specially and unique elaborateness [113].

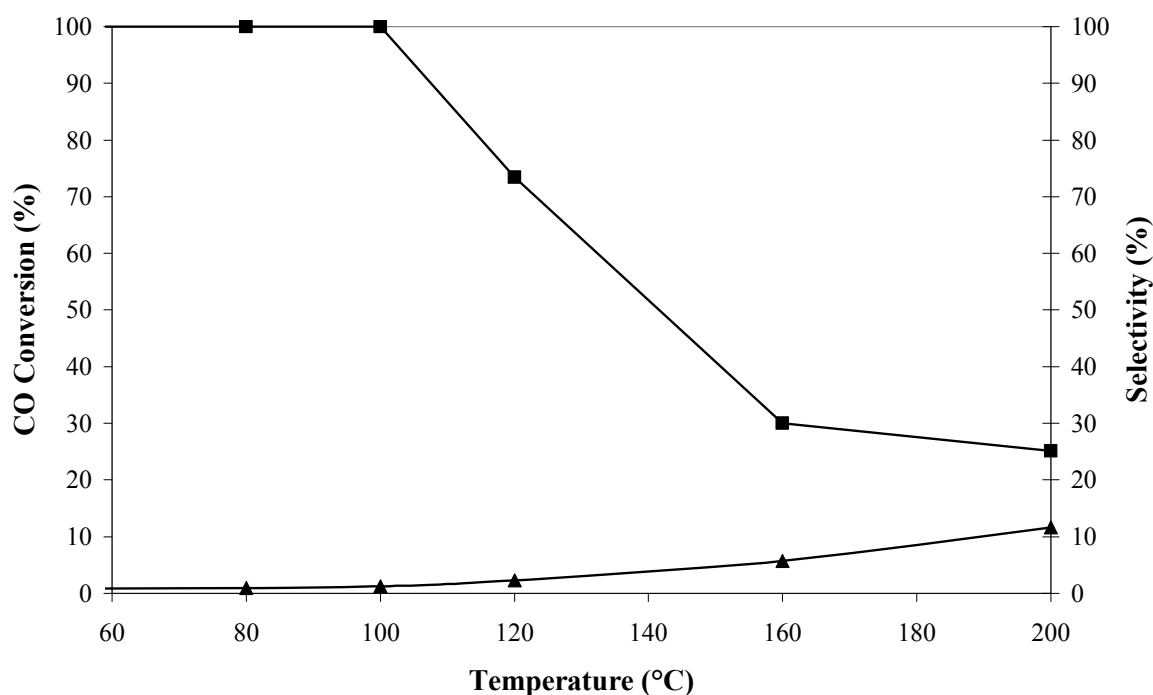


**Figure 34:** CO conversion and selectivity achieved vs. reaction's temperature over 0.5 wt.% Pt/Mordenite catalyst, feed O/CO = 3, WHSV = 180 Ndm<sup>3</sup>/h·g<sub>cat</sub>, (▲) conversion and (■) selectivity.

In the case presented in Figure 32 and in Figure 34, the platinum-mordenite catalyst does not show significant abilities to catalyze selectively carbon monoxide oxidation. Although pretreatment conditions, reported in literature [114] (1 hour at 300 °C in 60 ml/min H<sub>2</sub> flow), were followed, the results obtained were not encouraging.

Recently, it was reported that platinum-iron/mordenite exhibited higher carbon monoxide

conversion and selectivity than platinum/mordenite catalyst [114]. For this purpose a catalyst was prepared and the results are depicted in Figure 35.

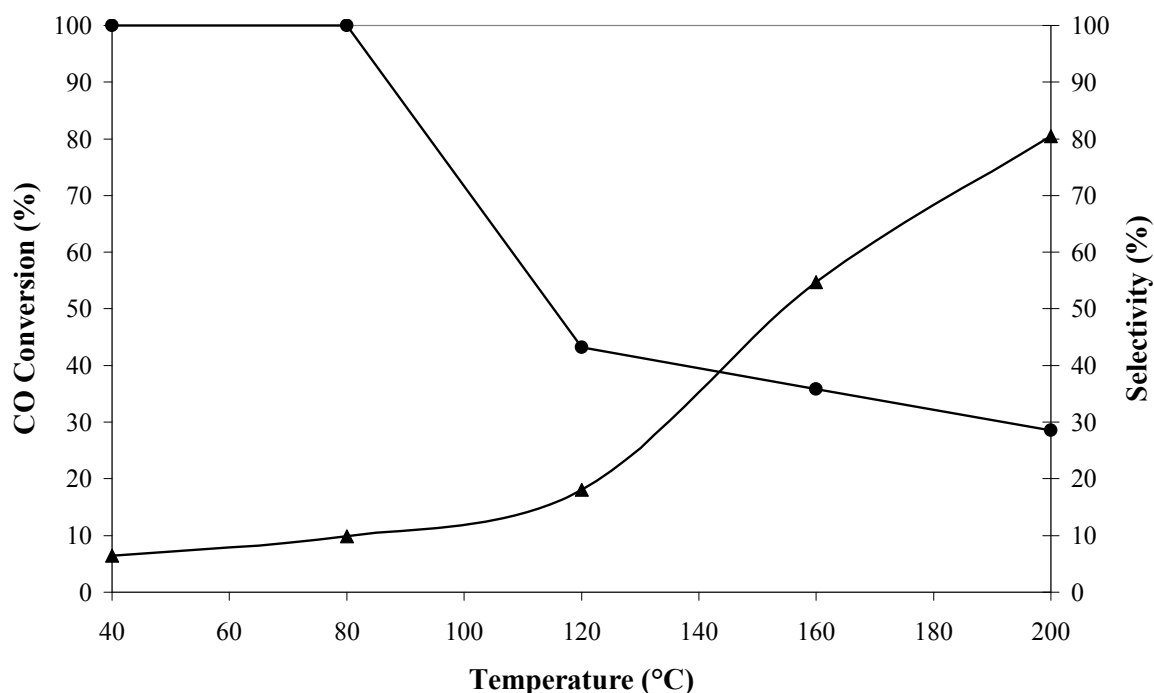


**Figure 35:** *CO conversion and selectivity achieved vs. reaction's temperature over platinum-iron/mordenite catalyst, feed O/CO = 2, WHSV = 180 Ndm<sup>3</sup>/h·g<sub>cat</sub> (▲) conversion and (●) selectivity.*

There are remarkable prospects for some catalysts, namely platinum supported in ZSM-5/100 and platinum-iron ion-exchanged in mordenite.

Although platinum-mordenite and iron-mordenite had negligible activity for the preferential oxidation of carbon monoxide, it is believed that platinum sites act as adsorption sites for carbon monoxide and for hydrogen, while iron (dominantly FeO) sites only for oxygen. In this way, the addition of iron to platinum-mordenite can preserve oxygen adsorption sites for the preferential oxidation reaction, even in excess of hydrogen gas flow. The poor reactivity of platinum-mordenite can be ascribed to the lack of carbon monoxide and of oxygen adsorption as the essential requisite for the Langmuir-Hinshelwood mechanism. This was proposed as a bifunctional mechanism for the distinctive performance at platinum-iron/mordenite, where the platinum site acts as a carbon monoxide adsorption site and the iron site acts as an oxygen dissociative-adsorption site and enhances the surface reaction between the reactants on the neighboring sites [113 – 115].

Several parameters, originally assumed to have minor effect, unexpectedly played a significant role for the activity (e.g. heating rate, flow rate during calcination and reduction).

Calcination temperature and heating rate as well, seem to be crucial to the catalyst performance. The necessity to use a very low heating rate, near 0.2 °C/min, is explained by the slow desorption of water and ammonia from the microporous zeolite in combination with the stabilization of mobile platinum species by the cavity walls of zeolite. Besides, greater heating rate leads to unstable zeolite pores. The calcinations must be done under continuous flow in order to secure the complete water sewerage from zeolite pores [116].

### 2.3.3 Other noble metal catalysts

For low temperature fuel cells the final removal of residual carbon monoxide in the hydrogen is of importance. It is presently achieved by oxidation with various noble metal containing catalysts. However, these suffer under unselective oxidation and thus also reduce the hydrogen content. Highly active and selective carbon monoxide oxidation catalysts are required. Hence, the conversion and the selectivity achieved in a single microreactor coated with a Pt-Rh/ $\gamma$ -Al<sub>2</sub>O<sub>3</sub> catalyst developed at the Institut für Mikrotechnik and a Pt<sub>0.5</sub>Al<sub>1</sub>Mn<sub>7</sub>Co<sub>91.5</sub>O<sub>x</sub> catalyst synthesized at the University of Saarbrücken for the preferential oxidation of carbon monoxide in the presence of excess hydrogen were examined and presented in Figure 36 and Figure 37, respectively. These platinum-based catalysts were selected as reference catalysts.

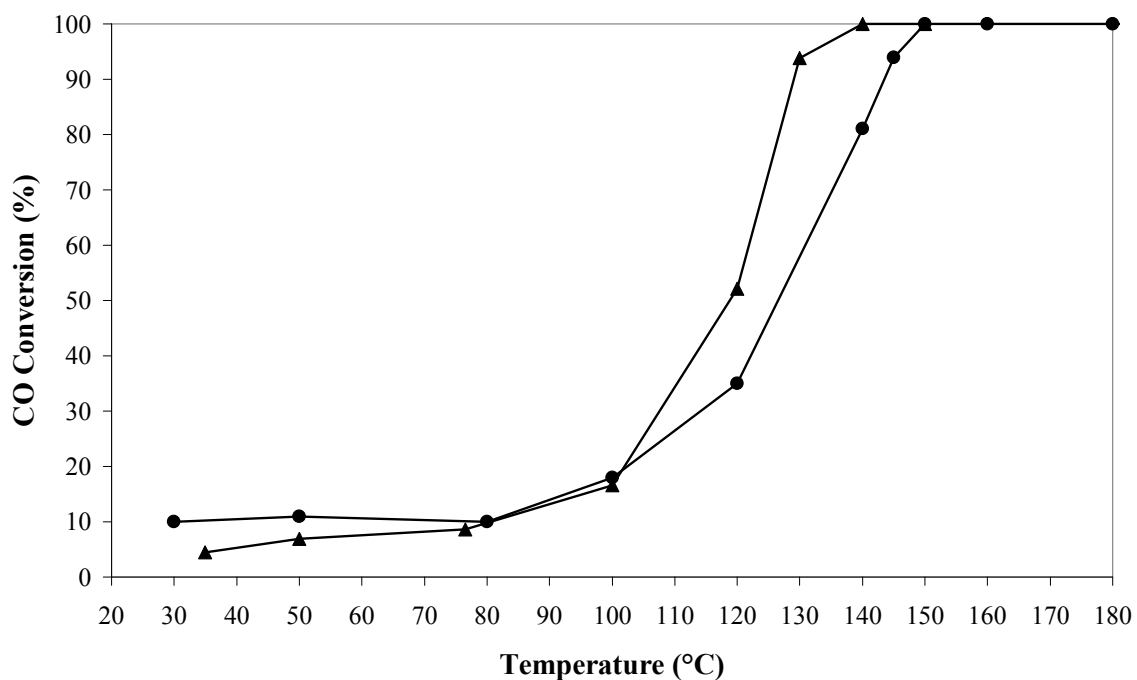


**Figure 36:** CO conversion achieved vs. reaction's temperature at WSHV = 180 Ndm<sup>3</sup>/h·g<sub>cat</sub>, feed O/CO = 4 over (▲) Pt<sub>0.5</sub>Al<sub>1</sub>Mn<sub>7</sub>Co<sub>91.5</sub>O<sub>x</sub> and (●) Pt-Rh/ $\gamma$ -Al<sub>2</sub>O<sub>3</sub> catalyst.

Important parameter for the selection and the comparison of those two catalysts was the platinum content in the mass of the catalysts. Platinum is not abundant and its high price is a drawback. However, the low content of platinum in the CoMn-catalyst, which was only 10% of that of the alumina catalyst, was a big advantage for the former.

Among the two catalysts tested, the  $\text{Pt}_{0.5}\text{Al}_1\text{Mn}_7\text{Co}_{91.5}\text{O}_x$  sample was the most active and the most selective as well, especially at lower temperatures. Indeed, under these conditions ( $\text{WHSV} = 180 \text{ Nl/h}\cdot\text{g}_{\text{cat}}$  and  $\text{O}/\text{CO} = 4$ ), the temperature at which 50% conversion of carbon monoxide was obtained,  $T_{50}$ , was found equal to  $118 \text{ }^\circ\text{C}$  ( $S_{\text{CO}} = 49\%$ ) and  $127 \text{ }^\circ\text{C}$  ( $S_{\text{CO}} = 22\%$ ) for the  $\text{Pt}_{0.5}\text{Al}_1\text{Mn}_7\text{Co}_{91.5}\text{O}_x$  and  $\text{Pt-Rh}/\gamma\text{-Al}_2\text{O}_3$  respectively. The maximum carbon monoxide conversion achieved over the  $\text{Pt}_{0.5}\text{Al}_1\text{Mn}_7\text{Co}_{91.5}\text{O}_x$  sample was 100% ( $S_{\text{CO}} = 25\%$ ) at  $140 \text{ }^\circ\text{C}$ . The temperature at which full carbon monoxide conversion was obtained with the  $\text{Pt-Rh}/\gamma\text{-Al}_2\text{O}_3$  was  $150 \text{ }^\circ\text{C}$  ( $S_{\text{CO}} = 25\%$ ).

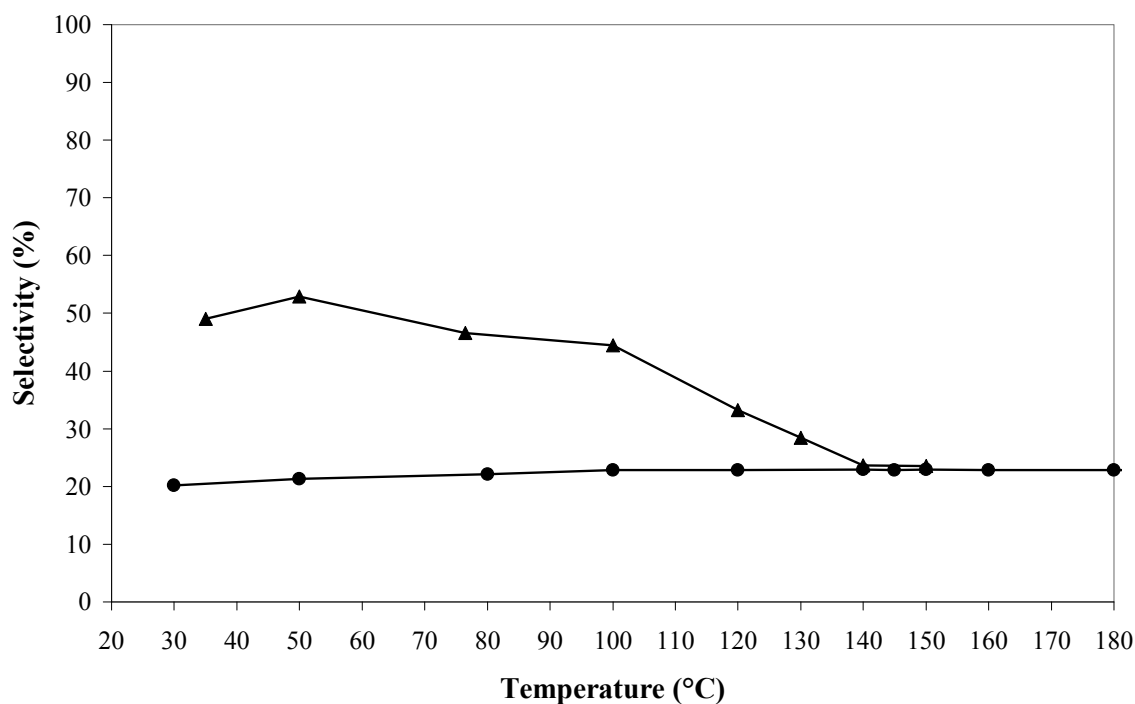


**Figure 37:** CO selectivity achieved vs. reaction's temperature at  $\text{WSHV} = 180 \text{ Ndm}^3/\text{h}\cdot\text{g}_{\text{cat}}$ , feed  $\text{O}/\text{CO} = 4$  over (▲)  $\text{Pt}_{0.5}\text{Al}_1\text{Mn}_7\text{Co}_{91.5}\text{O}_x$  and (●)  $\text{Pt-Rh}/\gamma\text{-Al}_2\text{O}_3$  catalyst.

As seen from the same figures, the influence of the reaction temperature on selectivity depends strongly on the nature of the catalyst. For the  $\text{Pt}_{0.5}\text{Al}_1\text{Mn}_7\text{Co}_{91.5}\text{O}_x$  sample, the increase of the reaction temperature is accompanied with a continuous decrease of the selectivity. Over the  $\text{Pt-Rh}/\gamma\text{-Al}_2\text{O}_3$  catalyst the selectivity remains in the range from 22 – 25% for the whole temperature range of our experiment, although the conversion of

carbon monoxide greatly increases from 10 to 100%.

### A. Effect of O/CO ratio

The process parameter  $\lambda = 2 \cdot [\text{O}_2]/[\text{CO}]$  defines the oxygen excess with respect to stoichiometric amount to oxidize carbon monoxide. As hydrogen oxidation competes with carbon monoxide oxidation in such a system, an optimum catalyst formulation must show high activity and selectivity towards carbon monoxide oxidation. Therefore, the O/CO ratio influence on the activity had to be examined.

As the selectivity is inversely proportional to the oxygen content, an ideal catalyst should be active even with low oxygen contents (low  $\lambda$  values) in order to maintain selectivity at acceptable values.

Figure 38 and Figure 39 show that with increasing oxygen concentration and within the temperature range between 80 °C and 160 °C the carbon monoxide conversion increased for both  $\text{Pt}_{0.5}\text{Al}_1\text{Mn}_7\text{Co}_{91.5}\text{O}_x$  and  $\text{Pt-Rh}/\gamma\text{-Al}_2\text{O}_3$  catalysts. Thus, with both catalysts full carbon monoxide conversion was achieved at O/CO ratio of 2 or higher.

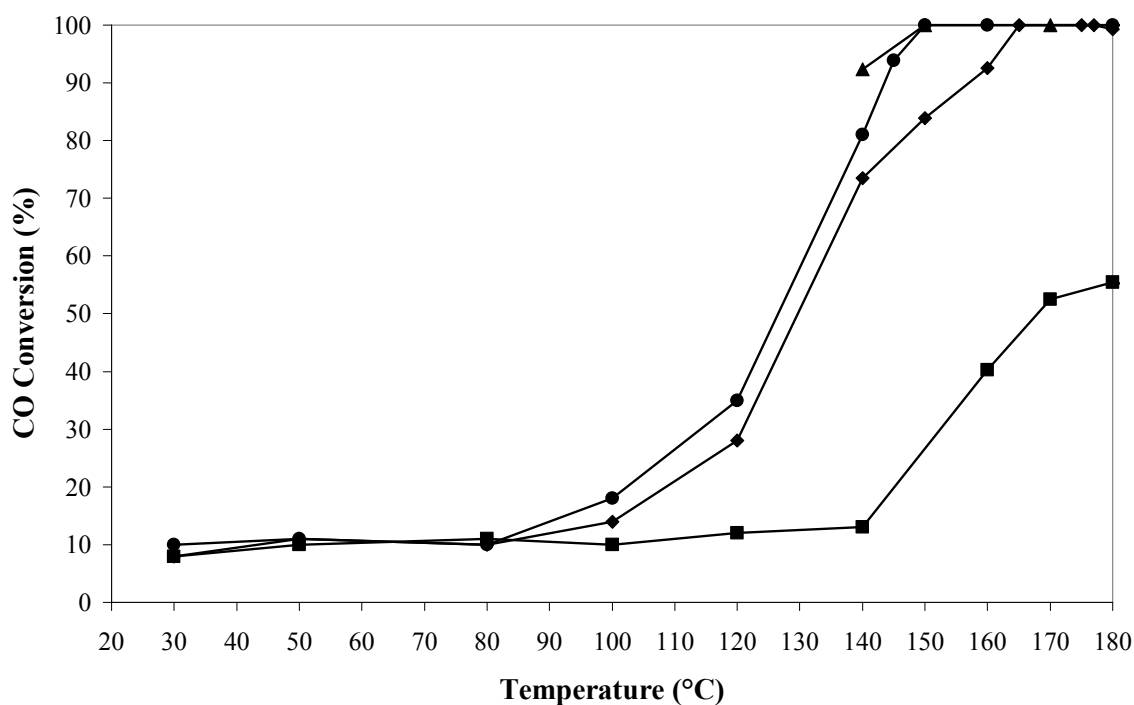


**Figure 38:** CO conversion achieved vs. reaction's temperature at  $WSHV = 180 \text{ Ndm}^3/\text{h} \cdot \text{g}_{cat}$  over  $\text{Pt-Rh}/\gamma\text{-Al}_2\text{O}_3$  catalyst at feed (▲)  $O/CO = 8$ , (●)  $O/CO = 4$ , (◆)  $O/CO = 2$  and (■)  $O/CO = 1$ .

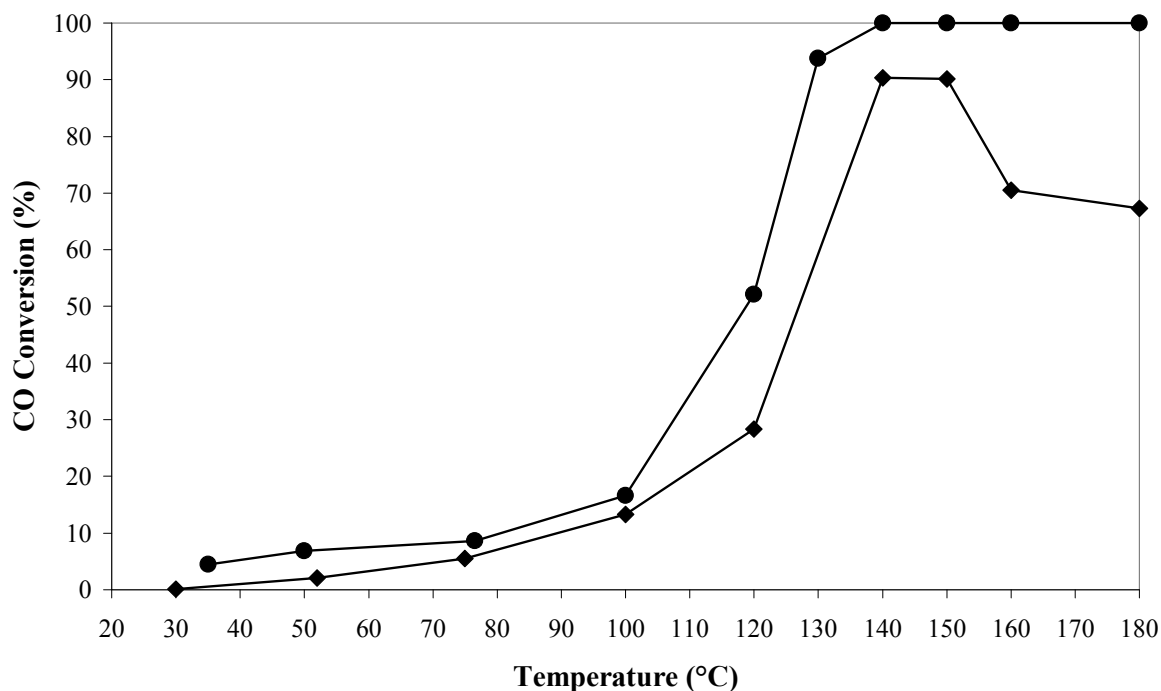


**Figure 39:** CO conversion achieved vs. reaction's temperature at  $WSHV = 180 \text{ Ndm}^3/\text{h}\cdot\text{g}_{cat}$  over  $\text{Pt}_{0.5}\text{Al}_1\text{Mn}_7\text{Co}_{91.5}\text{O}_x$  catalyst at feed (●)  $\text{O}/\text{CO} = 4$  and (◆)  $\text{O}/\text{CO} = 2$ .

Figure 40 and Figure 41 show the selectivity with varying O/CO ratio.

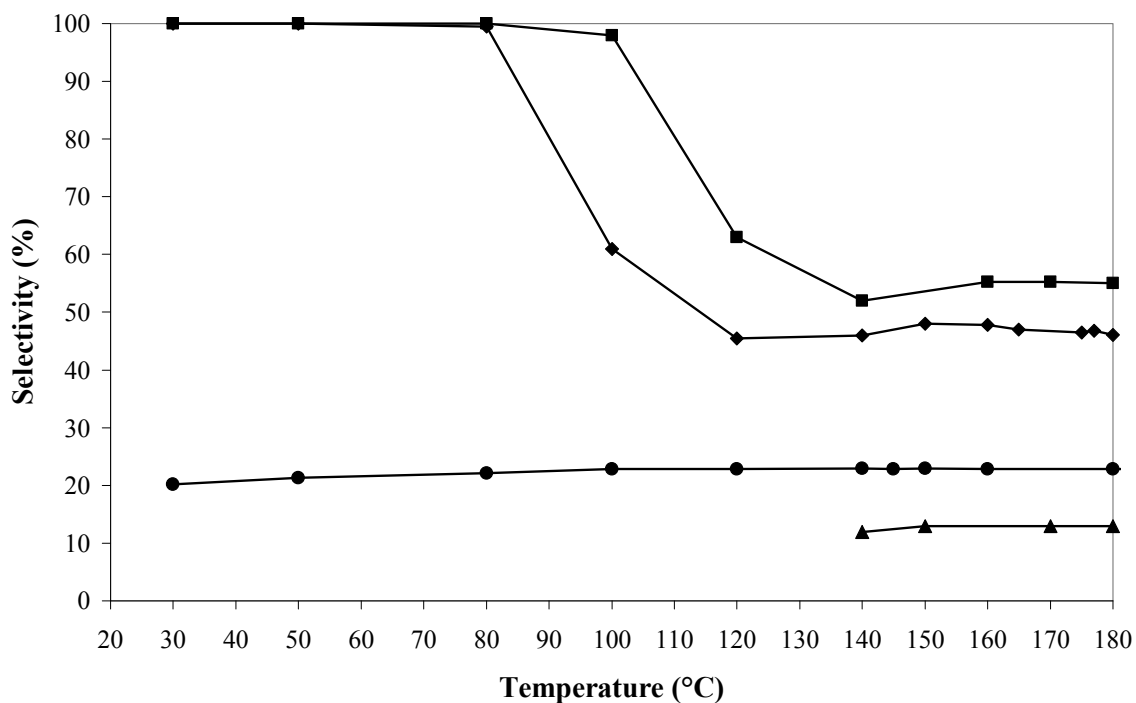


**Figure 40:** CO selectivity achieved vs. reaction's temperature at  $WSHV = 180 \text{ Ndm}^3/\text{h}\cdot\text{g}_{cat}$  over  $\text{Pt-Rh}/\gamma\text{-Al}_2\text{O}_3$  catalyst at feed (▲)  $\text{O}/\text{CO} = 8$ , (●)  $\text{O}/\text{CO} = 4$ , (◆)  $\text{O}/\text{CO} = 2$  and (■)  $\text{O}/\text{CO} = 1$ .

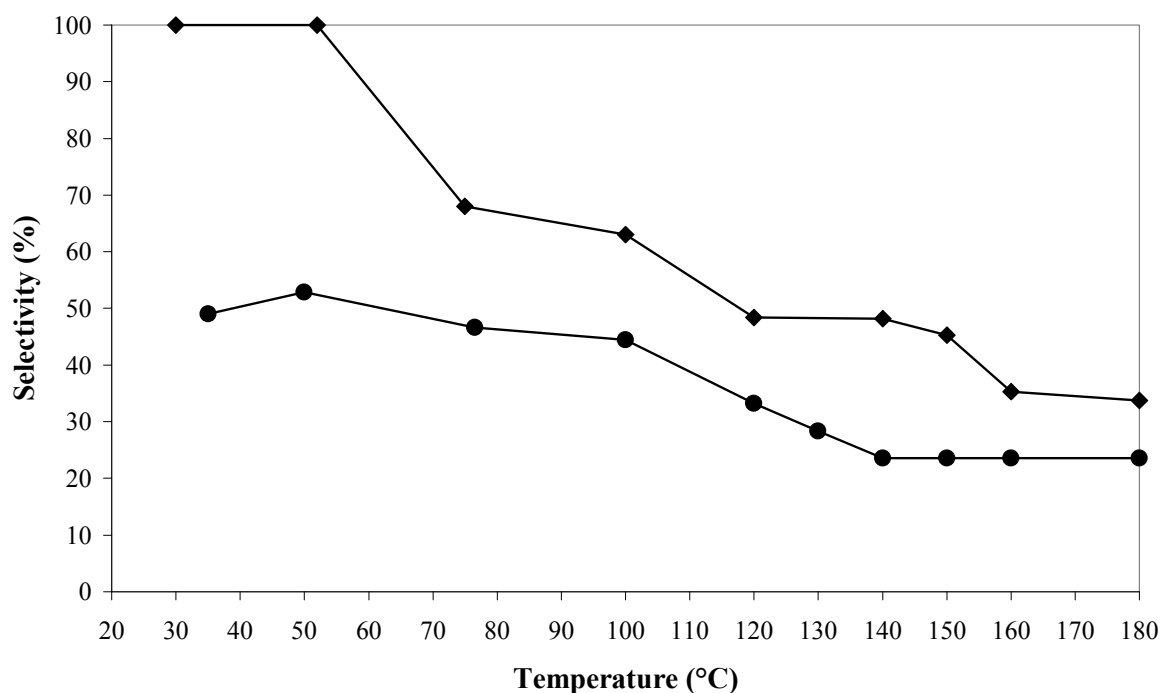


**Figure 41:** CO selectivity achieved vs. reaction's temperature at  $WSHV = 180 \text{ Ndm}^3/\text{h}\cdot\text{g}_{cat}$  over  $\text{Pt}_{0.5}\text{Al}_1\text{Mn}_7\text{Co}_{91.5}\text{O}_x$  catalyst at feed (●)  $O/CO = 4$  and (◆)  $O/CO = 2$ .

Raising the amount of oxygen inevitably led to an increase in hydrogen loss (lower selectivity). The  $\text{Pt}_{0.5}\text{Al}_1\text{Mn}_7\text{Co}_{91.5}\text{O}_x$  catalyst, which shows the higher activity and selectivity, has also limitations. It did not show stable activity at temperatures exceeding  $150 \text{ }^\circ\text{C}$  at  $O/CO = 2$ .

The reduced hydrogen consumption of the  $\text{Pt}_{0.5}\text{Al}_1\text{Mn}_7\text{Co}_{91.5}\text{O}_x$  catalyst may be attributed to a lack of  $\text{OH}^-$  groups present on its surface, as opposed to the  $\text{Pt-Rh}/\gamma\text{-Al}_2\text{O}_3$  catalyst. These  $\text{OH}^-$  groups are involved in the hydrogen oxidation mechanism and promote its conversion [46].

### B. Effect of $\text{CO}_2$ on the CO conversion over $\text{Pt}_{0.5}\text{Al}_1\text{Mn}_7\text{Co}_{91.5}\text{O}_x$

The influence of the presence of 15 Vol.%  $\text{CO}_2$  on the carbon monoxide conversion with  $\text{Pt}_{0.5}\text{Al}_1\text{Mn}_7\text{Co}_{91.5}\text{O}_x$  catalyst is shown in Figure 42 and Figure 43. Carbon dioxide generally decreases conversion slightly, which is quantified in an increase of the temperature  $T_{50}$  from  $115 \text{ }^\circ\text{C}$  to  $118 \text{ }^\circ\text{C}$ . Remarkable is the influence indicated on the selectivity, showing that carbon dioxide obviously blocks the active sites required for the hydrogen oxidation thus increasing the selectivity, especially at lower temperatures.

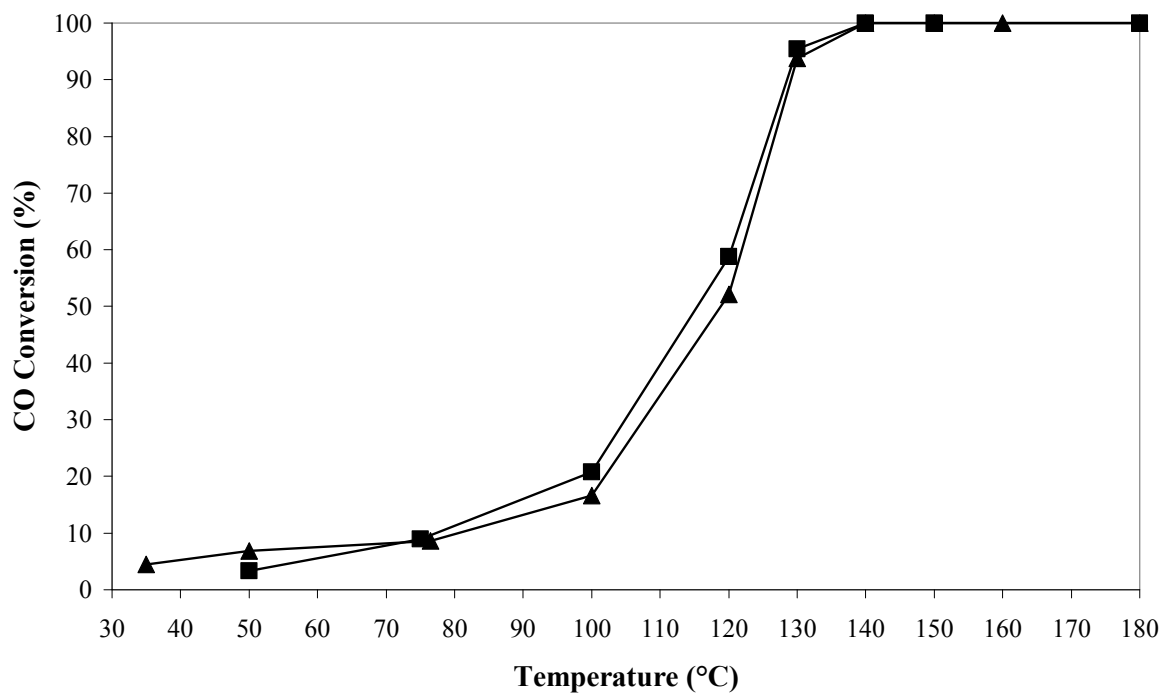


**Figure 42:** CO conversion achieved vs. reaction's temperature at  $WSHV = 180 \text{ Ndm}^3/\text{h}\cdot\text{g}_{cat}$ , feed  $O/CO = 4$  over  $Pt_{0.5}Al_1Mn_7Co_{91.5}O_x$  catalyst (■) in the absence of  $CO_2$  and (▲) in the presence of 15 Vol.%  $CO_2$ .

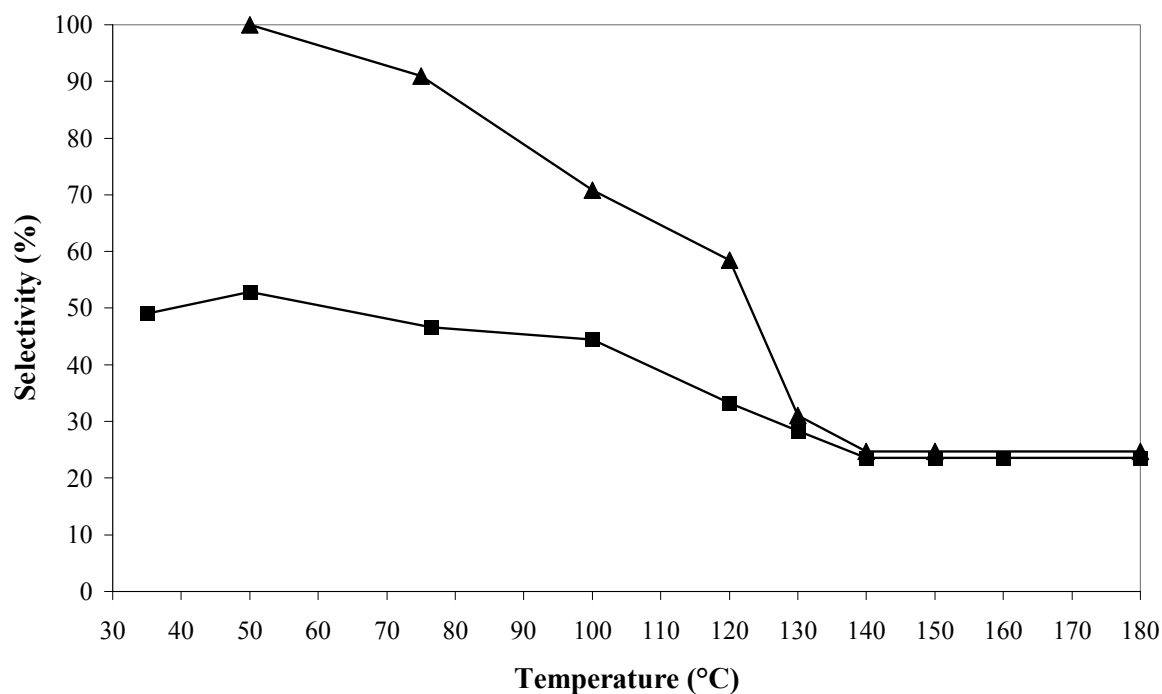


**Figure 43:** CO selectivity achieved vs. reaction's temperature at  $WSHV = 180 \text{ Ndm}^3/\text{h}\cdot\text{g}_{cat}$ , feed  $O/CO = 4$  over  $Pt_{0.5}Al_1Mn_7Co_{91.5}O_x$  catalyst (■) in the absence of  $CO_2$  and (▲) in the presence of 15 Vol.%  $CO_2$ .

This however is not a benefit under realistic operating conditions, because full conversion of carbon monoxide requires temperatures, where the selectivity increase through carbon dioxide becomes negligible (Figure 43).

### C. Effect of space velocity

As the application of the present preferential oxidation catalysts are fuel cell systems, it was important to determine the effect space velocity has on its performance as it reflects transient operating conditions. The Pt-Rh/ $\gamma$ -Al<sub>2</sub>O<sub>3</sub> catalyst showed full conversion at different WSHV between 90 and 270 Ndm<sup>3</sup>/h·g<sub>cat</sub>, at O/CO = 4 at 160 °C.

### D. Catalysts long term experiments

Prior to the long term testing of the Pt-Rh/ $\gamma$ -Al<sub>2</sub>O<sub>3</sub> catalyst its short term durability was investigated by stepwise increasing the reaction temperature as shown in Figure 44.

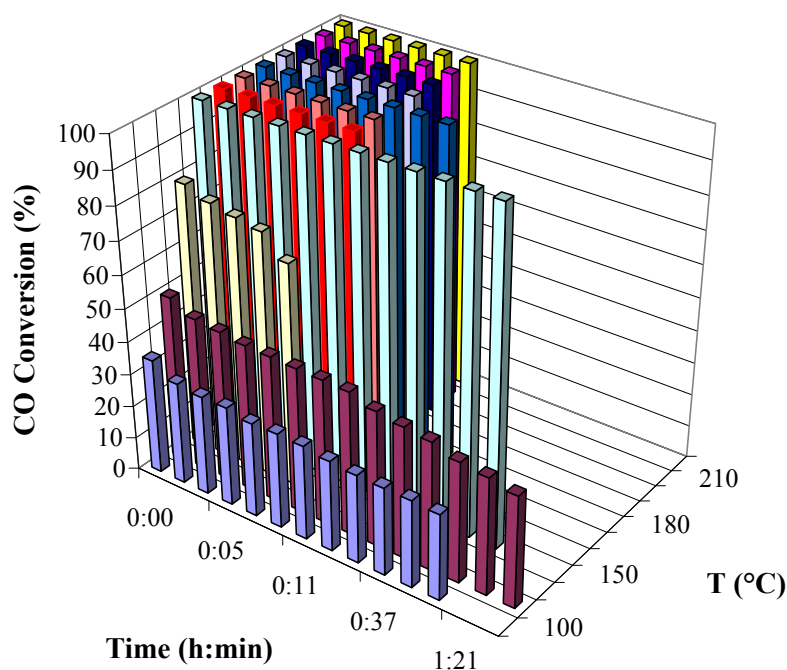


**Figure 44:** Pt-Rh/ $\gamma$ -Al<sub>2</sub>O<sub>3</sub> catalyst durability, feed O/CO = 4 and WSHV = 180 Ndm<sup>3</sup>/h·g<sub>cat</sub>.

With increasing temperature the durability and activity of the catalyst increased. At 120 °C full conversion was achieved but did last not more than 1 – 2 h. Above this temperature its durability and activity increased again showing full conversion up to 200 °C reaction temperature. The reaction temperature was then decreased to 160 °C and the reactor was

operated for 72 h at this temperature. The catalyst showed stable activity during this period. In addition, the catalyst exhibited a broad operating temperature window (from 160 °C to 200 °C); while the carbon monoxide content was below 10 ppm. This factor is important when considering temperature fluctuations typically experienced during operation of a fuel processor.

In Figure 45 and Figure 46, is shown  $Pt_{0.5}Al_1Mn_7Co_{91.5}O_x$  catalyst tested at 145 °C and 150 °C for 50 h and 70 h respectively.

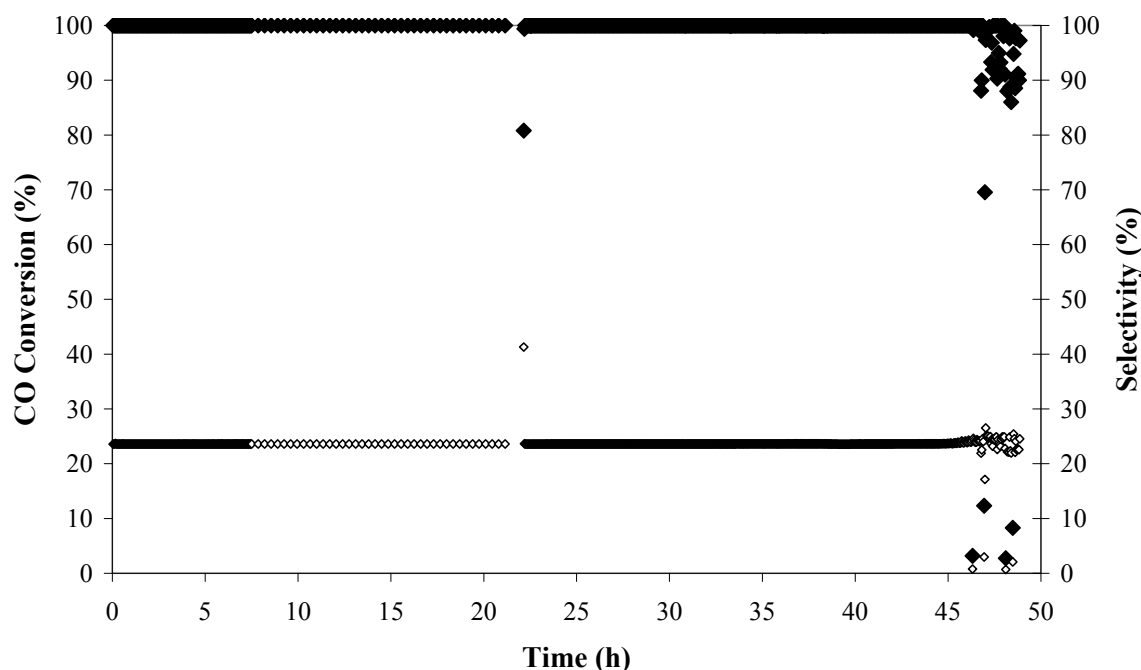


**Figure 45:** CO conversion and selectivity achieved vs. time over  $Pt_{0.5}Al_1Mn_7Co_{91.5}O_x$  catalyst at 145 °C,  $WSHV = 180 Ndm^3/h \cdot g_{cat}$ , feed  $O/CO = 4$ , (◆) Conversion and (◇) Selectivity.

Full conversion of carbon monoxide to concentrations below 10 ppm was initially achieved for both temperatures. However, at 145 °C reaction temperature, the catalyst showed rapid deactivation after 45 h.

When increasing the reaction temperature to 150 °C, the durability and the activity were again increased and were stable for the 72 h testing period.

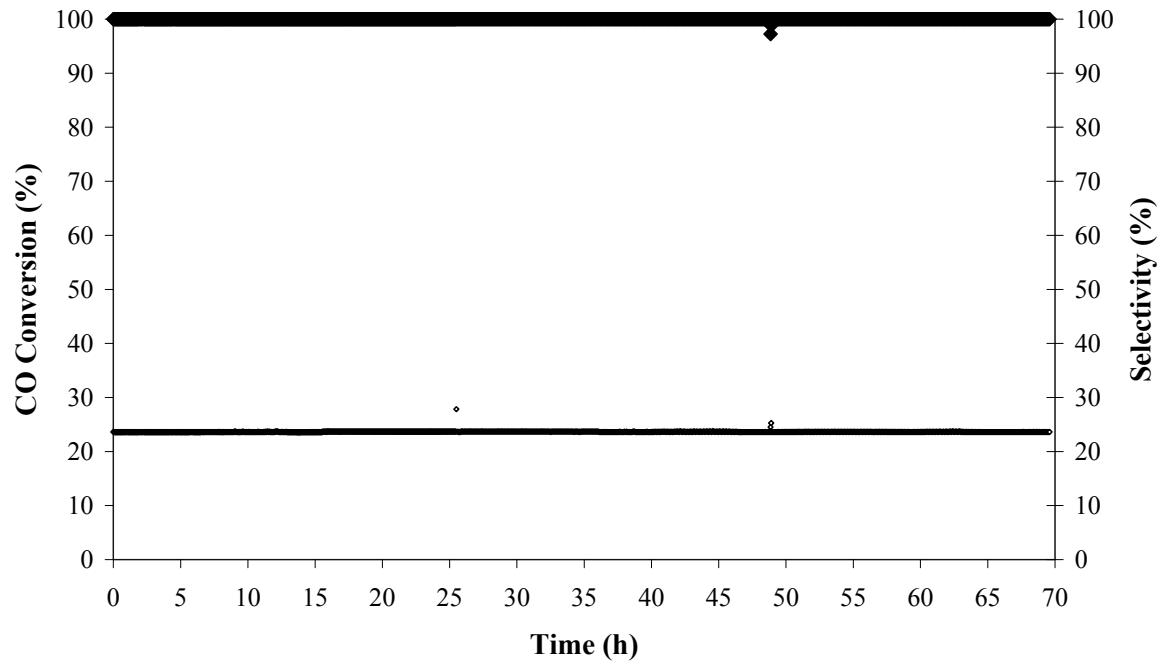


**Figure 46:** CO conversion and selectivity achieved vs. time over  $Pt_{0.5}Al_1Mn_7Co_{91.5}O_x$  catalyst at 150 °C,  $WSHV = 180 Ndm^3/h \cdot g_{cat}$ , feed  $O/CO = 4$ , (◆) Conversion and (◇) Selectivity.

## 2.4 Residence time distribution and reactor model

In practice the reactors used are never ideal; they can often be far from that. There are several reasons for this: the flow may have a preferable path in the reactor, it can circulate in the reactor or dead zones may exist [87].

In order to predict the behavior of a non-ideal reactor, the flow of matter through the single microreactor should be determined. This can be done by measuring for how long each molecule stays in the reactor, because typically molecules that travel different paths have different residence times. Marker experiments give the age distribution of the molecules in a flow. Figure 47 shows the results from the measurements performed at a feed flow rate of 100 ml/min (Standard Temperature and Pressure) through the recycle reactor at recycle ratio of 35. It is convenient to represent the RTD of the recycle setup used as normalized distribution.

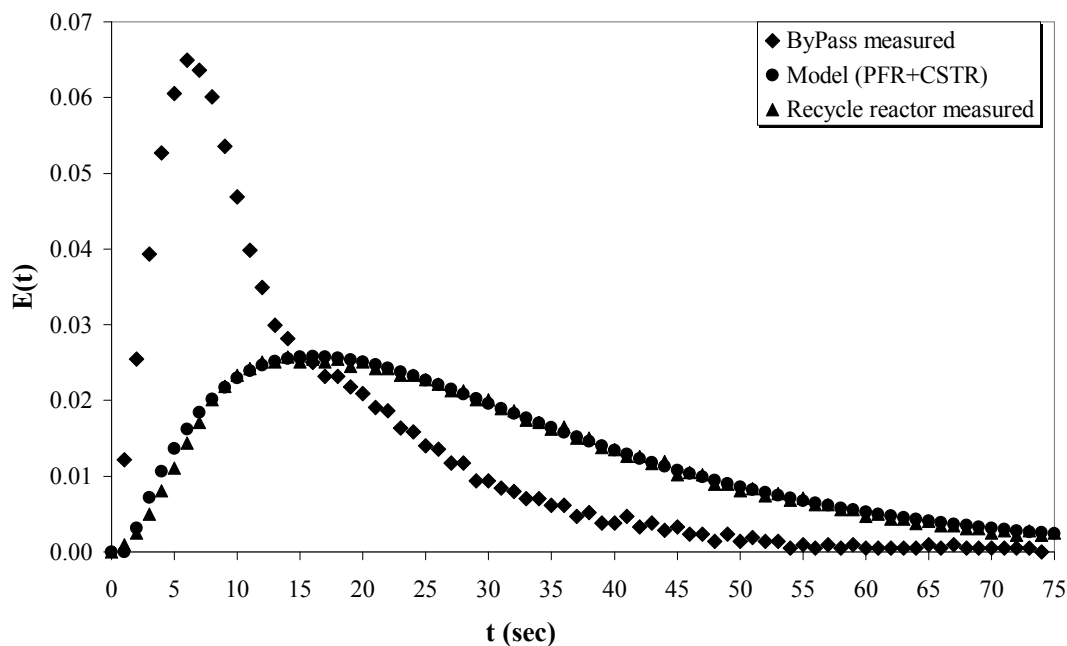


**Figure 47:** Residence time distribution for a Plug Flow Reactor followed by a Continuous Stirred Tank Reactor.

The tracer signal fed to the reactor was determined in bypass and fed to the reactor model. The bypass measurement shows the input signal fed to the recycle reactor (Figure 48a). The response of the recycle reactor is also plotted. This behavior deviates from the ideal CSTR. To represent this behavior different models were employed. A combination of a PFR connected in series with a CSTR (Figure 48b) agrees well with the experimental setup.

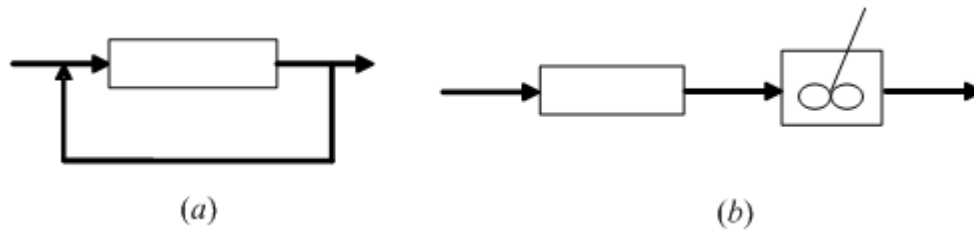


**Figure 48:** (a) Recycle reactor used and (b) PFR and CSTR reactors connected in series.

#### 2.4.1 Reactor model

The predicted model and the experimental results are in a good agreement as it is depicted. The delay of the reactor response observed (Figure 47) was thought to originate from the tube installed before and after the recycle reactor and connects the sample loop with the recycle reactor and the IR-sensor. This tube was modeled as the Plug Flow Reactor (PFR). The results obtained with this model (PFR + CSTR) revealed best agreement between predicted and experimentally determined reactor response. Table 7 provides a comparison of model parameters (reactor volumes) and the actual values of the experimental setup. For comparison purposes, the mean residence time ( $t_m$ ) was calculated by integrating the RTD:

$$t_m = \int_0^{\infty} tE(t)dt \quad (8)$$

**Table 7:** Characteristics of the model applied.

	Real	Model
<b>Volume (ml)</b>	19	19.2
<b>Mean residence time (sec)</b>	15.7	15.9
<b>Mean (%)</b>	2	

The good agreement of the model with the experiments justifies the assumption that the recycle loop behaves as a CSTR, while the pipes installed before and after the loop as a PFR. Additionally, high recirculation rates, mentioned above, also permit high gas velocities over the catalyst coating without the use of excessive quantities of reactants. Thus, mass transfer limitations can be eliminated even for very rapid reactions. Assuming that the overall rate of reaction is limited at low recirculation rates by the rate of mass transfer, then as the recirculation rate is increased the total conversion remains constant. When a certain recirculation rate is exceeded, any change of recirculation rate does not affect the conversion. This is shown in Figure 49.

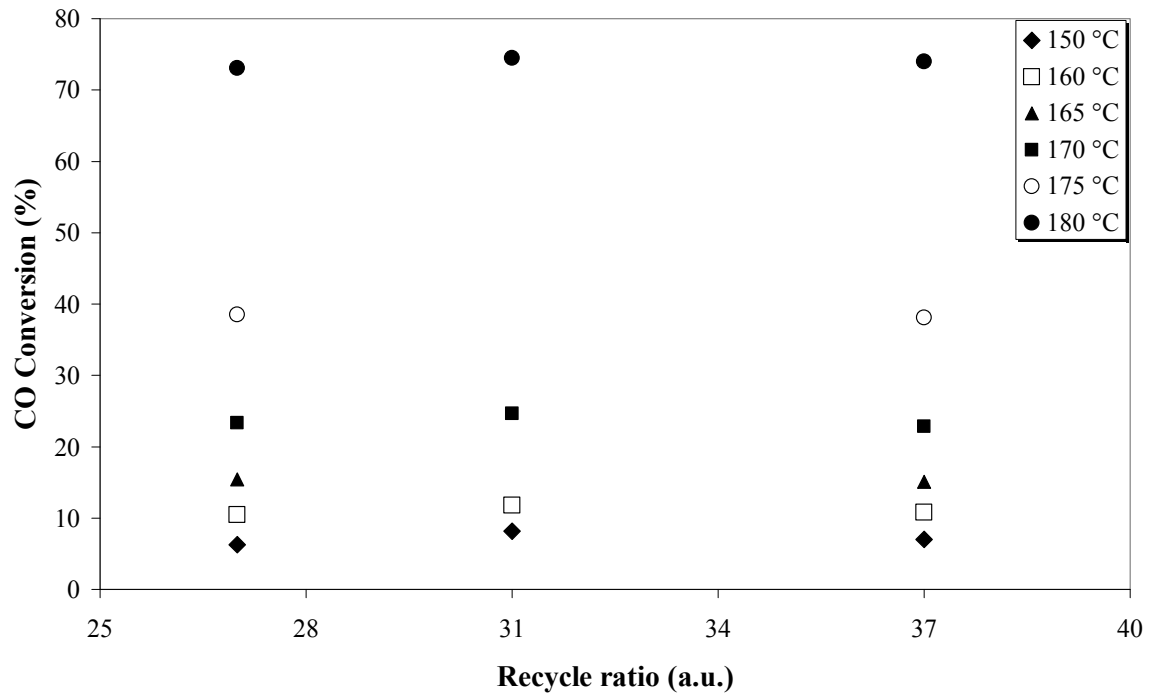


**Figure 49:** Effect of recirculation rate on CO conversion (0.5 Vol.% CO, O/CO = 4 and N<sub>2</sub> in balance).

Since the conversion of carbon monoxide is independent from the flow rate for the whole temperature-range and thus from the recirculation rate, the mass transfer limitation is negligible and can be ignored [117].

## 2.5 Kinetic measurements

In the following chapter, the conversion of the carbon monoxide oxidation in simulated reformer gas and how each component influences the reaction rate, will be discussed in detail. A proper method for the characterisation of the reactor will be also analysed. The standard method for the determination of reaction orders is to vary the inlet partial pressure or concentration of one of the reactants, while keeping all other reactants constant. In the present study, however, this approach was not followed, since it would entail measurements over a large range of O/CO ratios, which is undesirable for two reasons: (a) prime criterion for the preferential carbon monoxide oxidation is the minimization of hydrogen oxidation and thus the relevant range of the O/CO ratio was limited ( $\lambda \sim 1 - 4$ ); (b) a large variation between different reaction regimes, which would invalidate the experimental approach because of a change in mechanism. Therefore, the carbon monoxide concentration dependence was investigated by changing the carbon dioxide concentration at relatively constant O/CO ratio rather than at constant oxygen concentration and thus the use of the inclination as an exponent is implicit [50].

It will, however, be shown that it can be deduced from the measured data by means of a numerical fit of the  $r_{CO}$  data to a kinetic rate expression. This will provide an accurate method for data interpolation and will in turn allow the comparison between the reaction rates measured in this work and data resulting from the model. Finally we will discuss the effect of hydrogen, carbon dioxide and steam on the rate of carbon monoxide oxidation.

### 2.5.1 CO oxidation without $H_2$

The data for estimation of the parameters were obtained with the catalyst containing 5 wt.% Pt and 5 wt.% Rh. Maximum conversion under the test conditions was 15%, as it can be seen in Figure 50.

The rate of the carbon monoxide oxidation in the absence of any other gases can be described by equation (9):

$$r_{CO} = k_0 \cdot e^{-\frac{E_A}{R \cdot T}} \cdot [CO]^\alpha \cdot [O_2]^\beta \cdot [H_2]^\gamma \cdot [CO_2]^\delta \quad (9)$$

All experiments were accomplished with  $WHSV = 180 \text{ dcm}^3/\text{h} \cdot \text{g}_{\text{cat}}$ , which is a realistic value. The ranges of the experimental conditions covered are listed in Table 8.

**Table 8:** Range of experimental conditions during the CO oxidation over Pt-Rh/ $\gamma$ -Al<sub>2</sub>O<sub>3</sub>. N<sub>2</sub> is used in a balance.

<b>Total Feed [ml/min] (STP)</b>	100
<b>CO [ml/min] (STP)</b>	0.5 – 2.0
<b>O/CO ratio (-)</b>	1.0 – 4.0
<b>T (°C)</b>	130 – 180

The reformat temperature was kept below 180 °C to remain in a realistic range [45, 118 – 120].

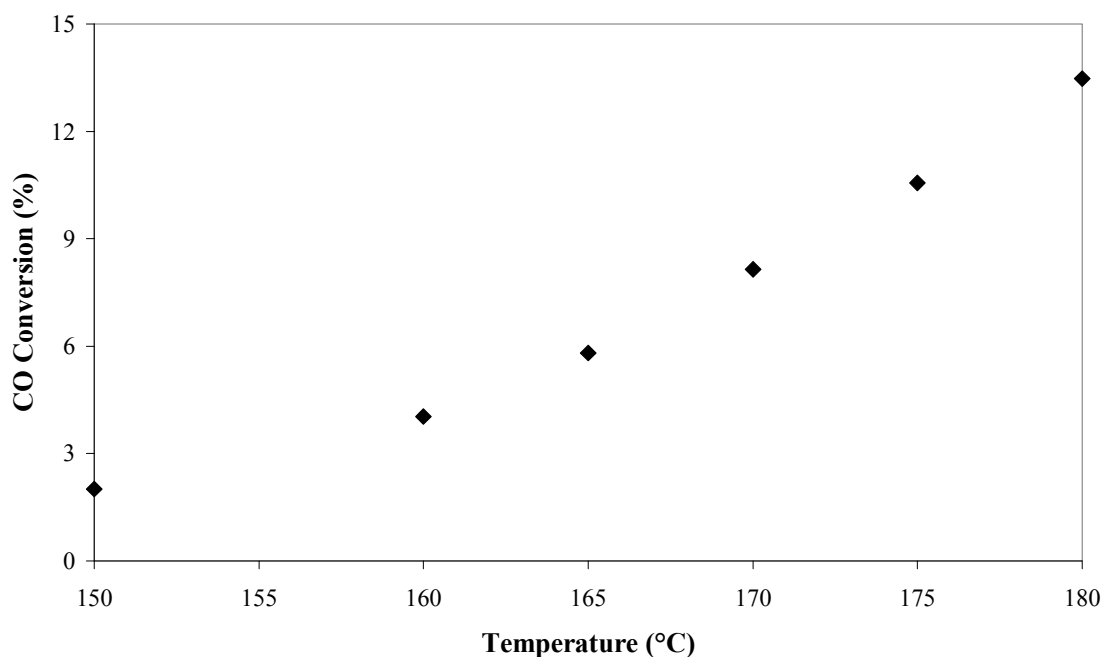
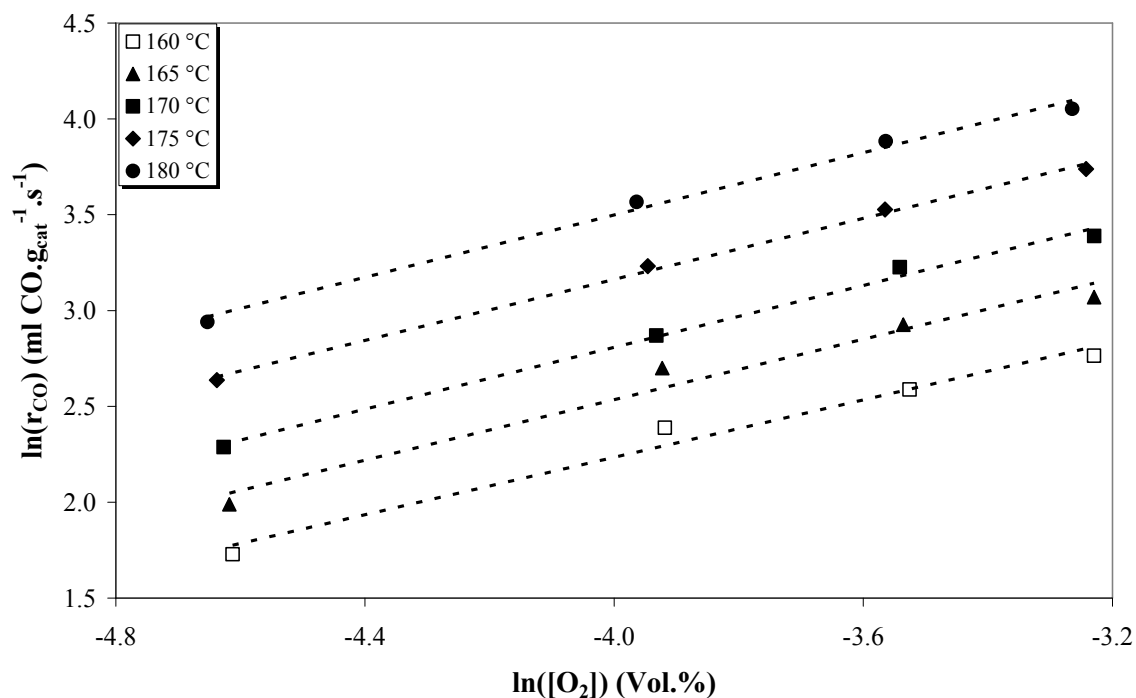


**Figure 50:** CO conversion achieved vs. reaction's temperature over Pt-Rh/ $\gamma$ -Al<sub>2</sub>O<sub>3</sub> catalyst (1.5 Vol.% CO, O/CO = 3 and N<sub>2</sub> in balance).

Figure 51 shows the oxidation rate as a function of oxygen output concentration for a carbon monoxide concentration of 2 Vol.%.

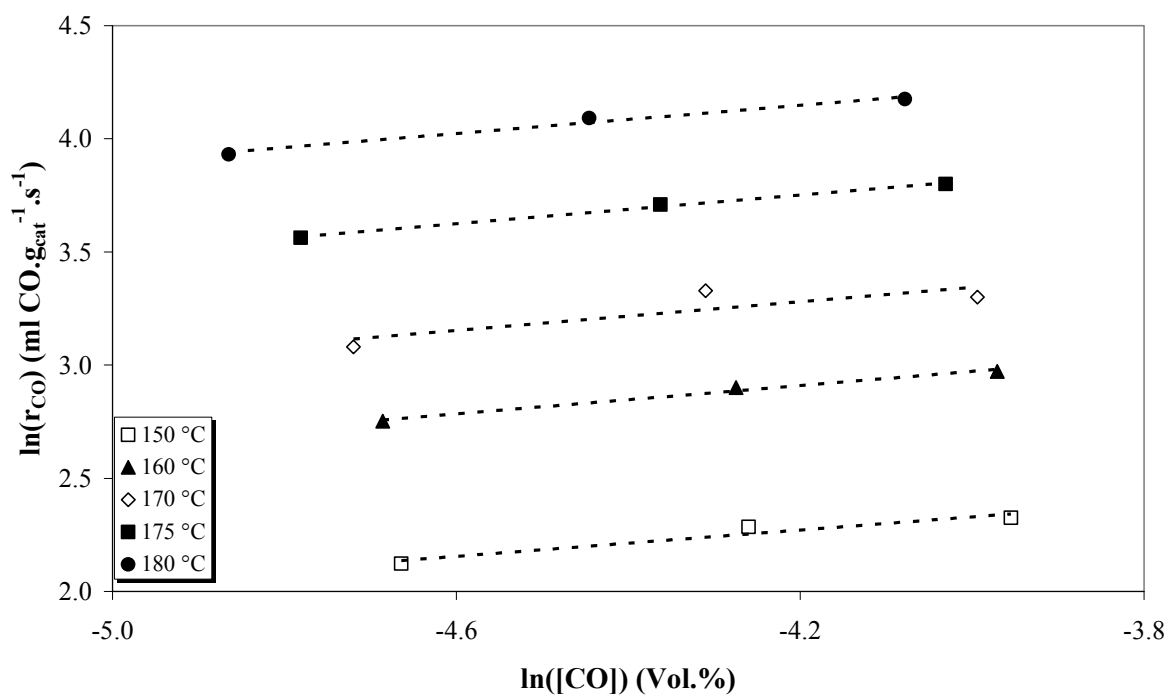
The least-squares regression line fitted the data with slope near 0.8, which corresponds to the exponent  $\beta$  for the oxygen concentration in equation (9).

Figure 52 shows the carbon monoxide oxidation rate versus carbon monoxide outlet concentration.



**Figure 51:** CO reaction rate vs.  $O_2$  concentration over  $Pt-Rh/\gamma-Al_2O_3$  catalyst (2 Vol.% CO,  $O_2$  and  $N_2$  in balance).

The reaction order of carbon monoxide was determined to  $\alpha_{CO} = -0.53$ . This is in reasonable agreement with the data found in literature [50 and 121].



**Figure 52:** CO reaction rate vs. CO concentration over  $Pt-Rh/\gamma-Al_2O_3$  catalyst ( $O/CO = 4$ , CO and  $N_2$  in balance).

With exponents being known, the rate constant can be readily determined. Figure 53 shows the temperature dependence of the rate in the range of 160 – 180 °C.

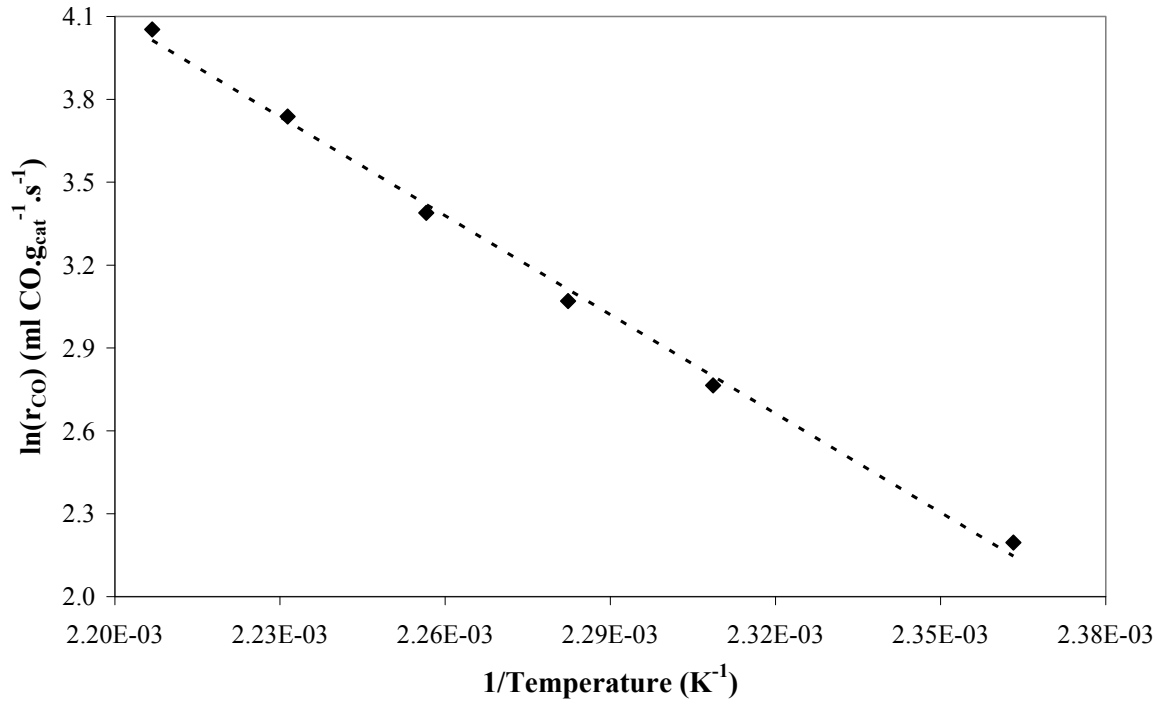


**Figure 53:** Arrhenius plot of the rate constant for CO oxidation over Pt-Rh/ $\gamma$ -Al<sub>2</sub>O<sub>3</sub> catalyst (O/CO = 4, 2.0 Vol.% CO and N<sub>2</sub> in balance).

The apparent activation energy from the least squares regression was 94.2 kJ/mole. The pre-exponential factor  $k_0$  was estimated near  $6.4 \times 10^{12} \text{ ml}^{0.74} \cdot \text{g}_{\text{cat}}^{-1} \cdot \text{s}^{-1}$ .

The confidence interval was 95 %. The parameters are summarized in Table 9.

**Table 9:** Confidence intervals of the kinetic parameters estimated by regression method for CO oxidation without H<sub>2</sub> for equation (9).

$\alpha$ (-)	-0.53±0.06
$\beta$ (-)	0.79±0.14
$\gamma$ (-)	0
$\delta$ (-)	0
$E_A$ (kJ/mole)	94.2±6.47
$k_0$ (ml <sup>0.74</sup> ·g <sub>cat</sub> <sup>-1</sup> ·s <sup>-1</sup> )	$6.4 \times 10^{12 \pm 0.87}$

From these calculated parameters, the rate model becomes:

$$r_{CO} = 6.4 \cdot 10^{12} \cdot e^{-\frac{94.2}{R \cdot T}} \cdot [CO]^{-0.53} \cdot [O_2]^{0.79} \quad (10)$$

Figure 54 shows a parity plot of the measured values and the data gained with the model described by the equation (10). The model applies for the whole temperature range investigated.

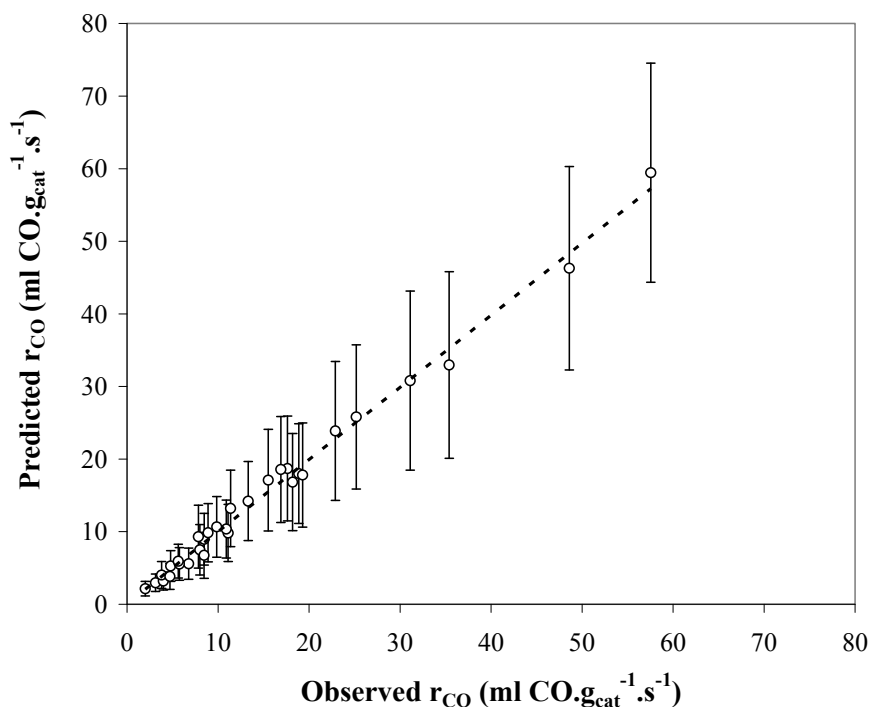


**Figure 54:** Parity plot for the CO oxidation in presence of  $O_2$ , CO and  $N_2$ .

The experiments described above revealed that the velocity of the carbon monoxide oxidation reaction in the presence of merely carbon monoxide, oxygen and nitrogen is proportional to the concentration of oxygen, but inversely proportional to the concentration of carbon monoxide. This indicates reaction inhibition by carbon monoxide, most likely due to competitive adsorption. Such a reaction behavior has been described before [122].

### 2.5.2 CO oxidation in the presence of $H_2$

The intrinsic kinetics of simultaneous carbon monoxide and hydrogen oxidation is well described by the same power-law expression [123] presented by equation (9). The data for estimation of the parameters were obtained over the same catalyst sample (5 wt.% of Pt and 5 wt.% of Rh). The range of experimental conditions covered is listed in Table 10.

**Table 10:** Range of experimental conditions during the CO oxidation over Pt-Rh/ $\gamma$ -Al<sub>2</sub>O<sub>3</sub> in the presence of H<sub>2</sub>. N<sub>2</sub> is used in a balance.

<b>Total Feed [ml/min] (STP)</b>	100
<b>CO [ml/min] (STP)</b>	0.5 – 2.0
<b>O/CO ratio (-)</b>	1.0 – 4.0
<b>H<sub>2</sub> [ml/min] (STP)</b>	0 – 60
<b>T (°C)</b>	130 – 180

As it is shown on Figure 55, for the oxidation of carbon monoxide the conversion in the presence of hydrogen is lower than without hydrogen.

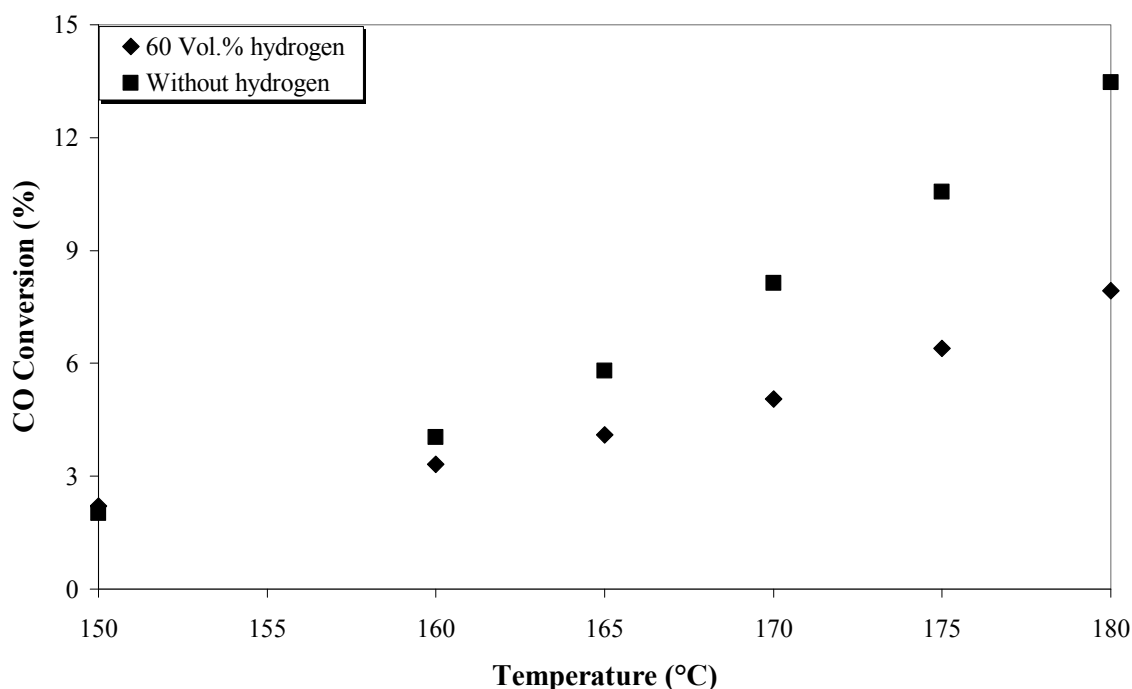


**Figure 55:** CO conversion achieved vs. reaction's temperature over Pt-Rh/ $\gamma$ Al<sub>2</sub>O<sub>3</sub> catalyst (60 Vol.%H<sub>2</sub>, 1.5 Vol.% CO, O/CO = 3 and N<sub>2</sub> in balance).

There are two possible reasons: competitive adsorption and reaction or removal of reactive oxygen by hydrogen. The system of molecularly adsorbed carbon monoxide and atomically adsorbed hydrogen co-adsorbed on metal surfaces provides mutual interactions [123]. The difference in adsorption strength between carbon monoxide and hydrogen provides a situation where carbon monoxide dominates the platinum metal surface, when both gases are present. The hydrogen competition with carbon monoxide for platinum metal site is much less favorable due to its lower adsorption strength, but its high concentration (here 60 Vol.%) relative to carbon monoxide (< 2 Vol.%) in the reformat may result in a reduced surface

coverage of carbon monoxide [10]. It is reported that the effect of hydrogen on the carbon monoxide oxidation rate depends on the support material and on the metal surface as well [50 and 124]. HCO- formation has already been proposed in earlier studies of interaction of carbon monoxide and hydrogen on metal surface, e.g. on supported rhodium, ruthenium or platinum catalysts [125 and 126], but no evidence for formaldehyde formation has been obtained. Such a formyl-formation has been discussed as a segregated over-layer developed on the surface. If this is extensive, its bond strength inhibits the dissociative chemisorption of oxygen. Practically oxygen cannot be adsorbed on carbon monoxide covered platinum anymore and hence both the carbon monoxide and hydrogen oxidation rates are low [49 and 124]. On the other hand, hydrogen may simply compete for surface oxygen and thus directly affect total carbon monoxide conversion. The latter is supported by the reaction orders determined.

Figure 56 – 58 show the oxidation rate as a function of oxygen, carbon monoxide and hydrogen output concentration respectively in a mixture of hydrogen, carbon monoxide, oxygen and nitrogen in balance.

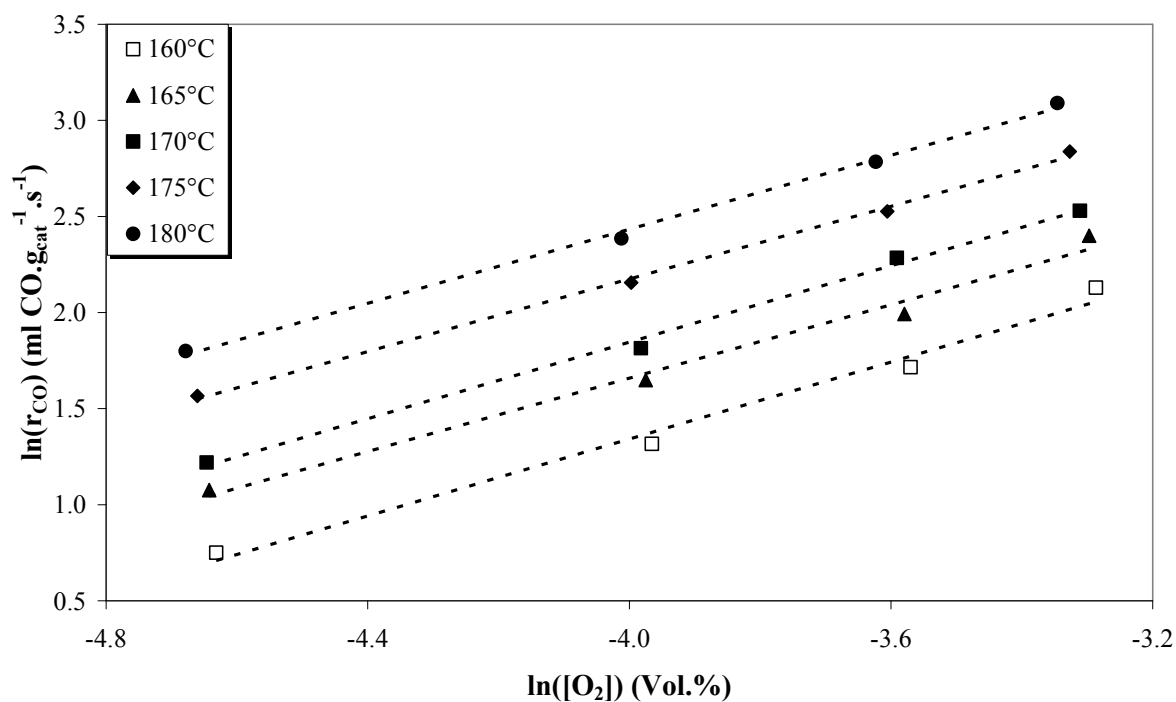


**Figure 56:** CO reaction rate vs. O<sub>2</sub> concentration over Pt-Rh/ $\gamma$ -Al<sub>2</sub>O<sub>3</sub> catalyst (2 Vol.% CO, 60 Vol.% H<sub>2</sub>, O<sub>2</sub> and N<sub>2</sub> in balance).

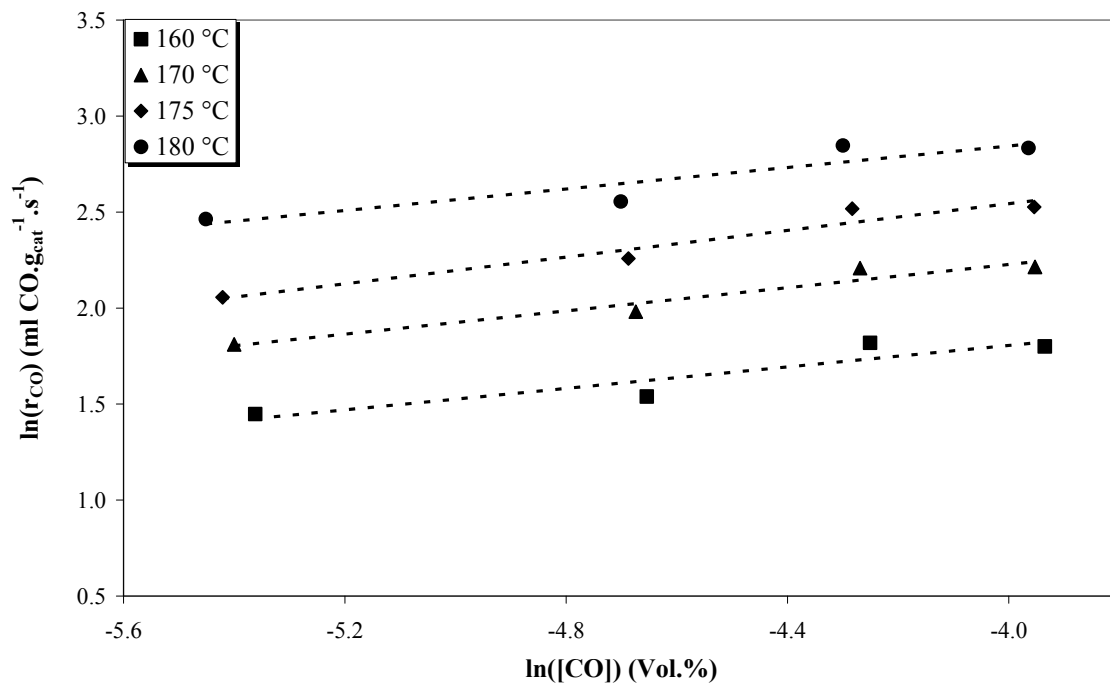


**Figure 57:** CO reaction rate vs. CO concentration over Pt-Rh/ $\gamma$ Al<sub>2</sub>O<sub>3</sub> catalyst ( $O/CO = 4$ , 60 Vol.% H<sub>2</sub>, CO and N<sub>2</sub> in balance).

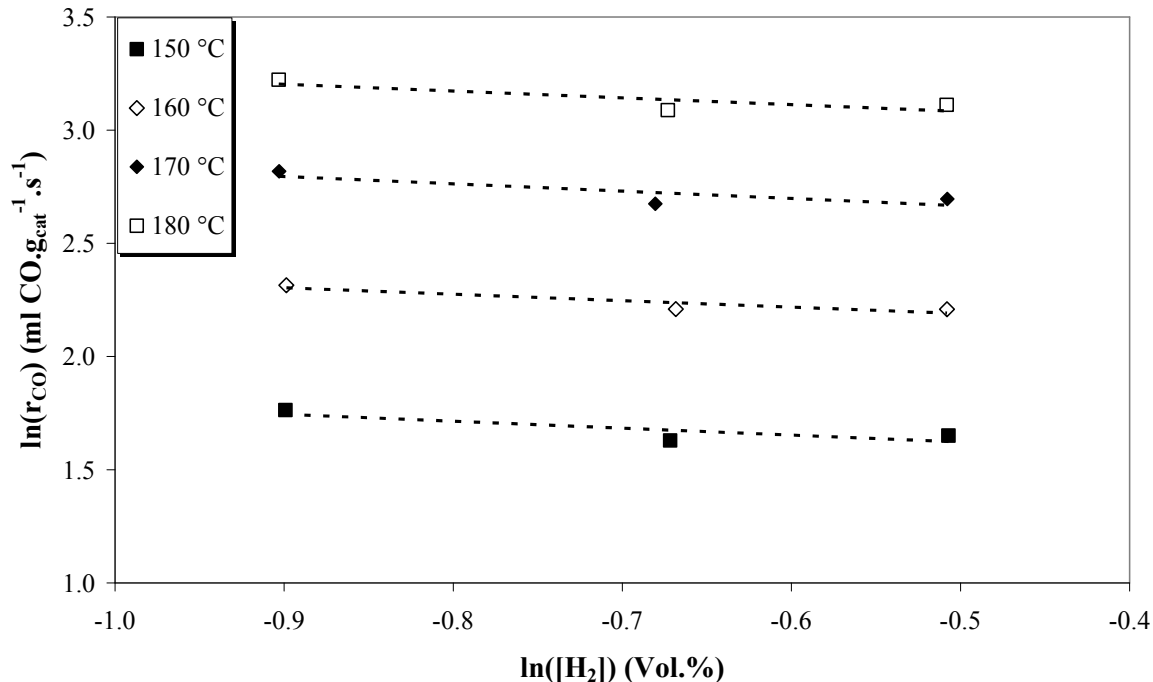


**Figure 58:** CO reaction rate vs. H<sub>2</sub> concentration over Pt-Rh/ $\gamma$ Al<sub>2</sub>O<sub>3</sub> catalyst ( $O/CO = 4$ , 1.5 Vol.% CO, H<sub>2</sub> and N<sub>2</sub> in balance).

Figure 59 shows the temperature dependence of the rate in the range of 150 °C to 180 °C.

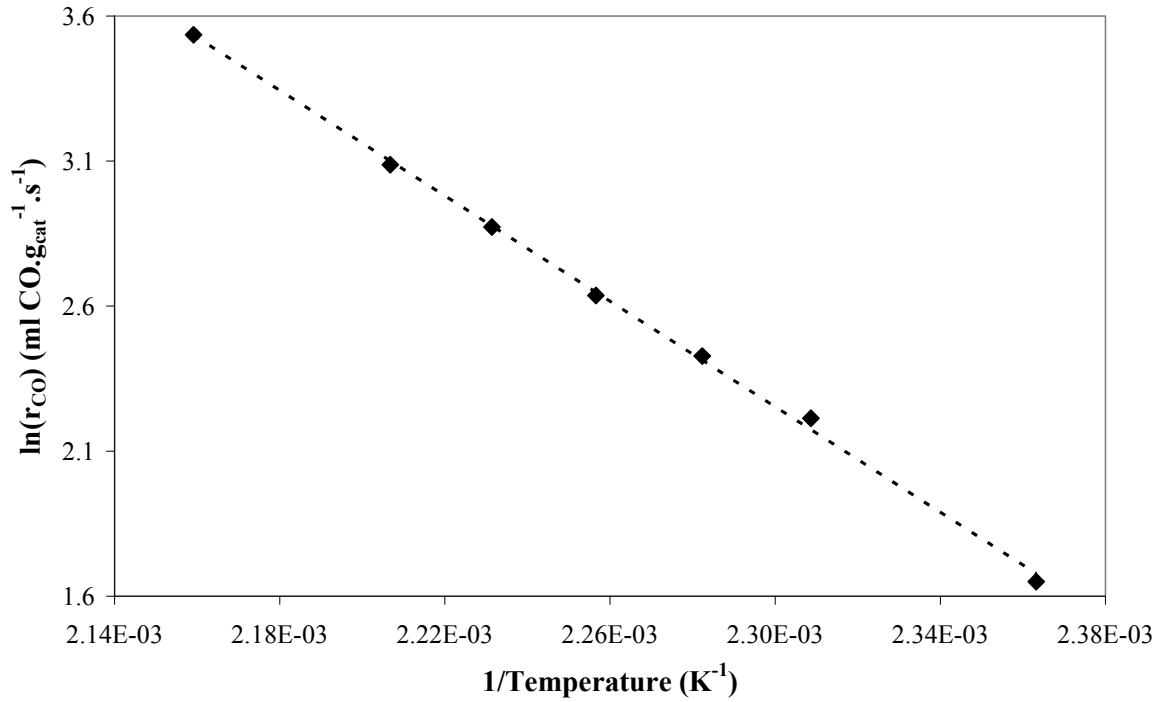


**Figure 59:** Arrhenius plot of the rate constant for CO oxidation over Pt-Rh/ $\gamma$ Al<sub>2</sub>O<sub>3</sub> catalyst (O/CO = 3, 1.5 Vol.% CO, 60 Vol.% H<sub>2</sub> and N<sub>2</sub> in balance).

The apparent activation energy from the least squares regression was 92.4 kJ/mole. The pre-exponential factor  $k_0$  was estimated near  $1.4 \times 10^{12}$  ml · g<sub>cat</sub><sup>-1</sup> · s<sup>-1</sup>. Table 11 shows the kinetic parameters along with their 95 % confidence interval.

**Table 11:** Confidence intervals of the kinetic parameters estimated by regression method for CO oxidation in the presence of H<sub>2</sub> for equation (9).

	1 <sup>st</sup> Model	2 <sup>nd</sup> Model
$\alpha$ (-)	-0.71±0.1	-0.68±0.1
$\beta$ (-)	1.00±0.08	1.00±0.08
$\gamma$ (-)	-0.30±0.67	0
$\delta$ (-)	0	0
$E_A$ (kJ/mole)	92.4±4.7	92.7±10.58
$k_0$ (ml <sup>0.68</sup> · g <sub>cat</sub> <sup>-1</sup> · s <sup>-1</sup> )	$1.4 \times 10^{12.0 \pm 0.9}$	$1.44 \times 10^{12.0 \pm 0.8}$
AIC (-)	27.694	27.701

Regression analysis of the first model described by equation (11) shows the influence of the reaction order of hydrogen on the rate of reaction.

$$r_{CO} = 1.4 \cdot 10^{12} \cdot e^{-\frac{92.4}{RT}} \cdot [CO]^{-0.71} \cdot [O_2]^{1.00} \cdot [H_2]^{-0.30} \quad (11)$$

However, t-test in the 1<sup>st</sup> model shows that  $\gamma$  parameter is statistically not significant and can be ignored in the 2<sup>nd</sup> model. To test a hypothesis on whether the means of two normally distributed populations are equal, t-test was performed. If the t value that is calculated is below the threshold chosen for statistical significance (here 0.05) then the two models do not differ. Additionally, AIC scores are very close and each model is equally likely to be correct. The 2<sup>nd</sup> model is the simpler model and it should fit worse. However, the change in sum of squares is not as large as expected from the change in number of parameters.

It is reported [118] that as long as the feed contains more than 10 Vol.% H<sub>2</sub>, as in the reformat, the carbon monoxide conversion is not affected by the hydrogen concentration. Therefore, the reaction order with respect to hydrogen is statistically not significant and thus,  $\gamma$  can be ignored ( $\gamma = 0$ ). It is also reported, [127] that because of the large excess of hydrogen there is no dependence on the partial concentration of hydrogen and the latter is part of the rate constant. Thus, the rate equation of carbon monoxide preferential oxidation in presence of hydrogen is described by equation (12).

$$r_{CO} = 1.44 \cdot 10^{12} \cdot e^{-\frac{92.7}{R \cdot T}} \cdot [CO]^{-0.68} \cdot [O_2]^{1.00} \quad (12)$$

The negative low order in hydrogen for the carbon monoxide conversion consist an evidence against competitive adsorption, while the increase of the reaction order for oxygen from 0.79 to 1.00 supports a relative reduction of surface oxygen as a result of the large amount of hydrogen being present.

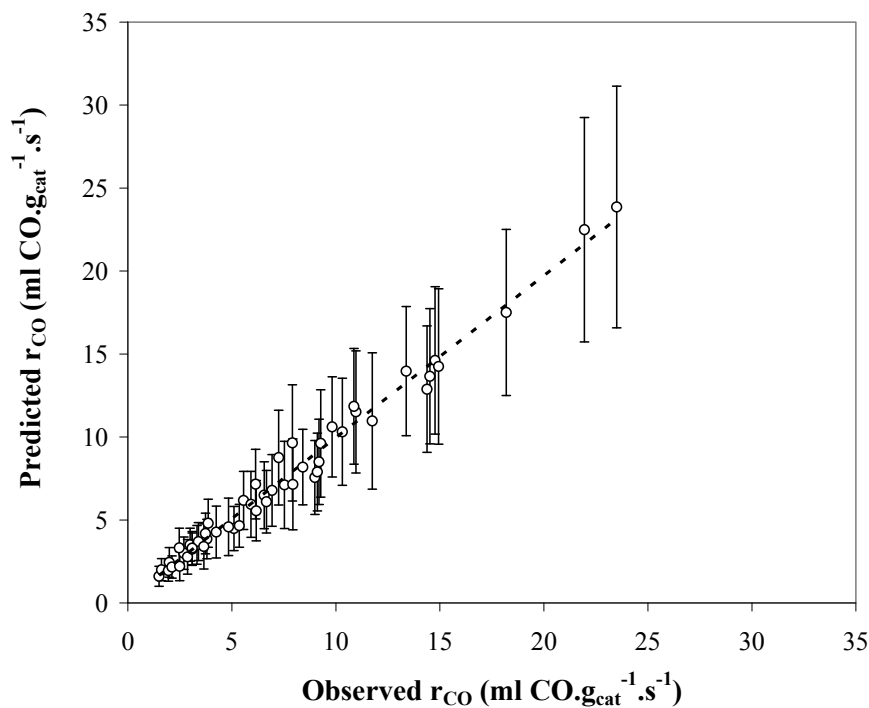


**Figure 60:** Parity plot for the CO oxidation in presence of CO, O<sub>2</sub>, H<sub>2</sub> and N<sub>2</sub>.

These values are in reasonable agreement with the data found in literature [50 and 118]. A parity plot comparing the measured values with the model described is shown in Figure 60.

### 2.5.3 CO oxidation in the presence of H<sub>2</sub> and CO<sub>2</sub>

In order to determine the kinetics of preferential oxidation of carbon monoxide in realistic reformat, reactions were performed in the presence of carbon dioxide and steam. Most experiments took place at a constant inlet concentration of 15 Vol.% CO<sub>2</sub>. Experiments were performed at temperatures exceeding 130 °C to avoid any condensation of steam. The range of experimental conditions covered is listed in Table 12.

**Table 12:** Range of experimental conditions during the CO oxidation over Pt-Rh/ $\gamma$ -Al<sub>2</sub>O<sub>3</sub> in the presence of H<sub>2</sub> and CO<sub>2</sub>. N<sub>2</sub> is used in a balance.

<b>Total Feed [ml/min] (STP)</b>	100
<b>CO [ml/min] (STP)</b>	0.5 – 2.0
<b>O/CO ratio (-)</b>	1.0 – 4.0
<b>H<sub>2</sub> [ml/min] (STP)</b>	0 – 60
<b>CO<sub>2</sub> [ml/min] (STP)</b>	0 – 20
<b>H<sub>2</sub>O [ml/min] (STP)</b>	0.0 – 2.5
<b>T (°C)</b>	130 – 190

The combined effect of carbon dioxide and hydrogen on the rate of carbon monoxide oxidation is shown in Figure 61.

As it is depicted the presence of carbon dioxide influences in negative way (negative inclination) the reaction. Carbon dioxide inhibits the preferential oxidation of carbon monoxide. The inhibition effect is strong and carbon dioxide participates in the reaction rate. Hence the reaction order is anticipated to be negative. The reaction order with respect to carbon monoxide seems to be different. It was determined lower as compared to the order determined without carbon dioxide, approximately -0.64 instead of -0.68. Nevertheless, the error of two results (with and without carbon dioxide in the feed) are different and overlap with each other; hence,  $-0.64 \pm 0.22$  (with carbon dioxide in the feed) and  $-0.68 \pm 0.1$  (without carbon dioxide in the feed), are statistically tied. This can be seen in the apparent activation energy values; i.e. within errors, the activation energies are not widely different.

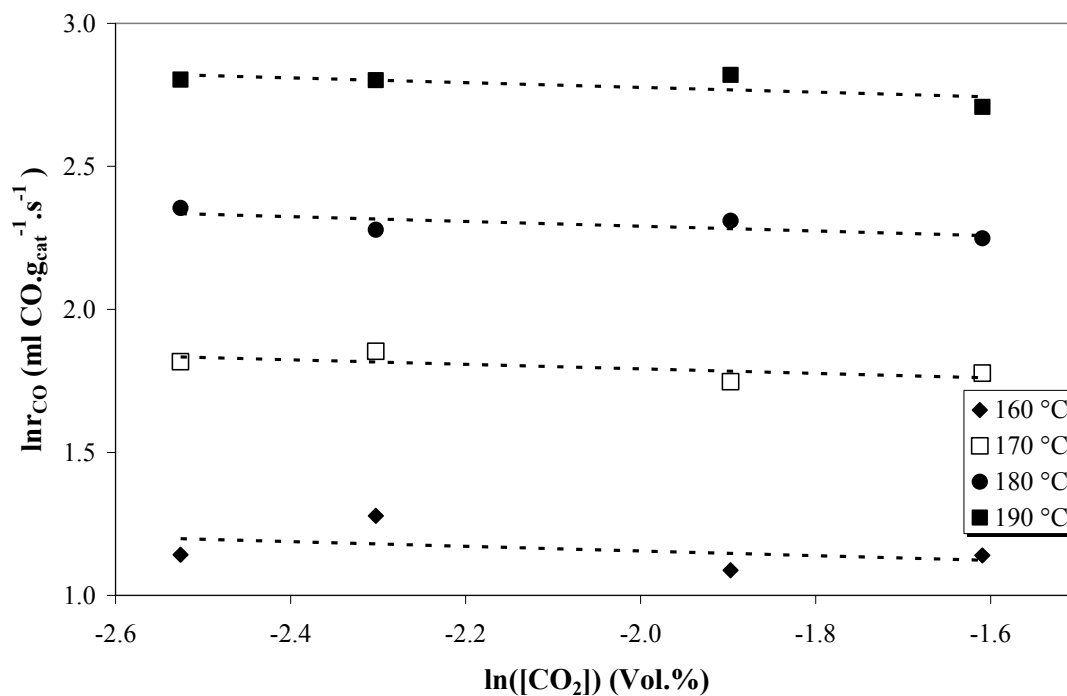


**Figure 61:** *CO reaction rate vs. CO<sub>2</sub> concentration over Pt-Rh/γAl<sub>2</sub>O<sub>3</sub> catalyst (1.5 Vol.% CO, O/CO = 4, 60 Vol.% H<sub>2</sub>, CO<sub>2</sub> and N<sub>2</sub> in balance).*

The reaction order of carbon dioxide,  $\delta$ , was found to be negative as expected, here -0.08.

From Arrhenius plot, depicted on Figure 62 and regression analysis we can extract the activation energy 92.5 kJ/mole.

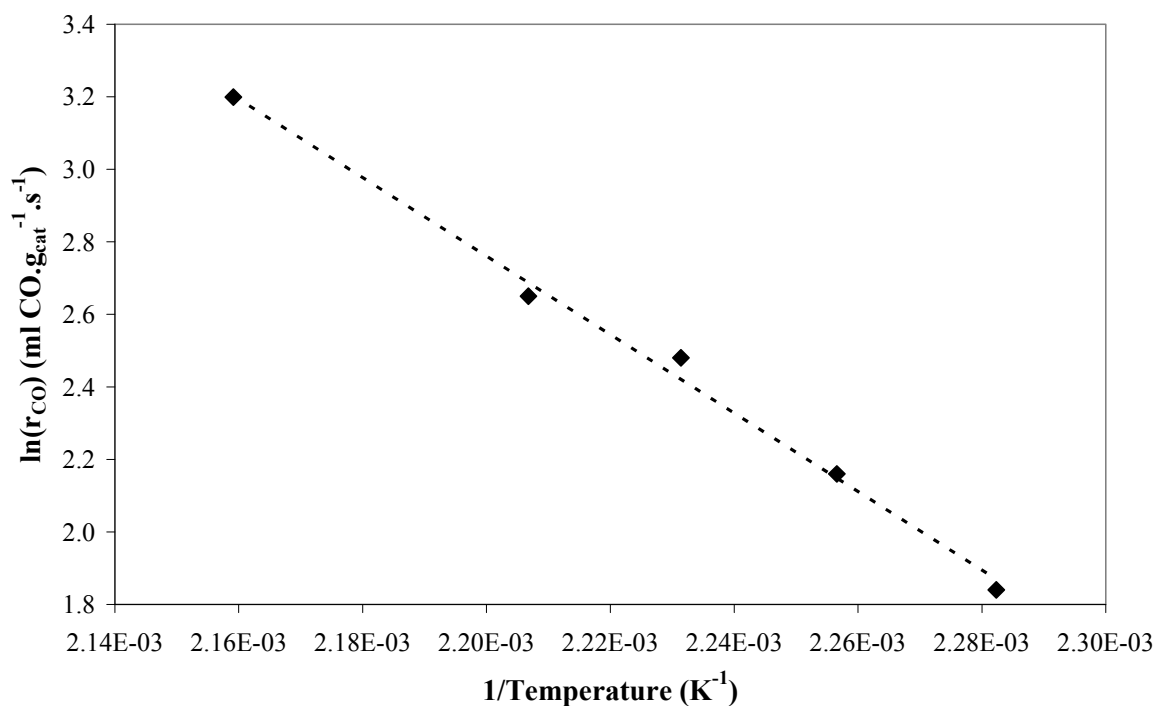


**Figure 62:** *Arrhenius plot of the rate constant for CO oxidation over Pt-Rh/γAl<sub>2</sub>O<sub>3</sub> catalyst (O/CO = 4, 2.0 Vol.% CO, 60 Vol.% H<sub>2</sub>, 15 Vol.% CO<sub>2</sub> and N<sub>2</sub> in balance).*

The rate equation of carbon monoxide oxidation in the presence of hydrogen and carbon dioxide takes the following form:

$$r_{CO} = k_0 \cdot e^{-\frac{E_A}{R \cdot T}} \cdot [CO]^\alpha \cdot [O_2]^\beta \cdot [H_2]^\gamma \cdot [CO_2]^\delta \quad (13)$$

From regression analysis, the pre-exponential factor  $k_0$  was found near  $3.46 \times 10^{11} \text{ ml} \cdot \text{g}_{\text{cat}}^{-1} \cdot \text{s}^{-1}$ . The confidence interval of the model predicted at 95 % and the parameters obtained are summarized in Table 13.

**Table 13:** Confidence intervals of the kinetic parameters estimated by regression method for CO oxidation in the presence of  $H_2$  and  $CO_2$  for equation (13).

	1 <sup>st</sup> Model	2 <sup>nd</sup> Model
$\alpha$ (-)	-0.64±0.22	-0.61±0.16
$\beta$ (-)	0.70±0.14	0.83±0.16
$\gamma$ (-)	-0.03±0.71	0
$\delta$ (-)	-0.08±0.39	0
$E_A$ (kJ/mole)	92.5±10.4	92.6±9.4
$k_0$ ( $\text{ml}^{0.78} \cdot \text{g}_{\text{cat}}^{-1} \cdot \text{s}^{-1}$ )	$3.46 \times 10^{11 \pm 1}$	$7.56 \times 10^{11 \pm 1}$
AIC (-)	44.004	44.083

The decrease of the reaction order with respect to oxygen is in agreement with literature [121] and can also be explained by the adsorption of carbon dioxide on the surface of the catalyst, which partially blocks the adsorption of all remaining reactants (here carbon monoxide, oxygen and hydrogen) [57, 62 and 128].

However, t-test shows that  $\gamma$  and  $\delta$  parameters are statistically not significant and can be ignored in the 2<sup>nd</sup> model. AIC scores are also very close and each model is equally likely to be correct.

Thus, the rate equation (13) takes the following form:

$$r_{CO} = 7.56 \cdot 10^{11} \cdot e^{-\frac{92.6}{R \cdot T}} \cdot [CO]^{0.61} \cdot [O_2]^{0.83} \quad (14)$$

A comparison between predicted and observed values of carbon monoxide oxidation rate is shown in a parity plot (Figure 63).

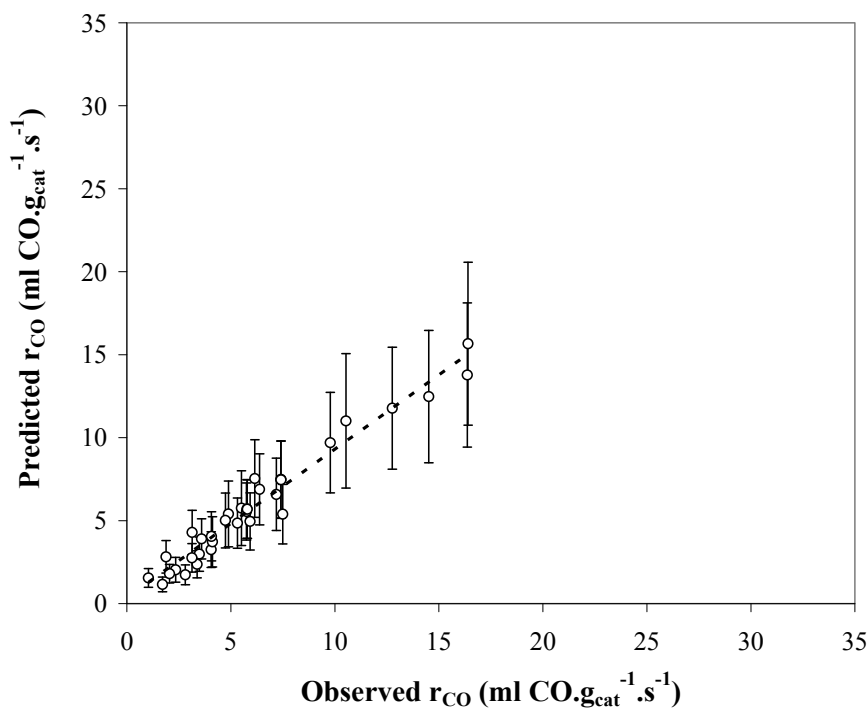


**Figure 63:** Parity plot for the CO oxidation in the presence of CO, O<sub>2</sub>, H<sub>2</sub> and CO<sub>2</sub>.

#### 2.5.4 CO oxidation in the presence of H<sub>2</sub>, CO<sub>2</sub> and steam

For the experiments the minimum catalyst temperature was kept above 120 °C so as to avoid condensation. As shown in Figure 64, steam had a dramatic effect on carbon monoxide conversion between the temperatures of 120 °C and 160 °C. At a temperature of 130 °C, no reaction was observed at all and thus, conversion was 0% when no steam was present in the feed while it reached 2% when 2.5 Vol.% H<sub>2</sub>O was added. In the temperature window from 130 °C to 160 °C the oxygen and hydrogen consumption was also negligible. However, the effect is limited to the temperature range between 160 °C and 190 °C.

This is in good agreement with earlier studies over similar catalyst from our group [46]. For the purpose of the present studies, the temperature range between 130 °C and 160 °C was not further investigated and the effect of steam was not included into the kinetic experiments.

Several authors have proposed an enhancement of the carbon monoxide oxidation rate in the presence of steam [46, 104 and 129]. The mechanism that describes the above statement could be the dissociation of water on the noble metal surface:



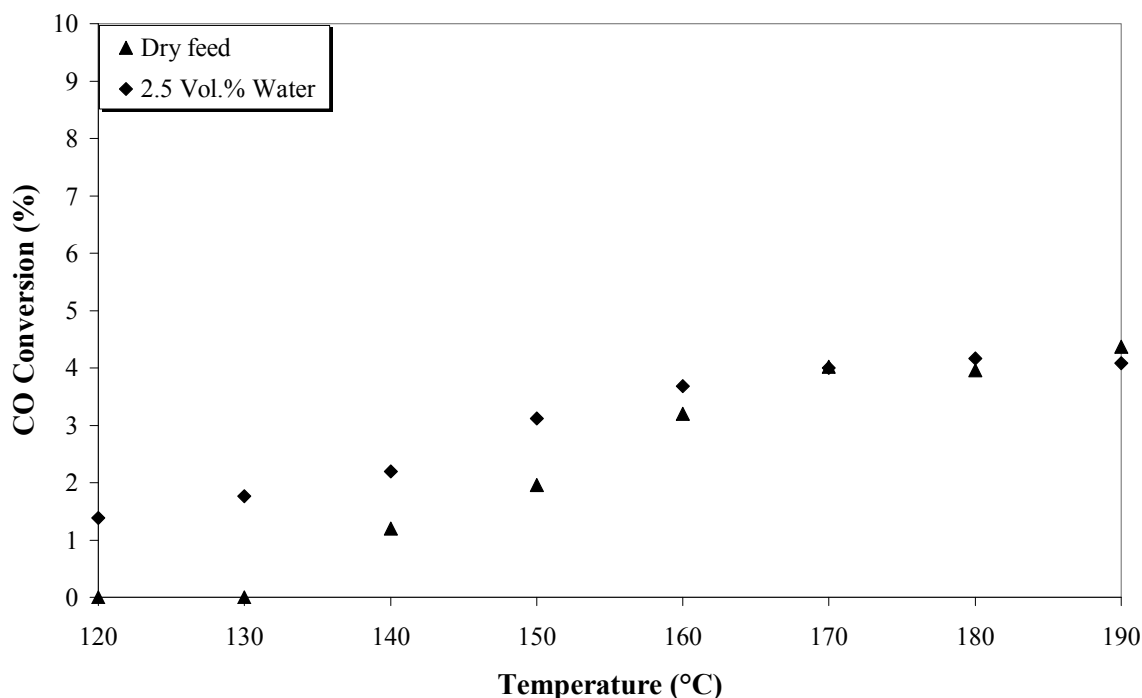


**Figure 64:** Effect of steam on CO conversion over Pt-Rh/ $\gamma$ Al<sub>2</sub>O<sub>3</sub> catalyst (0.5 Vol.% CO, O/CO = 2, 60 Vol.% H<sub>2</sub>, 15 Vol.% CO<sub>2</sub>, 2.5 Vol.% H<sub>2</sub>O and N<sub>2</sub> in balance).

And then, carbon monoxide can be removed by oxidation,



These reactions are also proposed also by Meng-Sheng Liao [129]. Similar observations have been made by Manasilp and Gulari [42] who investigated carbon monoxide oxidation over a Pt/Al<sub>2</sub>O<sub>3</sub> catalyst and by Yan et al [48] who investigated carbon monoxide oxidation over a Pt-Co/Al<sub>2</sub>O<sub>3</sub> catalyst. Manasilp and Gulari [42] proposed the possibility that the OH<sup>-</sup> groups formed on the catalyst upon steam adsorption are better oxidants than oxygen itself. An interesting mechanism for the influence of OH<sup>-</sup> groups on a Pt/SnO<sub>x</sub> catalyzed carbon monoxide oxidation reaction has also been suggested by Schryer et al [130] where modification of the Pt<sup>0</sup> and Pt(O)<sub>x</sub> sites takes place. They proposed that OH<sup>-</sup> groups on the surface of a Pt/SnO<sub>2</sub> catalyst (which are regarded as being a significant constituent of tin oxide surfaces) participate in the oxidation of carbon monoxide chemisorbed on adjacent platinum sites. Upon increasing the temperature, the rate of carbon monoxide desorption increases, and thus, the number of catalyst sites for oxygen adsorption, is increased. Carbon monoxide oxidation activity therefore increases [36 and 49].

### 2.5.5 Comparison with literature values

The reaction orders determined in this study are summarized in Table 14 and compared with the respective values for several other platinum or rhodium catalysts.

**Table 14:** Comparison between literature data for CO oxidation rate. Indexes e, f, c and d denote respectively Pt/ $\gamma$ -Al<sub>2</sub>O<sub>3</sub>, Rh(111), Rh/SiO<sub>2</sub>, Pt/SiO<sub>2</sub>.

Reference	Reaction Conditions	T-range (°C)	$\alpha$ (-)	$\beta$ (-)	$\gamma$ (-)	E <sub>A</sub> (kJ/mole)
[131] <sup>e</sup>	without H <sub>2</sub>	<200	-1.5	-1.0		101
[131] <sup>e</sup>	0 – 1% Vol. H <sub>2</sub>	<200	-0.7	0.7	-0.2	83
[132] <sup>e</sup>	without H <sub>2</sub>	<170	0 to -0.6	1.0		80
[133] <sup>e</sup>	without H <sub>2</sub>	>280	-0.6	1.0		125
[134] <sup>e</sup>	without H <sub>2</sub>	>230	-0.9	1.0		138
[135] <sup>f</sup>	without H <sub>2</sub>	~220	-1.0	1.0		106
[136] <sup>c</sup>	without H <sub>2</sub>	>200	-0.8	0.9		103
[136] <sup>d</sup>	without H <sub>2</sub>	>180	-0.2	0.9		56
[59] <sup>e</sup>	50% Vol. H <sub>2</sub>	150 – 350	-0.5	0.8		78
[75] <sup>e</sup>	75% Vol. H <sub>2</sub>	150 – 250	-0.4	0.8		71
This study	without H <sub>2</sub>	130 – 180	-0.53	0.79		94.2
This study	60% Vol. H <sub>2</sub>	130 – 180	-0.68	1.00	0.0	92.7
This study	60% Vol. H <sub>2</sub> 20% Vol. CO <sub>2</sub>	130 – 180	-0.61	0.83	0.0	92.6

### 2.5.6 H<sub>2</sub> oxidation

The hydrogen oxidation in the presence of carbon monoxide (or carbon dioxide) was difficult to be determined because of the phenomena taking place on the surface of the catalyst (mentioned in chapter 2.5.3). In the absence of carbon monoxide, hydrogen oxidation over the platinum surface is instantaneous, even at room temperature, and difficult to be controlled [118]. However, with carbon monoxide in the feed mixture, carbon monoxide covers the metal surface and inhibits the hydrogen oxidation. In an adsorption study of carbon monoxide on a platinum catalyst [118], the full coverage of carbon monoxide was observed at temperatures below 180 °C [36]. Despite this inhibition, the reaction rates of hydrogen

were extremely high. On the contrary, hydrogen conversion was low and in particular in the presence of carbon dioxide not possible to be measured accurately with the equipment used. Additionally, because of the large amount of hydrogen being present, as it is typical under the preferential carbon monoxide oxidation conditions, the hydrogen concentration throughout the reactor does not vary significantly.

$$r_{H_2} = k_0 \cdot e^{-\frac{E_A}{R \cdot T}} \cdot [H_2]^\pi \cdot [O_2]^v \cdot [CO]^\kappa \quad (17)$$

The Arrhenius plot shown in Figure 65 and regression analysis provides the activation energy of 12.73 kJ/mole and the pre-exponential factor of  $3054 \text{ ml}^{1.23} \cdot \text{g}_{\text{cat}}^{-1} \cdot \text{s}^{-1}$  respectively.

Following regression analysis method for equation (17), we obtained the regression parameters. Confidence interval was 95 % and the results are shown in Table 15.

**Table 15:** Confidence intervals of the kinetic parameters estimated by regression method for  $H_2$  oxidation in the presence of CO for equation (17).

$\pi$ (-)	-0.26±0.18
$v$ (-)	0.09±0.04
$\kappa$ (-)	-0.06±0.05
$E_A$ (kJ/mole)	12.73±2.84
$k_0$ ( $\text{ml}^{1.23} \cdot \text{g}_{\text{cat}}^{-1} \cdot \text{s}^{-1}$ )	3055±625
AIC (-)	273.65

The model proposed to describe the hydrogen oxidation in the presence of carbon monoxide is similar to the model describes carbon monoxide oxidation in the presence of hydrogen in equation (13) [Chapter 2.5.2].

Thus, the final form of the model for the oxidation of hydrogen is:

$$r_{H_2} = 3055 \cdot e^{-\frac{12.73}{R \cdot T}} \cdot [H_2]^{-0.26} \cdot [O_2]^{0.09} \cdot [CO]^{-0.06} \quad (18)$$

The results arising from the model presented by equation (18) are in reasonable agreement with the data obtained from experiments and with data found in literature [137].

The parity plot is presented in Figure 66. The deviation at higher temperatures of the reaction rate observed from the model is not surprising. At the higher end of temperatures (beyond 170 °C), carbon monoxide begins to desorb from the catalyst surface resulting in partial coverage of the surface by carbon monoxide, thus allowing the oxidation of hydrogen to proceed at a faster rate [36].

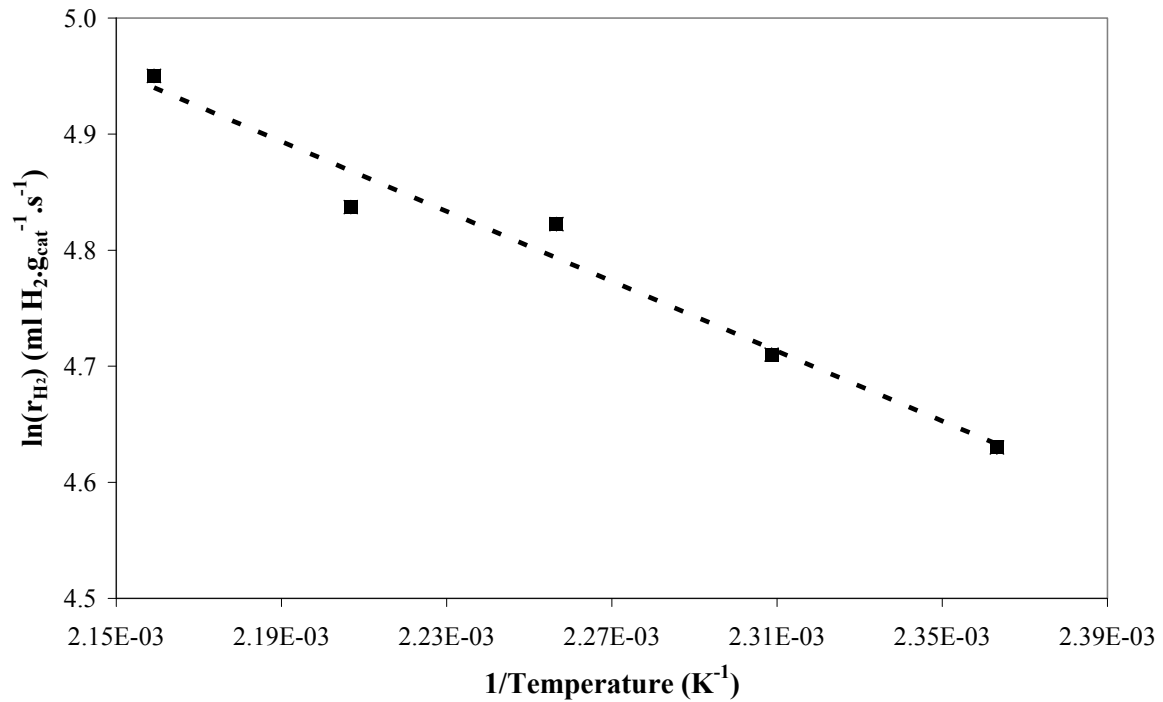


**Figure 65:** Arrhenius plot of the rate constant for  $H_2$  oxidation over  $Pt-Rh/\gamma Al_2O_3$  catalyst ( $O/CO = 4$ , 1.5 Vol.%  $CO$ , 40 Vol.%  $H_2$ , 15 Vol.%  $CO_2$  and  $N_2$  in balance).

It is also clear that the rate of hydrogen oxidation is around 5 to 10 times higher than that of the carbon monoxide oxidation.

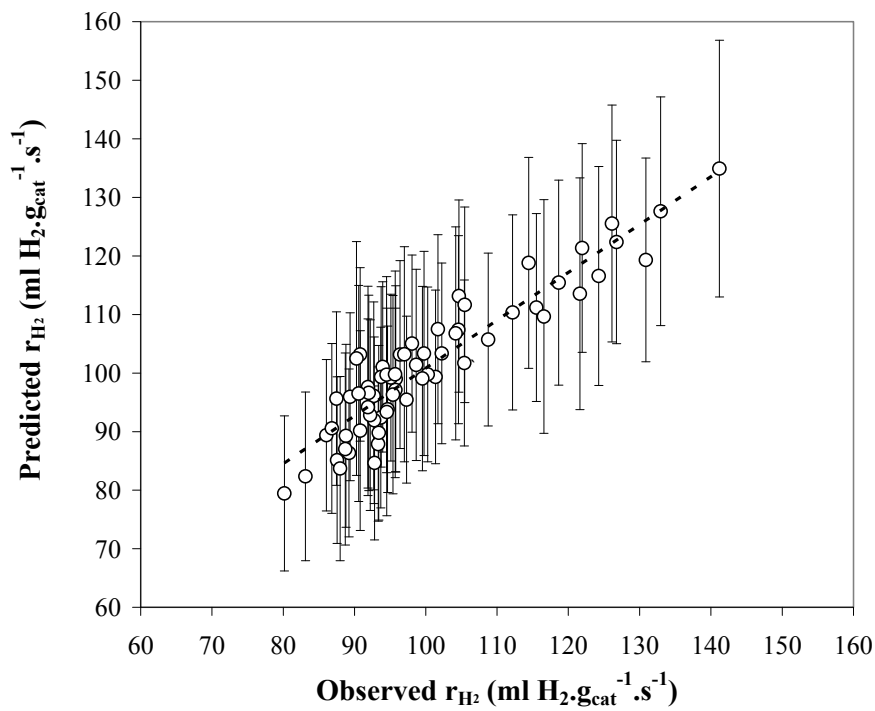


**Figure 66:** Parity plot for the  $H_2$  oxidation in the presence of  $CO$ ,  $O_2$ , and  $CO_2$ .

### 3.1 Synthesis of catalysts

#### 3.1.1 Gold catalysts

Active gold catalysts could be prepared using different methods. Coprecipitation, impregnation and deposition-precipitation are the most commonly used and they often result in quite different catalysts. Typically, coprecipitation or deposition-precipitation methods are more desirable than impregnation, especially when chloroauric acid is used as the precursor. Various synthesis parameters have been studied, which include mainly pH, calcination temperature and binding solution. Some of these studies have helped elucidate the underlying chemistry that causes variation in the properties of the final catalyst [138 – 142].

One of the better understood variables is pH in the coprecipitation procedure. In such a preparation method,  $\text{HAuCl}_4 \cdot 3\text{H}_2\text{O}$  is used as the metal gold precursor. The chloroauric anion hydrolyzes in solution to form  $\text{Au}(\text{OH})_x\text{Cl}_{4-x}^-$ . The extent of hydrolysis depends on the pH, gold and chlorine concentrations. The aqueous mixture of  $\text{HAuCl}_4$  and a nitrate solution of the corresponding metal oxide ( $\text{Co}_3\text{O}_4$ ,  $\text{TiO}_2$ ,  $\text{NiO}$ ,  $\text{Fe}_3\text{O}_4$ ,  $\text{CeO}_2$ ) support were poured drop wise into an aqueous stirred mixture of  $\text{Na}_2\text{CO}_3$ , which was used as a buffer solution to retain the pH at a constant value. In case where the influence of pH was examined, it was necessary to vary the pH from low or high values to the final pH value of 7 where the solvate precipitates. It has been found that preparation at a pH ranging from 7 to 8 was preferable depending on the oxide support [107]. At this pH, the value of  $x$  was close to 3. At lower pH's there is less hydrolysis of the gold-chlorine bond. Furthermore, at pH's below the isoelectric point of the support, the surface is dominated by positively charged gold species.

---

This results in not only a larger gold loading, but also a high concentration of chloride on the surface. The presence of chloride increases the mobility of gold on the support, leading to large gold particles. At pH's above the isoelectric point of the oxide, adsorption of the negatively charged  $\text{Au}(\text{OH})_x\text{Cl}_{4-x}^-$  complex decreases rapidly, resulting in a lower gold loading. However, there will also be less chloride at the catalyst surface and thus small particles can be formed. Therefore, there was a narrow range of pH where sufficient gold can be deposited onto the support with minimal chloride in the gold complex [143].

In addition to  $\text{Au}(\text{OH})_x\text{Cl}_{4-x}^-$ , chloride ions are adsorbed at the oxide. The amount of chloride adsorbed decreased rapidly as the isoelectric point is approached, when the oxide surface is no longer positively charged. The adsorbed chloride causes agglomeration of gold particles during calcination, such that the average gold particle size is larger in the samples.

To remove any stump of chlorine ions, the suspension was filtered and washed thoroughly with demineralized water at 80 °C. To examine the presence of ions, drops of  $\text{AgNO}_3$  were used as a test. The elimination of the ions was verified by the EDX-analysis, where no chloride-peaks were identified. The coprecipitate was then dried under vacuum over night and finally calcined in air at temperatures between 300 °C and 600 °C (heating rate 5 °C/min) for 4 h [144 – 147]. The gold content in the catalyst obtained was 1 – 5 wt.% and the mean particle diameter of gold was below 5 nm.

The binder, here polyvinyl alcohol, was dissolved in water in a beaker by stirring smoothly with a laboratory magnetic stir bar at 60 °C for 2 h and left without stirring overnight at room temperature [148]. The catalyst-powder was then added successively under stirring at room temperature. This mixture was then stirred at 65 °C for 2 h, cooled to room temperature and kept overnight under stirring. In order to remove air bubbles entrapped in the viscous mixture, a sufficient period of the self-release of the bubbles was necessary, typically ranging from 3 days to 2 weeks. The channels were then filled with the suspension and any excess on the top of the channel walls was wiped off.

The physical properties of the catalysts prepared are shown in Table 16.

**Table 16:** *Physical properties of  $\text{Au}/\text{Me}_x\text{O}_y$  catalysts.*

<b>Overall Au loading (wt.%)</b>	1 – 5
<b>Median pore diameter (nm)</b>	4 – 46
<b>BET specific surface area (<math>\text{m}^2/\text{g}</math>)</b>	10 – 179
<b>Overall catalyst mass per sample (mg)</b>	~9

### 3.1.2 Zeolite catalysts

One of the important issues in catalytic microreactors is the proper incorporation of the active catalyst within the microchannel. Typically, catalyst deposition over microreactors uses thin film techniques that are limited to metals and oxides. Growing a zeolite layer over a stainless steel microreactor is not trivial and few reports exist in the literature related to this subject [149].

In the work presented elsewhere [149], the synthesis conditions were optimized by studying different gel compositions and temperatures over stainless steel plates for the synthesis of a single layer ZSM-5 coating. However, the attempt to use the same recipes in the microchannels failed. It was not possible to selectively grow a coating on the microchannels. Rebrov et al. also observed that the thickness of the zeolite layer on the bottom of the microchannel was appreciably smaller [149].

In this work several syntheses of zeolite ZSM-5, Y and mordenite have been carried out on microreactors. The main procedure to make the synthesis was by means of a hydrothermal treatment of a Teflon lined autoclave.

The growth-method that was applied for the synthesis of zeolites (ZSM-5 with a silica to alumina ratio of 35 or 100, mordenite and zeolite-Y) over the microreactors consisted of two steps: i- hydrothermal treatment between 150 °C and 170 °C under pressure in an autoclave (Figure 67) and ii- a seeding step of the microchannels.

Zeolites were synthesized by mixing the raw materials to provide a “gel” that may be aged for a period (24 h at 25 °C) before reacting to provide the crystalline zeolite.



**Figure 67:** *Autoclave for zeolite synthesis.*

Two different gel compositions have been prepared for the hydrothermal synthesis of the ZSM-5 layers over the microreactors, with a molar composition of a tetrapropylammonium hydroxide complex  $\text{H}_2\text{O}:\text{SiO}_2:\text{NaOH}:\text{TPAOH}:\text{Al}_2\text{O}_3 = 987\cdot X:21:3:1:0.105$ , where X could be 1 or 2 for gel A or gel B respectively (tetrapropylammonium bromide, TPABr in case of ZSM-5/100 and TPAOH, in case of ZSM-5/35). The source of aluminium was sodium aluminate ( $\text{Na}_2\text{Al}_2\text{O}_4$ ) and for  $\text{SiO}_2$  was Ludox AS-40. The TPAOH/TPABr is added in a 1 M water solution.

Si and Al were the framework components. These components impact on the framework composition and on the properties of the material. A “mineralisation” component is essential in zeolite synthesis. This is usually a base. The base was added via an alkali metal, here NaOH and it can provide interesting changes in crystal size and morphology. TPAOH and TPABr are usually thought of as structure directing agents but they also play crucial roles in structure stabilisation.

The dominant component, by weight, was water. The use of water as the solvent in zeolite synthesis is widespread. For all the syntheses de-mineralised water was used to avoid the complicating effect of ions.

By this procedure, zeolite seeds were also produced. Since the seeds were added at 5 wt.% of the framework components ( $\text{SiO}_2$  and  $\text{Al}_2\text{O}_3$ ), the source of the seeds was actually from a synthesis carried out in a previous hydrothermal treatment. This colloidal suspension of silicalite seeds was prepared in order to seed beforehand the plates and have preferential growth layer. Additionally, the overall crystallisation time was reduced. The plates were seeded using a micro syringe.

By the hydrothermal treatment, two plates were introduced simultaneously in the autoclave, by stacking them together using teflon-tape. The “channel” side of both microreactors (Figure 68) was facing the gel. Samples were synthesised at 150 °C for gel A and 170 °C for gel B.

After the synthesis the supports were submitted to a calcination treatment at 480 °C for 8 h in order to eliminate the template out of the zeolite pores.

A solution used for the Y-type zeolite synthesis was prepared by mixing water glass,  $\text{NaAlO}_2$  and NaOH. The mole ratio of the initial composition of the solution was  $\text{H}_2\text{O}:\text{SiO}_2:\text{Na}_2\text{O}:\text{Al}_2\text{O}_3 = 975:12.8:17:1$ . This solution was stirred for 4 h at room temperature prior to the hydrothermal synthesis. Then the microreactor was placed into a tubular autoclave, which was filled with the synthesis solution. This tubular autoclave was then horizontally positioned in an oven, and maintained at 90 °C for 24 h. After the synthesis, the microreactor was washed using deionised water and dried for 12 h at room temperature.

---

For the preparation of mordenite, the synthesis solution consisted of  $\text{H}_2\text{O}:\text{SiO}_2:\text{Na}_2\text{O}:\text{Al}_2\text{O}_3$ , with a molar composition 80:1:0.38:0.025. Once prepared, the mordenite were subjected to post-synthetic treatment by vertical immersion in the autoclave containing an alkaline solution of  $\text{pH} = 10$  at  $180\text{ }^\circ\text{C}$  for 24 h [150].

The ZSM-5, mordenite and Y-type zeolites were ion-exchanged with an aqueous  $[\text{Pt}(\text{NH}_3)_4](\text{NO}_3)_2$  solution of 2.5 M by two different methods [151 and 152]. By the first method, the microreactor was impregnated with the solution for 24 h at room temperature. By the second method, the duration of the impregnation was reduced to 4 h but at elevated temperature of  $80\text{ }^\circ\text{C}$ . After this treatment, the reactor was washed with deionised water, and dried at room temperature overnight. The ion-exchanged zeolite was calcined in air at  $250\text{ }^\circ\text{C}$  for 3 h, and then reduced in a flow of hydrogen at  $250\text{ }^\circ\text{C}$  for 3 h. This method was used also by Hasegawa et. al. to obtain a platinum-loaded Y-type zeolite [61].

### 3.1.3 Other noble metal catalysts

#### A. Pt-Rh/ $\gamma$ - $\text{Al}_2\text{O}_3$ (4.8 wt.% Pt, 4.8 wt.% Rh)

In order to increase the surface area, a coating of a highly porous material, usually alumina, is applied. This procedure is known as washcoat. The coating of the plates was performed at the Institute für Mikrotechnik by Dr. R. Zapf, by initially applying a washcoat of a commercial Pt/ $\gamma$ - $\text{Al}_2\text{O}_3$  catalyst (Degussa) onto the entire length of the etched stainless steel channels. A 10 wt.% suspension was prepared from Pt/ $\gamma$ - $\text{Al}_2\text{O}_3$  and deionised water. The suspensions also contained 5 wt.% polyvinyl alcohol (Fluka) and 0.7 wt.% acetic acid. The channels were then filled with the suspension and any excess on the top of the channel walls was wiped off. The washcoated plates were then calcined for 6 h at a temperature of  $450\text{ }^\circ\text{C}$ . Then 20  $\mu\text{l}$  of a 9 wt.% solution of  $\text{Rh}(\text{NO}_3)_3$  was used to impregnate the Rh into the washcoat. After drying the impregnated plates were calcined for 6 h at  $450\text{ }^\circ\text{C}$  again.

The average thickness of each washcoat was about 25  $\mu\text{m}$ . The catalyst coated plates were incorporated into the microstructured reactor and were mildly reduced under a flow of 55 Vol.%  $\text{H}_2$  in nitrogen at 500 ml/min (STP) while initially being heated at a ramp rate of  $3\text{ }^\circ\text{C}/\text{min}$  from room temperature to  $130\text{ }^\circ\text{C}$ . This temperature was then kept stable for 1 hour. The reactor was afterwards purged with nitrogen while cooling down. Mild reduction conditions were chosen in order to avoid further loss of  $\text{OH}^-$  groups, due to high temperatures, since these groups are expected to play a role in the activity of the catalysts [153]. The physical properties of the catalyst prepared are shown in Table 17.

**Table 17:** *Physical properties of Pt-Rh/ $\gamma$ -Al<sub>2</sub>O<sub>3</sub> developed at the Institute für Mikrotechnik.*

<b>Overall metal loading (wt.%)</b>	9.6
<b>Median pore diameter (nm)</b>	17
<b>BET specific surface area (m<sup>2</sup>/g)</b>	223
<b>Overall catalyst mass (mg)</b>	8.97
<b>Median particle diameter (nm)</b>	1.4

The surface area and maximum pore diameter of the fresh catalysts were determined through BET measurements and BJH method respectively (nitrogen adsorption). Hydrogen chemisorption was used to qualitatively determine the mean particle size. A more detailed description of catalyst preparation and characterization is described elsewhere [46].

### B. Pt<sub>0.5</sub>Al<sub>1</sub>Mn<sub>7</sub>Co<sub>91.5</sub>O<sub>x</sub>

The catalyst was prepared by M. Krämer according to the following procedure. In a 250 ml glass flask 940.4 mg (4,586 mmole) Co(II)-propionate and 67.4 mg (0.335 mmole) Mn(II)-propionate have been stirred with 3.7 ml (50 mmole) propionic acid under heating to 150 °C until a clear solution was obtained. At 150 °C 500  $\mu$ l of a 0.1 M solution of Al(C<sub>2</sub>H<sub>5</sub>CH(CH<sub>3</sub>)O)<sub>3</sub> in 2-propanol and 250  $\mu$ L of a 0.1 M solution of Pt(NH<sub>3</sub>)<sub>4</sub>(NO<sub>3</sub>)<sub>2</sub> in purified water have been added. After about 50% of the propionic acid has been evaporated, the remaining hot solution was poured into a Petri-dish and allowed to cool. After 2 days in the hood a dark-red solid was obtained, which was heated with 1 °C/min to 300 °C and calcined at this temperature for 5 h.

The physical properties of the catalyst prepared are shown in Table 18.

**Table 18:** *Physical properties of Pt<sub>0.5</sub>Al<sub>1</sub>Mn<sub>7</sub>Co<sub>91.5</sub>O<sub>x</sub> catalyst synthesized at the University of Saarbrücken.*

<b>Overall metal loading (wt.%)</b>	0.5
<b>Max pore diameter (nm)</b>	4
<b>BET specific surface area (m<sup>2</sup>/g)</b>	66
<b>Overall catalyst mass (mg)</b>	15.35
<b>Median pore diameter (nm)</b>	12.8

A more detailed description of catalyst preparation and characterization is described elsewhere [65].

### 3.2 Temperature programmed reduction analysis

Temperature programmed reduction (TPR) experiments were carried out using a Power Supply model 40-102 GO- MAC Instrument.

The TPR apparatus consisted of a flow measuring and switching system, heated by a programmable furnace quartz tube in which the catalyst was placed along with the analysis system. The flow system was composed of high precision rota-meters and needle valves, 3-, 4- and 6-way valves and switching valves. The TPR cell was a quartz tube of 0.6 cm diameter and 25 cm length. A section at the centre of the tube was expanded to 2.4 cm diameter, in which the catalyst sample, approximately 0.1 g, was placed. A 1/16" thermocouple positioned at the center of the cell was used to determine the temperature at the catalyst bed. The TPR cell was placed in a cylindrical furnace of 3 cm diameter which was controlled by a linear temperature programmer (Omega, CN20IO). Prior to any experiments it was determined that the TPR cell or the tubing were not active in the adsorption and did not contribute to the mass spectrometer signal. It was also flushed with nitrogen at room temperature for 0.5 h before reduction. The procedure for each experiment was the following. The catalyst was placed in the TPR cell, supported by quartz wool. The cell was first cooled under argon flow. The argon flow was then switched to hydrogen-argon flow. Hydrogen concentration in this stream was kept constant at 5 Vol.% and the catalyst is submitted to a programmed temperature ramp of 5 °C/min from room temperature to 800 °C. Temperature programming was then initiated and the TPR profiles were obtained. After 15 min, the flow was switched to argon and the pipes were purged for 3 min. This procedure was found to give reproducible TPR results.

The effluent stream was passed through a molecular sieve trap in order to remove the water formed during reduction. The hydrogen concentration in the effluent was measured using a thermal conductivity detector. The detector output was calibrated using the reduction of bulk WO<sub>3</sub> powder (Aldrich, 99.99%). The detector was connected to a personal computer for instrument control, data acquisition and analysis.

---

### 3.3 Experimental Setup

#### 3.3.1 Microreactor as integral reactor

Two different types of reactors were used for these experiments. In both cases the reactors were operated in an integral mode during catalyst performance experiments to examine the effects of temperature, O/CO ratio, water, space velocity and catalyst preparation method on catalyst activity and selectivity. The reaction temperature was considered to be the temperature measured at the gas exit side by using a thermocouple 0.5 mm diameter.

The first reactor depicted in Figure 68, consisted of parallel channels with common inlet and outlet. The left-side is the inlet-section of the reactor, where the dot played the role of a mechanical support and flow barrier. The test reactors applied have a sandwich design with two micro-structured platelets being attached face to face. The platelets carried 14 channels each, which were 25 mm long, 500  $\mu\text{m}$  wide and 250  $\mu\text{m}$  deep. The channels together with the inlet and outlet region were prepared by wet chemical etching. Each couple of platelets was coated with the catalyst and subsequently sealed by laser welding. The amount of catalyst coated was approximately 9 mg. Inlet and outlet tubes were attached to the reactors by laser welding too. The welding procedure did not affect the catalyst performance as described elsewhere [154].

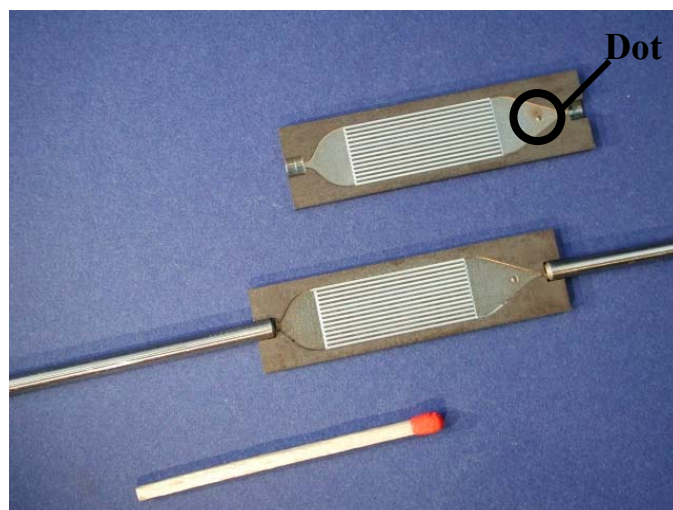


**Figure 68:** *Microreactors for single test.*

To heat up the reactor a heating cartridge of 200 W power was inserted into the borehole of a metal block. The temperature of the reactor was measured between the heating cartridge and the reactor. The heating block was insulated and therefore isothermal operation of the reactor

was assumed.

The second reactor depicted in Figure 69, offered the possibility of evaluating five different catalysts at the same time (primary screening). By using a Multi Position Valve one of the five outlet streams was collected and directed to the gas chromatograph which performed a complete analysis in less than 2 minutes.



**Figure 69:** Five fold screening reactor, Institut für Mikrotechnik, Mainz, 2005.

As it is depicted in Figure 70 the reactor consisted of the front-plate, as inlet ①, the main reactor ②, where the reactor-plates (Figure 71) were placed and the exit part ③.

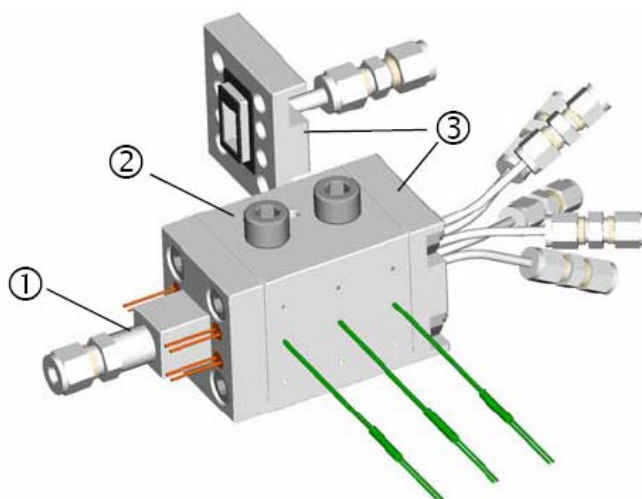


**Figure 70:** Drawing of the five fold reactor.

There were 12 channels in these plates with a cross sectional profile. The microchannels were 500  $\mu\text{m}$  wide, 300  $\mu\text{m}$  deep and 50 mm long.

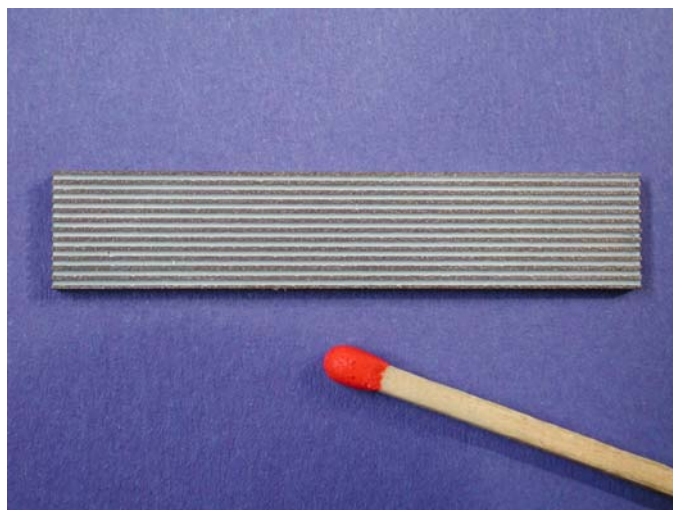


**Figure 71:** *Microreactors for screening tests.*

The inlet part of the reactor, depicted in Figure 72, had the form of a pyramid ④. Graphite seals were incorporated to achieve leak tightness ⑤.

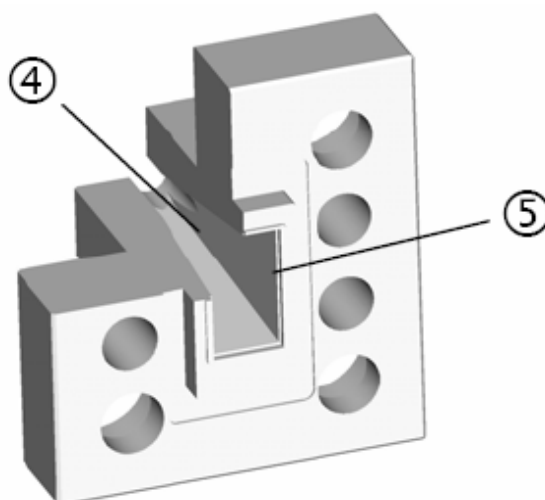


**Figure 72:** *Front-side of the screening reactor.*

The sketch presented in Figure 73 shows the position of the five plates inside the main reactor body ②. The plates were inserted by the use of drawers ⑥. To avoid leakages, sealing-frames were put ⑦ between the drawers and the main housing. The five drawers are covered by a top plate. In addition two screws ⑧ compressed the drawers from the top achieving satisfactory sealing between the plates and no cross-talking between the plates.

In order to check if fluidic cross-talk exists, the five microreactors were coated with five different catalysts. The active catalysts were positioned on the bottom (1<sup>st</sup> row), in the middle (3<sup>rd</sup> row) and on top (5<sup>th</sup> row) of the reactor core, next to the less active catalysts (2<sup>nd</sup> and 4<sup>th</sup>

row). The result was that the three active reactors did not influence the two neighboring less active reactors. Thus, cross-talk was not observed.

The heating of the reactors was performed by 4 heating cartridges ⑨ of 150 W power each at both sides of the drawers. To control their temperature, they were equipped with integrated thermocouples. Parallel to the reactor-plates there were also 3 thermocouples for temperature-measurement ⑩.

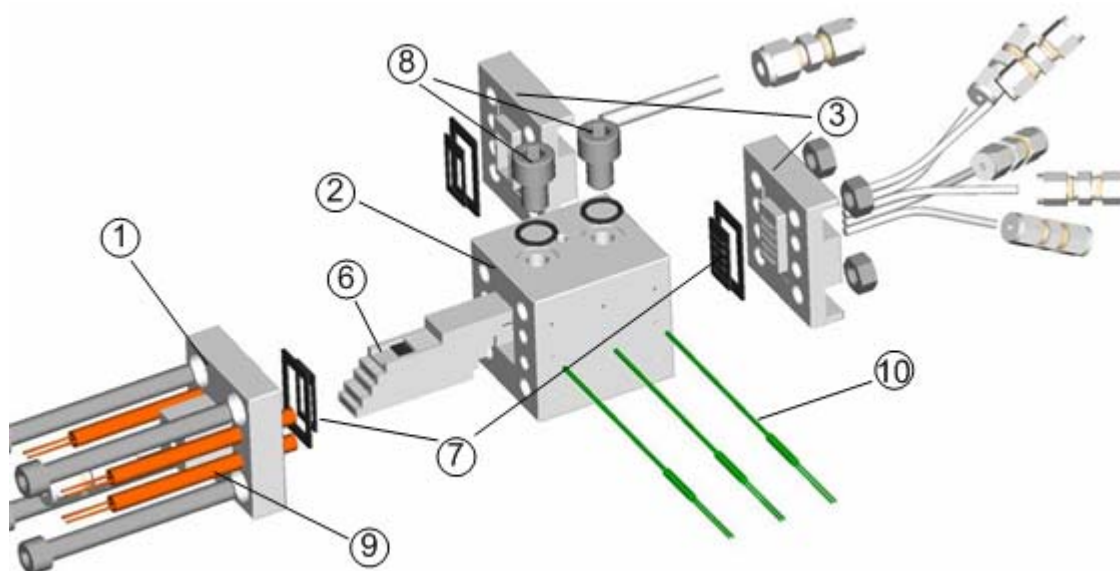


**Figure 73:** Drawing of the five fold reactor (detailed view).

To test leak tightness and pressure stability of the screening-reactor a leakage-test was performed, both at room temperature and at 120 °C, at 7 bar pressure.

Table 19 provides the results for both sealing-materials, which were excellent, since no significant pressure drop was observed.

**Table 19:** Pressure at various temperatures and for different sealing materials.

Temperature (°C)	Pressure loss (%/hour)	
	Graphite	Viton
23	1.92	0
120	2.01	0.30

Furthermore, to scrutinize the temperature profile, the reactor was heated up to various temperatures. With an infrared camera the temperature distribution of the reactor was

mapped (Figure 74). At low temperatures a homogeneous distribution of the temperature was formed, where at higher temperatures, above 100 °C some oscillations were observed.

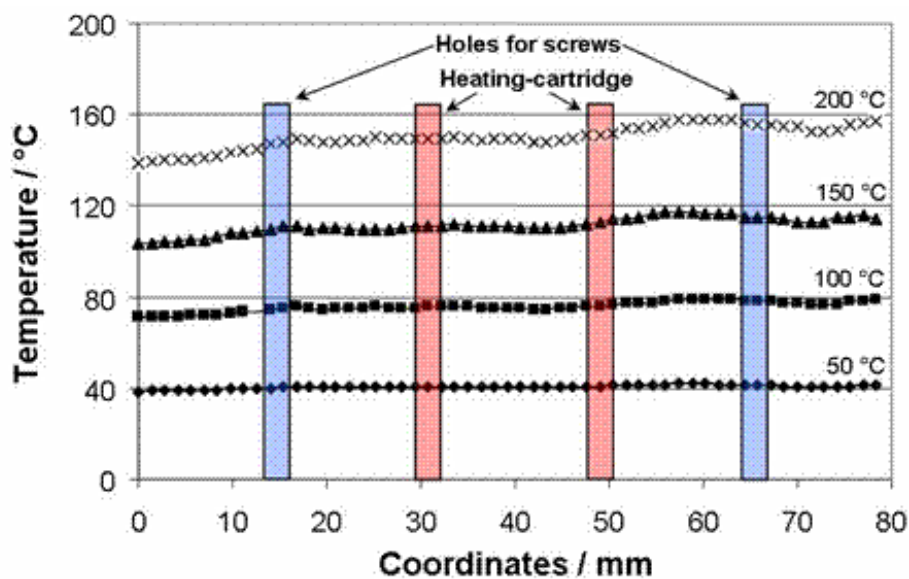
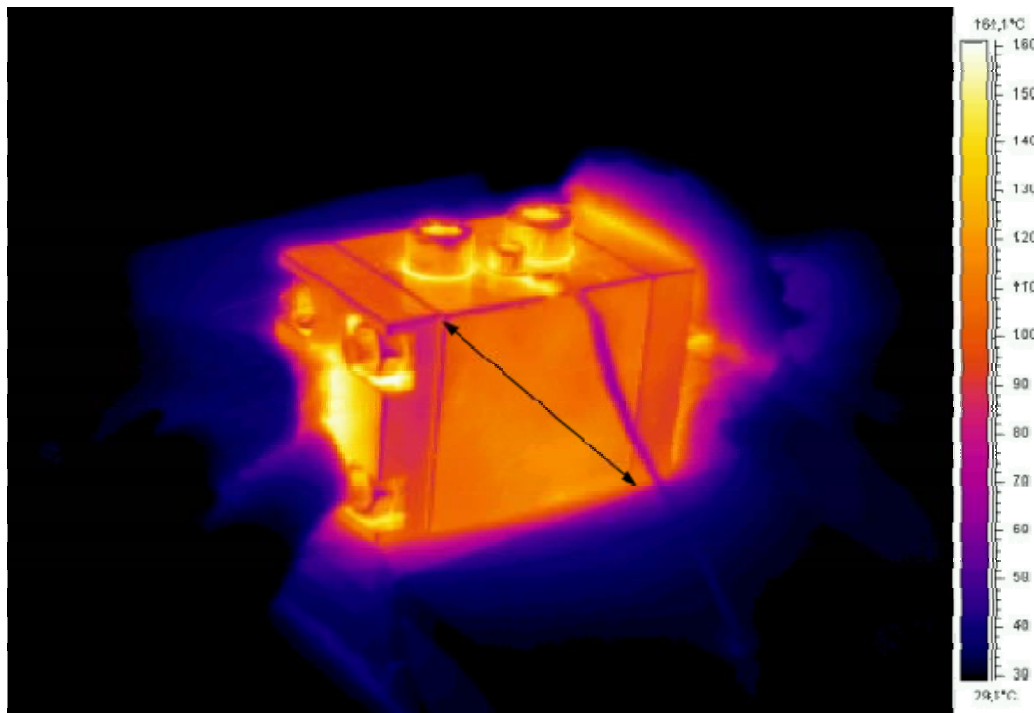


**Figure 74:** *Temperature distribution of the screening reactor (from up-left to down-right).*

In particular, at positions where the heating cartridges were plugged, no profile was indicated. The observed deviations at higher temperatures could be caused by a variable nature of surface. In both reactors, tests were carried out under atmospheric pressure and a total flowrate of 27 ml/min (STP) over each platelet which corresponds to a weight hourly

---

space velocity (WHSV) of  $180 \text{ dm}^3 \cdot \text{h}^{-1} \cdot \text{g}_{\text{cat}}^{-1}$  for each microreactor. WHSV was here defined as the ratio of the volumetric flowrate of the feed stream at STP to the weight of the catalyst coated onto the channels.

Gas flows were regulated by Bronkhorst mass flow controllers. A premixed gas mixture consisting only of hydrogen, carbon dioxide and carbon monoxide was obtained from Linde AG gas (class 1). The dry feed simulating the reformat stream was composed of 72 Vol.%  $\text{H}_2$ , 21 Vol.%  $\text{CO}_2$ , 1.27 Vol.%  $\text{CO}$ , 0.6 – 4.8 Vol.%  $\text{O}_2$  (depending on O/CO ratio), balance  $\text{N}_2$ . The ratio of nitrogen to oxygen at the feed was approximately that of air as would be the real case in a fuel processor. It was only varied when carrying out experiments with different O/CO ratios.

All feeds were heated before entering the microstructured device while pure nitrogen was used in all cases to simulate the cooling stream coming from the fuel cell side. Product gases flowed through a heated line before entering the gas chromatograph in order to avoid any water condensation.

### *3.3.2 Determination of the residence time distribution*

To find the exit age distribution curve,  $E(t)$ , for the recycle reactor, pulse (marker) experiments were performed. Such marker experiments, like the stimulus-response experiment, provide the age distribution of the molecules in a flow.

The marker must fulfil certain requirements: It must not affect the bulk flow of the process, it must mix perfectly with the bulk flow and it must be detectable. Carbon dioxide fulfilled all 3 requirements and was therefore selected.

The residence time distribution (RTD) was determined experimentally by injecting a  $9 \mu\text{l}$  volume, by means of a valve actuator described in section 3.3.3, of the inert chemical tracer into the reactor. The reactor was that depicted in Figure 68 without any catalyst on each surface to avoid adsorption of carbon dioxide inside the catalyst's pores. Great care was taken of synchronizing the pulse input with the initiation of data accumulation with an infrared sensor for RTD analysis. The valve actuator and the sensor were connected before and after the reactor respectively with a stainless steel pipe. Main consideration was to install a short as possible pipe to reduce dead volume which causes delay. For all of these experiments data were taken at 1 s intervals. The RTD was obtained from these data by normalization.

---

### 3.3.3 Valve actuator

To ensure that a specific quantity of tracer was entering the reactor, a valve actuator (GILSON Valvemate Rheodyne 7010) was applied for the determination of the RTD.

It consisted of a conventional six-port sample valve, which was used to inject the tracer into the continuous flow passing through the reactor.

The tracer-quantity (sample loop volume) used in RTD experiments amounted to 9  $\mu\text{l}$ .

### 3.3.4 TCOD IR-Sensor

Carbon dioxide was selected as suitable tracer. For measuring the tracer concentration, a carbon dioxide IR-Sensor (Winter GmbH Gas-Warnanlagen, Transducer TCOD-IR-5, Item Nr. 85785) connected with a data logger (Testo 125) for online analysis was used. Standard measuring range of the sensor was 0 – 5 Vol. % and the dead volume of the device was 0.5 ml. Response time was below 1 sec and the signal output between 4 mA and 20 mA on a logarithmic scale.

### 3.3.5 Pump

A cross-sectional view of the pump, (Metal Bellows, Senior Operations, INC. MB-HT 21 H.T. P/N 40075/27508) is shown in Figure 75. For metal bellow pumps welded metal bellows technology is used. This allows for unique features that are not available with conventional pumps or compressors. The pump was temperature-resistant up to 220 °C and suitable in cases where toxic, radioactive or explosive gases (here hydrogen) are processed.

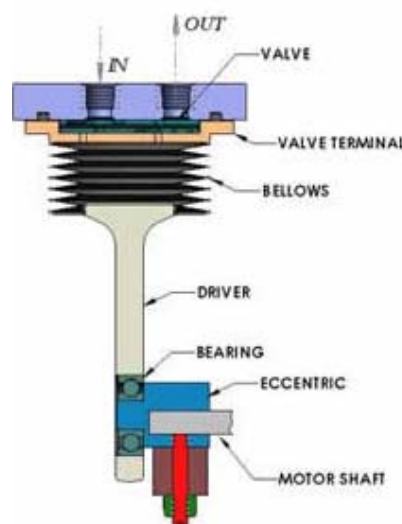


**Figure 75:** Metal bellows pump.

The central component of this pump is a welded diaphragm metal bellows, constructed from stainless steel. Because all the wetted surfaces are made of stainless steel and there are no wearing surfaces, these units are suitable for use in extreme environments where zero leakage, high reliability, and long life are required. The pump was heated by a heating cable to a temperature similar to that of the reactor.

### 3.3.6 Gas chromatograph

For the determination of the reaction rates, the product composition was monitored by online gas chromatography (Varian CP-4900 Micro-GC). It consisted of four different channels each with a separate thermal conductivity detector (TCD) and oven. Channel 1 had a 10 m long Molsieve column which could separate oxygen, nitrogen and carbon monoxide, channel 2 had a similar column to separate hydrogen and methane, channel 3 had a Porapak U column to separate carbon dioxide, water and HC-species up to butane. Channel 4 was not used. All channels used helium as carrier gas, which has a high thermal conductivity, with the exception of channel 2, which used nitrogen as carrier gas. The column pressure was in all cases 150 kPa. Each analysis lasted for 1 min, while it was possible to have an analysis cycle of ca. 1.5 min.

### 3.3.7 Microreactor as recycle reactor

The recycle reactor system had several advantages. Perfect mixing was achieved and negligible mass transfer was established, by external recycling of the gaseous phase with recycle ratios  $R$  ( $R = F_R/F_{in}$ ) greater than 25 [155 and 156].

Recirculation was succeeding by the recycle pump as depicted in Figure 76.

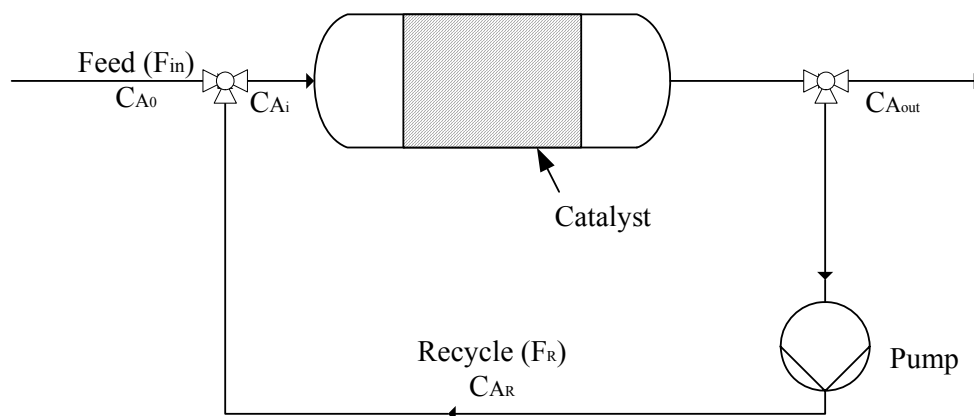


**Figure 76:** Process diagram of a recycle reactor.

The rotation speed of the recycle pump was controlled by an Opto 22™ control system. Flow rate was obtained by the careful and repeated calibration of the pump speed. This calibration was performed before each experiment to assure measurement accuracy.

The setup applied for the kinetic studies is depicted in Figure 77. The reactor presented in Figure 68 was used to determine the kinetic parameters. The test-bench consisted of a number of thermal mass flow controllers (BRONKHORST), which ensured a steady flow of gases. The feed gases were mixed in the tubing upstream the reactor by turbulent flow.



1. Flow controllers
2. Reactor inlet
3. Reactor (Figure 68)
4. Temperature controller
5. Bypass
6. To gas analysis equipment (GC)
7. Recycle pump

**Figure 77:** *Experimental setup for the determination of kinetics.*

Tests were carried out at a pressure of 1.3 bar. For experiments carried out without carbon dioxide and hydrogen in the reaction mixture, the feed was composed only of 0.5 – 2.0 Vol.% CO, O<sub>2</sub> (depending on O/CO ratio), and N<sub>2</sub> in balance. For experiments carried out with hydrogen in the reaction mixture, the feed was composed of 0 – 60 Vol.% H<sub>2</sub>, 0.5 – 2.0 Vol.% CO, O<sub>2</sub> (depending on O/CO ratio), and N<sub>2</sub> in balance. Finally, the feed simulating the reformat stream in the presence of carbon dioxide and hydrogen was composed of 0 – 60 Vol.% H<sub>2</sub>, 0 – 20 Vol.% CO<sub>2</sub>, 0.5 – 2.0 Vol.% CO, O<sub>2</sub> (depending on O/CO ratio), and N<sub>2</sub>

in balance. The ratio of nitrogen to oxygen in the feed was approximately that of air as it would be the case of a fuel processor. It was only varied when carrying out experiments with different O/CO ratios ( $\lambda$  ratio). The O/CO ratio was kept below 4. However, these differences were considered not to have any influence on the results. All feed components were preheated before entering the microstructured device.

When steam was added to the feed, bi-distillated water was fed from tanks to a microstructured electrically heated evaporator at 150 °C. To avoid condensation and minimize adsorption at the steel surface, all tubings and valves, including the pump, were heated to temperatures exceeding 120 °C.

The reactor was operated as a continuous stirred tank reactor (CSTR) also during experiments to examine the effects of temperature, O/CO ratio, and concentration of hydrogen, carbon dioxide and water on the reaction rate.

The Pt-Rh/Al<sub>2</sub>O<sub>3</sub> catalyst used was prepared according to the procedure described in 3.1.3. The total mass of catalyst amounted to 8.97 mg Pt-Rh/Al<sub>2</sub>O<sub>3</sub> catalyst which was washcoated onto the plates. Both method and catalyst were developed by IMM. The catalyst sample had passed a 1,000 h stability test [19] prior to the experiments described here and thus a stable performance was expected. In addition, to ensure that during the experiments no catalyst-deactivation occurred, activity-tests of the catalyst were performed after each set of experiments by simply isolating the reactor from the recycle-loop using two valves installed, which are shown in Figure 76.

To generate the recycle flow, a bellow-pump (see below) was used. The pump could achieve flow rates up to 4000 ml/min (STP) at a net feed flow rate of 100 Nml/min (STP). This corresponded to a recycle ratio of 40. A recycle ratio near 35 was chosen which was proven to be sufficient by residence time experiments to simulate an ideal CSTR [93]. The high recycle rates applied also excluded mass transfer limitations, which additionally was verified by the following estimations:

The extent of reaction per pass through the catalyst was very small; consequently isothermal conditions were established. The feed flow rate of 3,500 Nml/min was very high and corresponded to a WHSV of  $[=3.5 \cdot 60 / 0.00897] = 25,059 \text{ NI}/(\text{h} \cdot \text{g}_{\text{catalyst}})$ . To achieve stable and full conversion of carbon monoxide, the catalyst applied had to be operated at a WHSV  $[ \sim 0.03 \cdot 60 / 0.00897 ] \sim 215 \text{ NI}/(\text{h} \cdot \text{g}_{\text{catalyst}})$  in fuel processing applications. Thus, by applying a recycle ratio of 35, the conversion achieved did not exceeded 15%.

---

### 3.4 Calculations

#### 3.4.1 Material balance of a CSTR

The recycle loop of the setup had a defined volume  $V$  ( $\text{cm}^3$ ) through which the fluid flow  $F_R$  ( $\text{cm}^3/\text{s}$ ) is passed. The tracer introduced into the fluid entering the reactor, and the concentration of tracer leaving the reactor was recorded. The material balance of a CSTR is defined as follows:

$$V \frac{dC(t)}{dt} = F_R \cdot (C_1(t) - C(t)) \quad (19)$$

Dividing both sides with  $F_R$  and applying Laplace transformation the equation becomes:

$$G(s) = \frac{1}{\frac{V}{F_R} s + 1} = \frac{1}{\tau_{CSTR} \cdot s + 1} \quad (20)$$

$V/F_R$  is the residence time  $\tau$ . The inverse transformation gives the time-domain response (residence time distribution):

$$g_{CSTR}(t) = \frac{1}{\tau_{CSTR}} e^{-\frac{t}{\tau_{CSTR}}} \quad (21)$$

Applying the same for a plug flow reactor we get:

$$g_{PFR}(t) = t - \tau_{PFR} \quad (22)$$

For a system consisting of a series operation of a PFR and CSTR the overall transform equation derives by multiplying the individual transfer function and applying the inverse Laplace transformation on the result [87]:

$$E(t) = \frac{(t - \tau_{PFR})}{\tau_{CSTR}} e^{-\frac{(\tau_{PFR} - t)}{\tau_{CSTR}}} \quad (23)$$

#### 3.4.2 CO conversion and selectivity

The conversion and the selectivity of carbon monoxide were defined as follows:

$$CO \text{ conversion} = \frac{[CO]_{initial} - [CO]_{final}}{[CO]_{initial}} \quad (24)$$

And selectivity

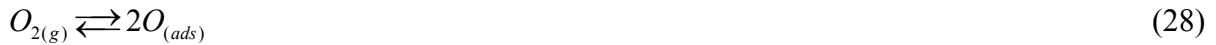
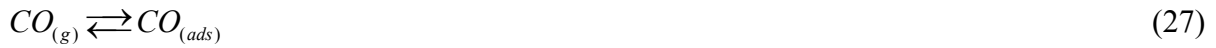
$$Selectivity = 0.5 \times \frac{[CO]_{final} - [CO]_{initial}}{[O_2]_{initial} - [O_2]_{final}} \quad (25)$$

The O/CO ratio, called  $\lambda$ , is defined as:

$$\lambda = \frac{2 \cdot [O_2]}{[CO]} \quad (26)$$

### 3.4.3 Mechanism of preferential oxidation reaction

In the preferential oxidation of carbon monoxide, water is also formed among to the presence of hydrogen. The overall reaction in the carbon monoxide oxidation process includes the equations (27), (28) and (29). On precious metal surfaces (e.g. platinum) the carbon monoxide oxidation reaction is generally believed to follow a Langmuir-Hinshelwood mechanism of the following type:



As carbon dioxide is comparatively weakly-bound to the surface, the desorption of this product is relatively fast and in many circumstances is the surface reaction between the two adsorbed species the rate determining step (rds) [157].

If the two adsorbed molecules are mobile on the surface, the rate of the reaction will be determined by the following rate expression for the bimolecular surface combinations step:

$$r = k \cdot \theta_{CO} \cdot \theta_O \quad (30)$$

In case carbon monoxide adsorbed as molecule and oxygen adsorbed dissociatively, are competing for the same adsorption sites then the relevant expressions are [91]:

$$\theta_{CO} = \frac{b_{CO} P_{CO}}{1 + b_{CO} P_{CO} + \sqrt{b_{O_2} P_{O_2}}} \quad (31)$$

$$\text{and } \theta_{O_2} = \frac{\sqrt{b_{O_2} P_{O_2}}}{1 + b_{CO} P_{CO} + \sqrt{b_{O_2} P_{O_2}}} \quad (32)$$

where  $b$  is a function of temperature and contains an exponential term of the form  $e^{E_A/RT}$ .

Substituting these into the rate expression (30) gives [91]:

$$r = k \cdot \frac{b_{CO} P_{CO} \sqrt{b_{O_2} P_{O_2}}}{\left(1 + b_{CO} P_{CO} + \sqrt{b_{O_2} P_{O_2}}\right)^2} \quad (33)$$

Assuming that carbon monoxide is much more strongly bound to the surface such that  $b_{CO} P_{CO} \gg 1 + b_{O_2} P_{O_2}$

and thus equation (30) simplifies to give [91]:

$$r_{CO} = k_0 \cdot e^{-\frac{E_A}{R \cdot T}} \cdot [CO]^\alpha \cdot [O_2]^\beta \quad (34)$$

This leaves only the partial concentration of carbon monoxide and oxygen in the reaction term.

However, the carbon monoxide oxidation reaction is frequently applied for the purification of reformer off-gas dedicated for PEM fuel cell supply and owing to the very limited carbon monoxide tolerance of low temperature PEM fuel cell catalysts [19]. In case steam reforming is applied, the reformat contains not only carbon monoxide but also hydrogen, carbon dioxide and steam. Therefore not only the kinetics of carbon monoxide oxidation was under investigation in the current work but also the effect of these reactants. Thus, we may assume the rate of the carbon monoxide oxidation as [122]:

$$r_{CO} = k_0 \cdot e^{-\frac{E_A}{R \cdot T}} \cdot [CO]^\alpha \cdot [O_2]^\beta \cdot [H_2]^\gamma \cdot [CO_2]^\delta \quad (35)$$

#### 3.4.4 Akaike's Information Criterion (AIC)

When fitting experimental data with regression, the main objective is to discriminate between different models or to test whether the data are more consistent with one possible mechanism relative to another.

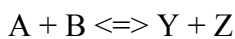
A statistic method for comparing models is Akaike's Information Criterion, abbreviated AIC. Accepting the assumption of regression, the AIC is defined by the equation (36):

$$AIC = N \cdot \ln\left(\frac{SS}{N}\right) + 2 \cdot K \quad (36)$$

where N is the number of data points, K is the number of parameters fit by the regression plus one and SS is the sum of square of the vertical distances of the points from the curve. The model with the lower AIC score is the model more likely to be correct.

#### 3.4.5 Arrhenius equation

For a reaction of the form:



the temperature dependence of the equilibrium constant:

$$\frac{d \ln K_C}{dT} = \frac{\Delta U^0}{R \cdot T^2} \quad (37)$$

$\Delta U^0$ : standard internal energy change of the reaction.

$K_c$ : equilibrium constant.

Knowing that the following relationships are true:

$$\Delta U^0 = E_1 - E_{-1} \text{ and } K_C = k_1/k_{-1}$$

The equation (37) can be rearranged to:

$$\frac{d \ln \left( \frac{k_1}{k_{-1}} \right)}{dT} = \frac{E_1 - E_{-1}}{R \cdot T^2} \Rightarrow \frac{d \ln k_1}{dT} - \frac{d \ln k_{-1}}{dT} = \frac{E_1}{R \cdot T^2} - \frac{E_{-1}}{R \cdot T^2} \quad (38)$$

And thus,

$$k_1 = A_1 \cdot e^{-E/RT} \text{ and } k_{-1} = A_{-1} \cdot e^{-E'/RT}.$$

The Arrhenius equation can also be written as:

$\ln(k) = \ln(A) - E/RT$ . A plot of  $\ln(k)$  vs.  $1/T$  yields a straight line with slope  $-E/R$  and slope  $\ln A$ . Figure 78 shows a plot of an Arrhenius Equation.

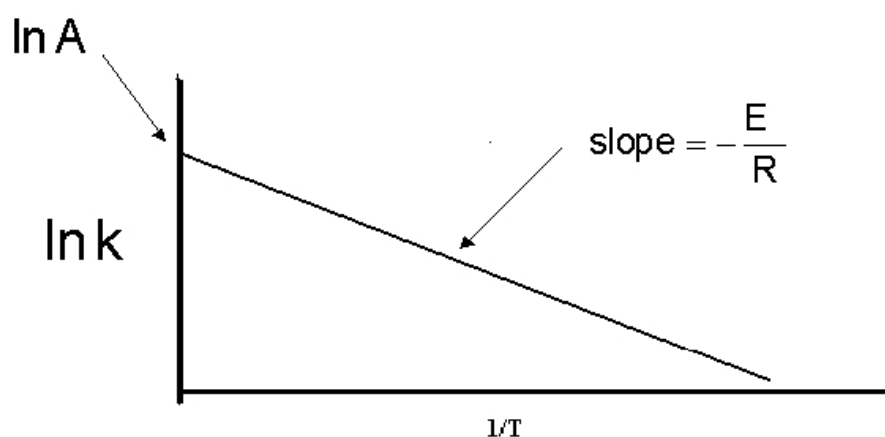


**Figure 78:** Plot of Arrhenius equation.

If we consider a simple reaction such as the one describe above, a collision between two molecules initiates the reaction and yields products. The vast majority of collisions are ineffective. The molecules have to be oriented in the correct way when they collide. Simple gas phase reaction will not occur unless the molecules are oriented in a “proper” way.

Molecules are held together with strong chemical bonds. In order to break these bonds, the colliding molecules need to have a large amount of kinetic energy from the collision. If they do not have enough energy, the reaction will not occur.

Reactions with large activation energies are slower at given temperature than reactions with small activation energies. As temperature increases, the rate of the reaction increases as well.

The fraction of collisions with an energy greater than  $E$  is represented by  $e^{-E/RT}$  (Boltzmann principle). Arrhenius then concluded that the rate constant can be related to that fraction.

It seems that zeolites have remarkable prospects as catalysts for the preferential oxidation of carbon monoxide. Because of their high sensitivity in the synthesis procedure, a further investigation and optimization is required.

Calcination temperature and heating rate play an important role for the activity of the catalyst. Low heating rates near 0.2 °C/min are essential, since at higher rates unstable zeolite-structures may be formed. The calcination must be performed under continuous flow in order to secure the complete water sewerage from the zeolite-pores. The platinum-iron supported catalyst was found to be the most active one, where zeolite Y-type under specific optimized pretreatment could perform also in an excellent way.

The ability to prepare these high-activity zeolite catalysts reproducibly should be an important goal for further research. Thus, a clear understanding of the effects that various pre-treatment and preparation conditions may have on the activity of the catalyst is crucial. Along with these active zeolites, it would be desirable to understand how the zeolite coatings can be further stabilized in a way that stable samples, containing a high density of active sites, can be prepared in a reproducible manner.

Concerning gold-catalysts, the specific requirements of the active site according to the active site model and the sensitivity of the catalyst to chloride poisoning are among the reasons for wide variations of reported activities of similar compositions in literature and within this work. Additionally, the majority of the studies on the preferential carbon monoxide oxidation have been conducted in model atmospheres (“idealized reformat”), consisting only of carbon monoxide, oxygen, hydrogen and an inert component (nitrogen or helium). Realistic methanol steam reformat, however, contains up to 20 Vol.% CO<sub>2</sub> and 10 – 20 Vol.% H<sub>2</sub>O.

---

The influence of carbon dioxide on these catalysts was the most significant parameter. It is, thus, evident that the magnitude of the negative effect provoked by the presence of carbon dioxide on both the activity of the preferential carbon monoxide oxidation and the selectivity are strongly dependent on the nature of the gold-catalysts. Among the samples tested, the Au/Co<sub>3</sub>O<sub>4</sub> catalyst was the most sensitive, while the platinum based catalysts were the most resistant towards deactivation by carbon dioxide.

Based on the results presented in the present work, we may conclude that for low reaction temperatures (i.e.,  $T < 125$  °C), the Au/Co<sub>3</sub>O<sub>4</sub> catalyst was superior to the Pt-Rh/ $\gamma$ -Al<sub>2</sub>O<sub>3</sub> and Pt<sub>0.5</sub>Al<sub>1</sub>Mn<sub>7</sub>Co<sub>91.5</sub>O<sub>x</sub> for the preferential oxidation of carbon monoxide in the absence of carbon dioxide. At higher reaction temperatures the activity of Pt-Rh/ $\gamma$ -Al<sub>2</sub>O<sub>3</sub> and Pt<sub>0.5</sub>Al<sub>1</sub>Mn<sub>7</sub>Co<sub>91.5</sub>O<sub>x</sub> catalysts improved rapidly, as it was also the case in the presence of carbon dioxide in the reactant feed. Both catalysts exhibited good tolerance towards carbon dioxide, retaining their activity and selectivity when 20 Vol.% CO<sub>2</sub> was present in the reactant feed while for Au/Co<sub>3</sub>O<sub>4</sub> catalyst conversion dropped immediately.

Pt-Rh/ $\gamma$ -Al<sub>2</sub>O<sub>3</sub> and Pt<sub>0.5</sub>Al<sub>1</sub>Mn<sub>7</sub>Co<sub>91.5</sub>O<sub>x</sub> were found to oxidize carbon monoxide effectively in the presence of excess hydrogen and carbon dioxide and in the desired temperature range (140 – 180 °C). Both catalysts appeared to be quite stable under reaction conditions, especially with respect to selectivity. They exhibited stable activity in a dry feed for at least 70 h and succeeded in reducing the carbon monoxide concentration of the feed below 10 ppm from an inlet concentration of 1.2 Vol.% at different O/CO ratio (from 2 to 4).

The Pt<sub>0.5</sub>Al<sub>1</sub>Mn<sub>7</sub>Co<sub>91.5</sub>O<sub>x</sub> catalyst for the preferential carbon monoxide oxidation was found to be superior to the Pt-Rh/Al<sub>2</sub>O<sub>3</sub> catalyst. The Pt<sub>0.5</sub>Al<sub>1</sub>Mn<sub>7</sub>Co<sub>91.5</sub>O<sub>x</sub> catalyst was more active and selective while operating at lower reaction temperature, thus had substantial potential in preferential oxidation of carbon monoxide for commercial applications.

Another important factor was the platinum content, since platinum generally is not abundant and its price may strongly affect the market for fuel cells, a potential factor for this application. The low content of platinum in the CoMn-catalyst, which was only 10% of that of the reference catalyst, is a strong argument for the former. Since the content of platinum has not yet been optimized and thus may become even smaller than 0.5 wt.%, the CoMn-catalyst may become a realistic alternative to the state-of-the-art catalysts.

For the estimation of all parameters, a recycle reactor was set up, which had numerous advantages as it was mentioned in chapter 1.5. Perhaps the greatest advantage of this reactor was its ability to control the temperature of the catalysts more accurately. A further benefit persisted in the fact that due to perfect mixing, that can be achieved at high recycle ratios, the

material balances were the same like in the ideal, perfectly continuous stirred tank reactor (CSTR). Maintaining the recycle ratio above 25, the reactor behaved like a CSTR, which made the application of simple algebraic equations for the determination of the kinetics possible and thus to simplify the estimation of reaction kinetics.

The predictions of the residence time distribution (RTD) for a CSTR simulated by a microreactor with a recycle stream, operating in turbulent flow, has been shown to give an adequate approximation of experimental measurements.

We have shown that the kinetics of the preferential carbon monoxide oxidation and hydrogen oxidation on Pt-Rh/ $\gamma$ -Al<sub>2</sub>O<sub>3</sub> catalyst in simulated reformer gas in the microreactors is well described by a simple power-law expression. To our knowledge, the use of a microreactor operated as recycle reactor for the determination of reaction kinetics is a novel approach. Analysis of the differential data obtained with the catalyst containing 5 wt.% Pt and 5 wt.% Rh resulted in an activation energy ranging from 92.6 kJ/mole to 94.2 kJ/mole, depending on the reaction mixture (within errors are not widely different). In case where only carbon monoxide and oxygen are present in the reaction mixture, the exponents  $\alpha$  and  $\beta$ , of the partial concentrations, were found to be -0.53 and 0.79 respectively. Additionally,  $\alpha$  and  $\beta$  parameters found to be influenced, as expected, by the presence of large amounts of hydrogen and thus the increase of the oxygen reaction order from 0.79 to 1.0 is consistent with a lowering of the effective oxygen coverage. The exponent  $\alpha$ , of carbon monoxide partial concentration, was found to be -0.68 in the presence of hydrogen.

The inhibiting effect of carbon dioxide on both reaction rates may be explained by the adsorption of carbon dioxide on alumina, leading to the formation of carboxylate and carbonate species [121]. The latter species can decrease the reaction rate for both reactions by decreasing the alumina surface available for oxygen adsorption (competitive adsorption) and thus decreasing the concentration of adsorbed oxygen on alumina. This way the interface reaction is hindered. Another possible reason for this decrease can be the decrease of oxygen surface diffusion. The exponents  $\alpha$  and  $\beta$  of carbon monoxide and oxygen partial concentrations were found to be -0.61 and 0.83 respectively.

Furthermore, the undesired parallel reaction of the hydrogen oxidation was also investigated. The activation energy was found to be approximately 12.73 kJ/mole and the exponents of hydrogen, oxygen and carbon monoxide partial concentrations -0.26, 0.09 and -0.06 respectively.

The negative influence of hydrogen on both reactions is explained also as the effective removal of active oxygen through water formation. On the other hand, steam has no effect on

---

---

the catalyst performance at temperatures exceeding 160 °C, whereas it enhances oxidation rates at lower temperatures.

This system, and the conclusions made on these catalysts, has a substantial potential in advancing the knowledge in catalysis and in reaction engineering for commercial applications. The need to develop a model, applicable for all case-studies presented here, is intended. Therefore, various issues need to be addressed in future studies.

---

# 5

## REFERENCES

1. R. Wurster, "PEM fuel cell in stationary and mobile applications pathways to commercialization", 6th International Technical Congress, **1999**.
  2. G. P. Nowell, "The promise of methanol fuel cell vehicles", American Methanol Institute.
  3. A. J. Appleby, F. R. Foulkes, "Fuel Cell Handbook", Van Nostrand Reinhold, New York **1989**.
  4. A. Gavriilidis, P. Angeli, E. Cao, K. K. Yeong, Y. S. S. Wan, "Technology and applications of microengineered reactors", Chemical Engineering Research and Design **2002**, 80, 3-30.
  5. G. Cacciola, V. Antonucci, S. Freni, "Technology up date and new strategies on fuel cells", Journal of Power Sources **2001**, 100, 67-79.
  6. C. Hebling, A. Heinzl, D. Golombowski, T. Meyer, M. Müller, M. Zedda, "Fuel cells for low power applications", Proceedings of the 3rd International conference on microreaction technology, Germany **2000**, 383-393.
  7. D. L. Trimm, Z. I. Önsan, "Onboard fuel conversion for hydrogen-fuel-cell-driven vehicles", Catalysis Reviews **2001**, 43, 31-84.
-

- 
8. G. Avgouropoulos, T. Ioannides, H. K. Matralis, J. Batista, S. Hocevar, "CuO-CeO<sub>2</sub> mixed oxide catalysts for the selective oxidation of carbon monoxide in excess hydrogen", *Catalysis Letters* **2001**, 73, 33-40.
  9. H. Igarashi, H. Uchida, M. Suzuki, Y. Sasaki, M. Watanabe, "Removal of carbon monoxide from hydrogen-rich fuels by selective oxidation over platinum catalyst supported on zeolite", *Applied Catalysis, A: General* **1997**, 159, 159-169.
  10. X. Liu, O. Korotkith, R. Farrauto, "Selective catalytic oxidation of CO in H<sub>2</sub>: structural study of Fe oxide-promoted Pt/alumina catalyst", *Applied Catalysis, A: General* **2002**, 226, 293-303.
  11. J. Holladay, E. Jones, D. R. Palo, M. Phels, Ya-Huei Chin, R. Dagle, J. Hu, Y. Wang, E. Baker, "Miniature fuel processors for portable fuel cell power supplies", *Materials Research Society Symposium Proceedings* **2004**, Vol. 756.
  12. R. W. McCabe, P. J. Mitchell, "Synergism between palladium and silver in methanol and carbon monoxide oxidation over an alumina-supported palladium-silver catalyst" *Journal of Catalysis* **1987**, 103, 419-425.
  13. M. J. M. Mies, E. V. Rebrov, M. H. J. M. de Croon, J. C. Schouten, "Design of a molybdenum high throughput microreactor for high temperature screening of catalytic coatings", *Chemical Engineering Journal* **2004**, 101, 225-235.
  14. V. Hessel, S. Hardt, H. Löwe, "Chemical Micro Process Engineering - Fundamentals, Modelling and Reactions", Wiley-VCH, Weinheim, Germany **2004**.
  15. V. Hessel, H. Löwe, A. Müller, G. Kolb, "Chemical Micro Process Engineering – Processing and Plants", Wiley-VCH, Weinheim **2005**.
  16. K. Jähnisch, V. Hessel, H. Löwe, M. Baerns, "Chemistry in Microstructured Reactors", *Angewandte Chemie International Edition* **2004**, 43, 406-446.
-

- 
17. V. Hessel, P. Löb, H. Löwe, “Development of Microstructured Reactors to Enable Organic Synthesis Rather than Subduing Chemistry”, *Current Organic Chemistry*. **2005**, 8, 765-787.
  18. H. Pennemann, P. Watts, S. Haswell, V. Hessel, H. Löwe, “Benchmarking of microreactor applications”, *Organic Process Research and Development*. **2004**, 422-439.
  19. G. Kolb, V. Hessel, V. Cominos, C. Hofmann, H. Löwe, G. Nikolaidis, R. Zapf, A. Ziogas, E. R. Delsman, M. H. J. M. de Croon, J. C. Schouten, O. de la Iglesias, R. Mallada, J. Santamaria, “Selective Oxidations in Microstructured Catalytic Reactors – A review and an Overview of Own Work on Fuel Processing for Fuel Cells”, *Catalysis Today* **2006**, 120, 2-20.
  20. K. Schubert, W. Bier, G. Linder, D. Seider, “Herstellung und Test von kompakten Mikrowärmeüberträgern”, *Chemie Ingenieur Technik* **1989**, 61, 172-173.
  21. G. Ondrey, “Microreaction engineering: birth of a new discipline?”, *Chemical Engineering Journal* **2001**, 56, 293-303.
  22. V. Cominos, V. Hessel, C. Hofmann, G. Kolb, H. Pennemann, R. Zapf, “Fuel processing in catalytically coated microreactors for low power fuel cell applications”, *Microreactor technology and process intensification*, ACS Symposium Series 914 (eds.: J. Wang and J. D. Holladay), ACS Books Department **2005**, 194-208.
  23. G. Kolb, V. Hessel, “Micro-structured reactors for gas phase reactions”, *Chemical Engineering Journal* **2004**, 98, 1-38.
  24. W. Ehrfeld, V. Hessel, H. Löwe, “Microreactors: new technology for modern chemistry”, Wiley-VCH, Weinheim, Germany **2000**.
  25. L. Kiwi-Minsker, A. Renken, “Microstructured reactors for catalytic reactions”, *Catalysis Today* **2005**, 110, 2-14.
-

- 
26. K. Jensen, "Microreaction engineering – is small better?", *Chemical Engineering Science* **2001**, 56, 293-303.
  27. K. Shah, X. Ouyang, R. S. Besser, "Microreaction for Microfuel Processing: Challenges and Prospects", *Chemical Engineering and Technology*. **2005**, 28, 303-313.
  28. S. M. Akam, E. V. Rebrov, M. H. J. M. de Croon, J. C. Schouten, "A kinetic study of the water gas shift reaction on two molybdenum carbide catalysts coatings with different morphologies", *Technische Univesiteit Eindhoven* **2006**.
  29. E. V. Rebrov, S. A. Duinkerke, M. H. J. M. de Croon, J. C. Schouten, "Optimisation of heat transfer characteristics, flow distribution, and reaction processing for a microstructured reactor/heat-exchanger for optimal performance in platinum catalysed ammonia oxidation", *Chemical Engineering Journal* **2003**, 93, 201-216.
  30. A. Manz, N. Graber, H. M. Widmer, "Miniaturized total chemical analysis systems: a novel concept for chemical sensing", *Sensors and Actuators B: Chemical* **1990**, 1, 244-248.
  31. A. Müller, K. Drese, H. Gnaser, M. Hampe, V. Hessel, H. Löwe, S. Schmitt, R. Zapf, "Fast preparation and testing methods using a microstructured modular reactor for parallel gas phase catalyst screening", *Catalysis Today* **2002**, 81, 377-391.
  32. D. C. Hendershot, "Process minimization: making plants safer", *Chemical Engineering Progress* **2000**, 96, 35-40.
  33. W. Ehrfeld, V. Hessel, V. Haverkamp, "Microreactors, Ullmann's encyclopedia of industrial chemistry", Wiley-VCH, Weinheim, Germany **1999**.
  34. S. Hasebe, "Design and operation of micro-chemical plants-bridging the gap between nano, micro and macro technologies", *Computers and Chemical Engineering* **2004**, 57-64.
  35. O. Wörz, K.-P. Jäckel, T. Richter, A. Wolf, "Microreactors-a new efficient tool for reactor development", *Chemical Engineering and Technology* **2001**, 24, 138-142.
-

- 
36. S. Srinivas, A. Dhingra, H. Im, E. Gulari, "A scalable silicon microreactor for preferential CO oxidation performance comparison with a tubular packed-bed microreactor", *Applied Catalysis A: General* **2004**, 274, 285-293.
  37. H. Igarashi, T. Fujimo, M. Watanabe, "Hydrogen electro-oxidation on platinum catalysts in the presence of trace carbon monoxide", *Journal of Electroanalytical Chemistry* **1995**, 391, 119-123.
  38. H. F. Oetjen, V. M. Schmidt, U. Stimming, F. J. Trila, "Performance Data of a Proton Exchange Membrane Fuel Cell Using H<sub>2</sub>/CO as Fuel Gas", *Electrochemical Society* **1996**, 143, 3838-3842.
  39. J. N. Armor, *Applied Catalysis B: Environmental Catalysis*. **1992**, 221-256.
  40. R. J. Farrauto, C. H. Bartholomew, "Fundamentals of Industrial Catalytic Processes", Blackie Academic and Professional, London **1999**.
  41. R. K. Herz, D. R. Badlani, D. R. Schryer, B. T. Upchurch, "Two-Component Catalysts for Low-Temperature CO Oxidation: A Monte Carlo Study", *Journal of Catalysis* **1993**, 141, 219-238.
  42. A. Manasilp, E. Gulari, "Selective CO oxidation over Pt/alumina catalysts for fuel cell applications", *Applied Catalysis B: Environmental* **2002**, 37, 17-25.
  43. L. Simonot, F. Garin, G. Maire, "A comparative study of LaCoO<sub>3</sub>, Co<sub>3</sub>O<sub>4</sub> and LaCoO<sub>3</sub>-Co<sub>3</sub>O<sub>4</sub> I. Preparation, characterisation and catalytic properties for the oxidation of CO", *Applied Catalysis B: Environmental* **1997**, 11, 167-179.
  44. W. Lin, M. Fytlzani-Stephanopoulos, "Total Oxidation of Carbon Monoxide and Methane over Transition Metal Fluorite Oxide Composite Catalysts: I. Catalyst Composition and Activity", *Journal of Catalysis* **1995**, 153, 304-316.
  45. M. Echigo, N. Shinke, S. Takami, S. Higashiguchi, K. Hirai, T. Tabata, "Development of residential PEFC cogeneration systems: Ru catalyst for CO preferential oxidation in reformed gas", *Catalysis Today* **2003**, 84, 209-215.
-

- 
46. V. Cominos, V. Hessel, C. Hofmann, G. Kolb, R. Zapf, A. Ziogas, E. R. Delsman, J. C. Schouten, "Selective oxidation of carbon monoxide in a hydrogen-rich fuel cell feed using a catalyst coated microstructured reactor", *Catalysis Today* **2005**, 110, 140-153.
  47. P. V. Snytnikov, V. A. Sobyanin, V. D. Belyaev, P. G. Tsyrunnikov, N.B. Shitova, D.A. Shlyapin, "Selective oxidation of carbon monoxide in excess hydrogen over Pt-, Ru- and Pd-supported catalysts", *Applied Catalysis A: General* **2003**, 239, 149-156.
  48. J. Yan, J. Ma, P Cao., P Li., "Preferential oxidation of CO in H<sub>2</sub>-rich gases over Co-promoted Pt-Al<sub>2</sub>O<sub>3</sub> catalyst", *Catalysis Letters* **2004**, 93, 55-60.
  49. C. D. Dudfield, R. Chen, P. L. Adcock, "Evaluation and modelling of a CO selective oxidation reactor for solid polymer fuel cell automotive applications", *Journal of Power Sources* **2000**, 85, 237-244.
  50. M. J. Kahlich, H. A. Gasteiger, R. J. Behm, "Kinetics of the selective CO oxidation in H<sub>2</sub>-rich gas on Pt/Al<sub>2</sub>O<sub>3</sub>", *Journal of Catalysis* **1997**, 171, 93-105.
  51. Y. J. Mergler, A. van Aalst, J. van Delft, B. E. Nieuwenhuys, "CO oxidation over promoted Pt catalysts", *Applied Catalysis B: Environmental* **1996**, 10, 245-261.
  52. Y. Cai, Harvey G. Stenger, Charles E. Lyman, "Catalytic CO oxidation over Pt-Rh/ $\gamma$ -Al<sub>2</sub>O<sub>3</sub> catalysts", *Journal of Catalysis* **1996**, 161, 123-131.
  53. G. W. Roberts, P. Chin, X. L. Sun, J. J Spivey, "Preferential oxidation of carbon monoxide with Pt/Fe monolithic catalysts: interactions between external transport and the reverse water-gas-shift reaction", *Applied Catalysis B: Environmental* **2003**, 46, 601-611.
  54. G. Chen, Q. Yuan, H. Li, S. Li, "CO selective oxidation in a microchannel reactor for PEM fuel cell", *Chemical Engineering Journal* **2004**, 101, 101-106.
  55. X. Ouyang, L. Bednarova, R. S. Besser, P. Ho, "Preferential oxidation (PrOx) in a thin-film catalytic microreactor: Advantages and limitations", *AIChE Journal* **2005**, 51, 1758-1772.
-

- 
56. S. H. Oh, R. M. Sinkevitch, "Carbon Monoxide removal from hydrogen rich fuel cell feedstreams by selective catalytic oxidation", *Journal of Catalysis* **1993**, 142, 254-262.
  57. T. Ince, G. Uysal, A. Nilgün Akin, R. Yildirim, "Selective low-temperature CO oxidation over Pt-Co-Ce/Al<sub>2</sub>O<sub>3</sub> in hydrogen-rich streams", *Applied Catalysis A: General* **2005**, 292, 171-176.
  58. Th. Ioannides, X. Verykios, "Influence of the carrier on the Interaction of H<sub>2</sub> and CO with Rh", *Journal of Catalysis* **1992**, 140, 353-369.
  59. D. H. Kim, M. S. Lim, "Kinetics of selective CO oxidation in hydrogen-rich mixtures on Pt/alumina catalysts", *Applied Catalysis A: General* **2002**, 224, 27-38.
  60. M. Watanabe, H. Uchida, H. Igarashi, M. Suzuki, "Pt catalyst supported on Zeolite for Selective oxidation of CO in reformed gases", *Chemistry Letters* **1995**, 24, 21-22.
  61. Y. Hasegawa, K. Kusajabem, S. Norooka, "Selective oxidation of carbon monoxide in hydrogen-rich mixtures by permeation through a platinum-loaded Y-type zeolite membrane", *Journal of Membrane Science* **2001**, 190, 1-8.
  62. G. Avgouropoulos, T. Ioannides, "Selective CO oxidation over CuO-CeO<sub>2</sub> catalysts prepared via the urea-nitrate combustion method", *Applied Catalysis A: General* **2003**, 244, 155-167.
  63. S. Y. Chin, O. S. Alexeev, M. D. Amiridis, "Preferential oxidation of CO under excess H<sub>2</sub> conditions over Ru catalysts", *Applied Catalysis A: General* **2005**, 286, 157-166.
  64. O. Korotkikh, R. Farrauto, "Selective catalytic oxidation of CO in H<sub>2</sub>: fuel cell applications", *Catalysis Today* **2000**, 62, 249-254.
  65. J. W. Sallfrank, W. F. Maier, "Doping, selection and composition spreads, a combinatorial strategy for the discovery of new mixed oxide catalysts for low temperature CO Oxidation", *Comptes Rendus Chimie* **2004**, 7, 483-494.
-

- 
66. J. W. Saalfrank, W. F. Maier, "Directed Evolution of Noble-Metal-Free catalysts for the Oxidation of CO at Room Temperature", *Angewandete Chemie* **2004**, 43, 2028-2031.
  67. W. F. Maier, J. W. Saalfrank, "Discovery, combinatorial chemistry and a new selective CO-oxidation catalyst", *Chemical Engineering Science* **2004**, 59, 4673-4678.
  68. M. Haruta, N. Yamada, T. Kobayashi, S. Iijima, "Gold catalysts prepared by coprecipitation for low temperature oxidation of hydrogen and of carbon monoxide", *Journal of Catalysis* **1989**, 115, 301-309.
  69. M. Haruta, S. Tsubota, T. Kobayashi, H. Kageyama, Michel J, Genete, B. Delmon, "Low-temperature oxidation of CO over Gold Supported on TiO<sub>2</sub>,  $\alpha$ -Fe<sub>2</sub>O<sub>3</sub> and Co<sub>3</sub>O<sub>4</sub>", *Journal of Catalysis* **1993**, 144, 175-192.
  70. H. H. Kung, M. C. Kung, C. K. Costello, "Supported Au catalysts for low temperature CO oxidation", *Journal of Catalysis* **2003**, 216, 425-432.
  71. G. K. Bethke, H. H. Kung, "Selective CO oxidation in a hydrogen-rich stream over Au/ $\gamma$ -Al<sub>2</sub>O<sub>3</sub> catalysts", *Applied Catalysis A: General* **2000**, 194-195, 43-53.
  72. G. R. Bamwenda, S. Tsubota, T. Nakamura, M. Haruta, "The influence of the preparation methods on the catalytic activity of platinum and gold supported on TiO<sub>2</sub> for CO oxidation", *Catalysis Letters* **1997**, 44, 83-87.
  73. S. K. Tanielyan, R. L. Augustine, "Effect of catalyst pretreatment on the oxidation of carbon monoxide over coprecipitated gold catalysts", *Applied Catalysis A: General* **1992**, 85, 73-87.
  74. M. M. Schubert, V. Plzakm, J. Garche, R. J. Behm, "Activity, selectivity, and long-term stability of different metal oxide supported gold catalysts for the preferential CO oxidation in H<sub>2</sub>-rich gas", *Catalysis Letters* **2001**, 76, 143-150.
-

- 
75. M. J. Kahlich, H. A. Gasteiger, R. J. Behm, "Kinetics of the Selective Low-Temperature Oxidation of CO in H<sub>2</sub>-Rich Gas over Au/ $\alpha$ -Fe<sub>2</sub>O<sub>3</sub>", *Journal of Catalysis* **1999**, 182, 430-440.
  76. D. E. W. Vaughan, "The synthesis and manufacture of Zeolites", Exxon research and Engineering Co., *Chemical Engineering Progress* **1988**, 25-31.
  77. N. Y. Chen, T. F. Degnan, "Industrial catalytic applications of zeolites", *Chemical Engineering Progress* **1988**, 32-41.
  78. IZA Structure commission Homepage, Stand **October 2002**,  
<http://www.iza-structure.org/databases>.
  79. Subhash Bhatia, *Zeolite Catalysis: Principles and Applications*, CRC Press, Inc., Boca Raton, Florida, **1990**.
  80. D. E. W. Vaughan, "Industrial uses of Zeolite catalysts", Davison Chemical Division, W. R. Grace & Co. Washington Research Center, 294-328.
  81. Süd Chemie Homepage, Stand **July 2007**,  
<http://www.sud-chemie.com/scmcms/web/content.jsp?nodeId=3680&lang=en>.
  82. S. Brunauer, P. H. Emmett, E. Teller, "Adsorption of gases in multimolecular layers", *Journal of American Chemical Society*. **1938**, 60, 309-319.
  83. X-ray Diffraction Mineralogy with Impact K/T GeoServices, Inc. James Talbot, 4993 Kiowa Trail, Argyle TX 76226-1573 USA.
  84. Jones Alan, "Temperature-Programmed Reduction for Solid Materials Characterization", Marcel Dekker, ISBN: 9780824775834, New York **1996**.
  85. D. B. Williams, C. B. Carter, "Transmission Electron Microscopy", Books 1 to 4, Plenum Press **1996**.
  86. P. Stremple, "Analytical Gas Chromatography", Academic Press; 2nd edition (November 15, 2006), ISBN-13: 978-0123843579.
-

- 
87. O. Levenspiel, *Chemical Reaction Engineering*, 3rd Edition, John Wiley & Sons, **1999**.
  88. M. Čurlin, H. Korajlija, M. Matošić, I. Mijatović, Ž. Kurtanjek, “Effect of hydraulic residence time and mixing on wastewater treatment in a membrane bioreactor”, 1st EMCO Workshop 20-21 October **2005**, Dubrovnik, Croatia.
  89. T. Jokinen 2.10.1999 / Cesa Hölttä 31.8.2001, Tracer Experiment, Helsinki University of Technology, Control Engineering Laboratory.
  90. M. I. Temkin, “Gradientless methods fore the determinations of reaction rates”, Translated from *Kinetica I Kataliz*, **1962**, 3, 509-517.
  91. School of Biological and Chemical Sciences, Queen Mary, University of London, Mile End Road, London E1 4NS. Stand **July 2007**,  
<http://www.chem.qmul.ac.uk/surfaces/scc/>
  92. J. L. Ayastuy, M. P. Gonzalez-Marcos, A. Gil-Rodriguez, J. R. Gonzalez-Velasco, M. A. Gutierrez-Ortiz, “Selective CO oxidation over  $Ce_xZr_{1-x}O_2$ -supported Pt catalysts”, *Catalysis Today* **2006**, 116, 391-399.
  93. J. M. Berty, “Testing commercial Catalysts in recycle reactors”, *Catalysis Reviews- Science and Engineering* **1979**, 20, 75-96.
  94. J. J. Carberry, “Designing laboratory catalytic reactors”, *Industrial and Engineering Chemistry* **1964**, 56, 39-46.
  95. M. Burriela, G. Garciaa, J. Santisoa, A. N. Hanssonb, S. Linderothb, A. Figueras, “ $Co_3O_4$  protective coatings prepared by Pulsed Injection Metal Organic Chemical Vapour Deposition”, *Thin Solid Films* **2005**, 473, 98-103.
  96. A. C. Gluhoi, H. S. Vreeburg, J. W. Bakker, B. E. Nieuwenhuys, “Activation of CO,  $O_2$  and  $H_2$  on gold-based catalysts”, *Applied Catalysis A: General* **2005**, 291, 145-150.
  97. L. Ilieva, J. W. Sobczak, M. Manzoli, B. L. Su, D. Andreeva, “Reduction behavior of nanostructured gold catalysts supported on mesoporous titania and zirconia”, *Applied Catalysis A: General* **2005**, 291, 85-92.
-

- 
98. M. Nakamoto, M. Yamamoto, "New Type of Organically Capped Gold Nanoparticles prepared by Controlled Thermolysis of Gold Complexes", Osaka Municipal Technical Research Institute, Morinomiya, Joto-ku, Osaka, 536-8553, Japan.
  99. J. Jingxi, Z. Cangfeng, Z. Lixiong, X. Nanping, "Continuous synthesis of zeolite NaA in a microchannel reactor", *Chemical Engineering Journal* **2006**, 116, 115-121.
  100. I. N. Remediakis, N. Lopez, J. K. Norskov, "CO oxidation on gold nanoparticles: Theoretical studies", *Applied Catalysis A: General* **2005**, 291, 13-20.
  101. J. M. C. Soares, M. Bowker, "Low temperature CO oxidation on supported and unsupported gold compounds", *Applied Catalysis A: General* **2005**, 291, 136-144.
  102. B. E. Solsona, T. Garcia, C. Jones, S. H. Taylor, A. F. Carley, G. J. Hutchings, "Supported gold catalysts for the total oxidation of alkanes and carbon monoxide", *Applied Catalysis A: General* **2006**, 312, 67-76.
  103. E. D. Park, J. S. Lee, "Effects of pretreatment conditions on CO oxidation over supported Au catalysts", *Journal of Catalysis* **1999**, 186, 1-11.
  104. R. J. H. Grisel, B. E. Nieuwenhuys, "Selective oxidation of CO over supported Au catalysts", *Journal of Catalysis* **2001**, 199, 48-59.
  105. Offenlegungsschrift DE 102 05 873 A1.
  106. C. Yeong-Jey, Y. Chuin-Tih, "Deposition of highly disperse gold on Alumina support", *Journal of Catalysis* **2001**, 200, 59-68.
  107. <http://www.subtleenergies.com/ormus/research/precip.htm>
  108. M. Date, M. Haruta, "Moisture effect on CO oxidation over Au/TiO<sub>2</sub> catalyst", *Journal of Catalysis* **2001**, 201, 221-224.
  109. T. V. Choudhary, D. W. Goodman, "Catalytically active gold: The role of cluster morphology", *Applied Catalysis A: General* **2005**, 291, 32-36.
-

- 
110. A. de Lucas, M. J. Ramos, F. Dorado, P. Sanchez, J. L. Valverde, "Influence of the Si/Al ratio in the hydroisomerization of n-octane over platinum and palladium beta zeolite-based catalysts with or without binder", *Applied Catalysis A: General* **2005**, 289, 205-213.
111. C. Jen-Ho, L. Jiunn-Nan, K. Yih-Ming, Y. Wen-Yueh, K. Chien-Nan, W. Ben-Zu, "Preparation of nano-gold in zeolites for CO oxidation: Effects of structures and number of ion exchange sites of zeolites", *Applied Catalysis A: General* **2005**, 291, 162-169.
112. C. Jen-Ho, L. Jiunn-Nan, K. Yih-Ming, Y. Wen-Yueh, K. Chien-Nan, W. Ben-Zu, "Preparation of platinum in zeolites for CO Oxidation: Effects of structures and number of ion exchanges sites of zeolites", *Applied Catalysis A: General* **2005**, Article in Press.
113. M. Kotobuki, T. Shido, M. Tada, H. Uchida, H. Yamashita, Y. Iwasawa, M. Watanabe, "XAFS Characterization of Pt-Fe/zeolite Catalysts for Preferential Oxidation of CO in Hydrogen Fuel Gases", *Catalysis Letters* **2005**, 103, 263-269.
114. M. Kotobuki, A. Watanabe, H. Uchida, H. Yamashita, M. Watanabe, "Reaction mechanism of preferential oxidation of carbon monoxide on Pt, Fe, and Pt-Fe/mordenite catalysts", *Journal of Catalysis* **2005**, 23, 262-269.
115. M. Kotobuki, H. Uchida, T. Shido, Y. Iwasawa, M. Watanabe, "Design and analysis of bimetal supported zeolite catalysts for selective CO oxidation in reforming gas for fuel cells", *Photon factory activity report* **2003**, 9A, 10B/2002G282.
116. K. Naonobu et. al., "Standardization of catalyst preparation using reference catalyst: ion exchange of mordenite type zeolite 1. Remarkable dealumination accompanying ion exchange", *Applied Catalysis A: General* **2005**, 283, 63-74.
117. St. Walter, St. Malmberg, B. Schmidt, M. A. Liauw, Mass transfer limitations in microchannel reactors, *Catalysis Today* **2005**, 110, 15-25.
-

- 
118. D. H. Kim, M. S. Lim, "Kinetics of selective CO oxidation in hydrogen-rich mixtures on Pt/alumina catalysts", *Applied Catalysis A: General* **2002**, 224, 27-38.
  119. G. Kolb, V. Cominos, C. Hoffmann, H. Pennemann, J. Schürer, D. Tiemann, M. Wichert, R. Zapf, V. Hessel, H. Löwe, "Integrated microstructured fuel processors for fuel cell applications", *Chemical Engineering Research and Design* **2005**, 83, 626-633.
  120. T. Caputo, R. Pirone, G. Russo, "CuO/CeO<sub>2</sub> catalysts for the Preferential Oxidation of CO in excess H<sub>2</sub>", *Chemical Engineering Transactions* **2004**, 4, 259-264.
  121. R. H. Nibbelke, M. A. Campman, J. H. B. J. Hoebink, G. B. Marin, "Kinetic study of the CO oxidation over Pt/ $\gamma$ -Al<sub>2</sub>O<sub>3</sub> and Pt/Rh/CeO<sub>2</sub>/ $\gamma$ -Al<sub>2</sub>O<sub>3</sub> in the presence of H<sub>2</sub>O and CO<sub>2</sub>", *Journal of Catalysis* **1997**, 171, 358-373.
  122. L. Irving, "The mechanism of the catalytic action of platinum in the reactions  $2\text{CO} + \text{O}_2 = 2\text{CO}_2$  and  $2\text{H}_2 + \text{O}_2 = 2\text{H}_2\text{O}$ ", *Transactions of Faraday Society* **1922**, 17, 621-654.
  123. B. Riedmüller, D. C. Papageorgopoulos, B. Berenbak, R. A. van Santen, A. W. Kleyn, "'Magic' island formation of CO coadsorbed with H on Ru (0001)", *Surface Science* **2002**, 515, 323-336.
  124. T. Ioannides, X. Verykios, "Influence of the carrier on the interaction of H<sub>2</sub> and CO with supported Rh", *Journal of Catalysis* **1993**, 140, 353-369.
  125. M. M. Schubert, A. H. Gasteiger, R. J. Behm, "Surface formats as side products in the selective CO oxidation on Pt/ $\gamma$ -Al<sub>2</sub>O<sub>3</sub>", *Journal of Catalysis* **1997**, 172, 256-258.
  126. S. Zh. Todorova, G. B. Kadinov, "Infrared spectroscopy of adsorption and coadsorption of carbon monoxide and hydrogen on Ru/Al<sub>2</sub>O<sub>3</sub>", *Research on Chemical Intermediates* **2002**, 28, 291-301.
  127. M. Schuessler, M. Portscher, U. Limbeck, "Monolithic integrated fuel processor for the conversion of liquid methanol", *Catalysis Today* **2003**, 79-80, 511-520.
-

- 
128. G. Avgouropoulos, T. Ioannides, H. K. Matralis, J. Batista, S. Hocevar, "CuO-CeO<sub>2</sub> mixed oxide catalysts for the selective oxidation of carbon monoxide in excess hydrogen", *Catalysis Letter* **2001**, 73, 33-40.
  129. M. S Liao, R. C. Carlos, Y. Ishikawa, "A theoretical study of CO adsorption on Pt, Ru and Pt-M (M = Ru, Sn, Ge) clusters", *Surface Science* **2000**, 445, 267-282.
  130. D. R. Schryer, B. T. Upchurch, B. D. Sidney, K. G. Brown, G. B. Hoflund, R. K. Herz, "A proposed mechanism for Pt/SnO<sub>x</sub>-catalyzed CO oxidation", *Journal of Catalysis* **1991**, 130, 314-317.
  131. H. Muraki, S. Matunaga, H. Shinjoh, M. Wainwright, "The effect of steam and hydrogen in promoting the oxidation of carbon monoxide over a platinum on alumina catalyst", *Journal of Chemical Technology and Biotechnology* **1991**, 52, 415-424.
  132. P. J. Berlowitz, C. H. F. Peden, D. W. Goodman, "Kinetics of CO oxidation on single-crystal Pd, Pt, Ir", *Journal of Physical Chemistry* **1988**, 92, 5213-5221.
  133. G. S. Zafiris, R. J. Gorte, "CO oxidation on model Pt/ $\gamma$ -Al<sub>2</sub>O<sub>3</sub>(0001): Evidence for structure sensitivity", *Journal of Catalysis* **1993**, 140, 418-423.
  134. J. A. Rodriguez, D. W. Goodman, "High-pressure catalytic reactions over single crystal metal surfaces", *Surface Science Report* **1991**, 14, 1-107.
  135. C. H. F. Peden, D. W. Goodman, D. S. Blair, P. J. Berlowitz, G. B. Fisher, S. H. Oh, "Kinetics of CO oxidation by O<sub>2</sub> or NO on Rh(111) and Rh(100) single crystals", *Journal of Physical Chemistry* **1988**, 92, 1563-1567.
  136. N. W. Cant, P. C. Hicks, B. S. Lennon, "Steady-state oxidation of carbon monoxide over supported noble metals with particular reference to platinum", *Journal of Catalysis* **1978**, 54, 372-383.
  137. V. Gorodetskii, G. Panov, V. Sobyenin, N. Bulgakov, "Low temperature oxidation of hydrogen on platinum", *Reaction Kinetics Catalysis Letters* **1978**, 9, 239-244.
-

- 
138. M. Haruta, T. Kobayashi, H. Sano, N. Yamada, "Novel Gold catalysts for the oxidation of Carbon Monoxide at a Temperature far below of 0 °C", *Chemistry Letters* **1987**, 405-408.
  139. S. D. Gardner, G. B. Hoflund, B. T. Upchurch, D. R. Schryer, E. J. Kielin, J. Schryer, "Comparison of the performance characteristics of Pt/SnO<sub>x</sub> and Au/MnO<sub>x</sub> catalysts for low-temperature CO oxidation", *Journal of Catalysis* **1991**, 129, 114-120.
  140. S. Kandoi, A. A. Gokhale, L. C. Grabow, J. A. Dumesic, M. Mavrikakis, "Why Au and Cu are more selective than Pt for preferential oxidation of CO at low temperature", *Catalysis Letters* **2004**, 93, 93-100.
  141. Note, "Selective Oxidation of CO in Hydrogen over Gold supported on Manganese Oxides", *Journal of Catalysis* **1997**, 168, 125-127.
  142. S. Akinobu, M. Haruta, "Simulations of pathways for CO oxidation over Au nano-clusters by paired interacting orbitals (PIO) analysis", *Applied Catalysis A: General* **2005**, 291, 6-12.
  143. L. M. Molina, B. Hammer, "Some recent theoretical advances in the understanding of the catalytic of Au", *Applied Catalysis A: General* **2005**, 291, 21-31.
  144. R. Zanella, L. Delannoy, C. Louis, "Mechanism of deposition of gold precursors onto TiO<sub>2</sub> during the preparation by cation adsorption and deposition-precipitation with NaOH and urea", *Applied Catalysis A: General* **2005**, 291, 62-72.
  145. M. A. Debeila, N. J. Coville, M. S. Scurrell, G. R. Hearne, "The effect of calcination temperature on the adsorption of nitric oxide on Au-TiO<sub>2</sub>: Drifts studies", *Applied Catalysis A: General* **2005**, 291, 98-115.
  146. M. Khoudiakov, M. C. Gupta, S. Deevi, "Au/Fe<sub>2</sub>O<sub>3</sub> nanocatalysts for CO oxidation: A comparative study of deposition-precipitation and coprecipitation techniques", *Applied Catalysis A: General* **2005**, 291, 151-161.
-

- 
147. H. Sakurai, T. Akita, S. Tsubota, M. Kiuchi, M. Haruta, "Low temperature activity of Au/CeO<sub>2</sub> for water gas shift reaction, and characterization by ADF-STEM, temperature-programmed reaction, and pulse reaction", *Applied Catalysis A: General* **2005**, 291, 179-187.
148. R. Zapf, C. Becker-Willinger, K. Berresheim, H. Bolz, H. Gnaser, V. Hessel, G. Kolb, P. Löb, A.-K. Pannwitt, A. Ziogas, "Detailed characterization of various porous alumina-based catalyst coatings within microchannels and their testing for methanol steam reforming", *Trans IChemE* **2003**, 81, 721-729.
149. E. V. Rebrov, G. B. F. Seijger, H. P. A. Calis, M. H. J. M. de Croon, C. M. van den Bleek, J. C. Schouten, "The preparation of highly ordered single layer ZSM-5 coating on prefabricated stainless steel microchannels", *Applied Catalysis A: General* **2001**, 206, 125-143.
150. A. Navajas, R. Mallada, C. Tellez, J. Coronas, M. Menendez, J. Santamaria, "Study on the reproducibility of mordenite tubular membranes used in the dehydration of ethanol", *Journal of Membrane Science*, **2007**, 299, 166-173.
151. Y. S. S. Wan, J. L. H. Chau, A. Gavriilidis, K. L. Yeung, "Design and fabrication of zeolite-based microreactors and membrane microseparators", *Microporous and Mesoporous Materials* **2001**, 42, 157-175.
152. Y. S. S. Wan, J. L. H. Chau, A. Gavriilidis, K. L. Yeung, "TS-1 zeolite microengineered reactors for 1-pentene epoxidation", *Chemical Communications* **2002**, 8, 878-879.
153. D. R. Schryer, B. T. Upchurch, J. D. Van Norman, K. G. Brown, J. Schryer, "Effects of pre-treatment conditions on a Pt/SnO<sub>2</sub> catalyst for the oxidation of CO in CO<sub>2</sub> lasers", *Journal of Catalysis* **1990**, 122, 193-197.
-

- 
154. G. Kolb, H. Pennemann, R. Zapf, "Water-gas shift reaction in micro-channels – Results from catalyst screening and optimization", *Catalysis Today* **2005**, 110, 121-131.
  155. E. G. Christoffel, "Laboratory reactors and heterogeneous catalytic processes", *Catalysis Reviews - Science and Engineering* **1982**, 24, 159-232.
  156. L. K. Doraiswamy, "Laboratory catalytic reactors", *Catalysis Reviews - Science and Engineering* **1974**, 10, 177-219.
  157. S. H. Oh, G. B. Fisher, J. E. Carpenter, D. W. Goodman, "Comparative kinetic studies of CO-O<sub>2</sub> and CO-NO reactions over single crystal and supported Rhodium catalysts", *Journal of Catalysis* **1996**, 100, 360-376.
-

## 6.1 Nomenclature

AIC	-	Akaike's Information Criterion
$C(t)$	moles/l	Output concentration of gas
$C_1(t)$	moles/l	Inlet concentration of gas
Cat.	-	Catalyst
$[i]$	Vol.%	Concentration of gas specie i
$E_A$	kJ/mole	Activation energy
$E$	$s^{-1}$	Residence time distribution
$F_{in}$	Nl/min	Inlet flow rate
$F_R$	Nl/min	Recycle flow rate
$k_0$	$ml^{1-(\alpha+\beta+\gamma+\delta)} \cdot g_{cat}^{-1} \cdot s^{-1}$	Pre-exponential factor
$R$	$kJ \cdot mole^{-1} \cdot K^{-1}$	Universal gas constant
$r$	$ml \cdot g_{cat}^{-1} \cdot s^{-1}$	Reaction rate
$t_m$	s	Mean residence time
$T$	K	Temperature
$V$	ml	Reactor volume
WHSV	$Nl \cdot h^{-1} \cdot g_{cat}^{-1}$	Weight Hourly Space Velocity

---

---

*Greek symbols*

$\alpha$	-	CO exponential factor in CO reaction rate
$\beta$	-	O <sub>2</sub> exponential factor in CO reaction rate
$\gamma$	-	H <sub>2</sub> exponential factor in CO reaction rate
$\delta$	-	CO <sub>2</sub> exponential factor in CO reaction rate
$\pi$	-	H <sub>2</sub> exponential factor in H <sub>2</sub> reaction rate
$\nu$	-	O <sub>2</sub> exponential factor in H <sub>2</sub> reaction rate
$\kappa$	-	CO <sub>2</sub> exponential factor in H <sub>2</sub> reaction rate
$\Delta H$	kJ/mole	Reaction enthalpy
$\theta$	-	Bragg's angle
$\theta_i$	-	Surface coverage of specie i
$\lambda$	-	2·[O <sub>2</sub> ]/[CO] ratio
$\tau$	s	Residence time

---